

Deactivation pathways in methane upgrading catalysis

Franz, R.P.M.

DOI

[10.4233/uuid:9ed1cff8-55b9-4be3-abc3-3ba05ec0bce4](https://doi.org/10.4233/uuid:9ed1cff8-55b9-4be3-abc3-3ba05ec0bce4)

Publication date

2021

Document Version

Final published version

Citation (APA)

Franz, R. P. M. (2021). *Deactivation pathways in methane upgrading catalysis*. [Dissertation (TU Delft), Delft University of Technology]. <https://doi.org/10.4233/uuid:9ed1cff8-55b9-4be3-abc3-3ba05ec0bce4>

Important note

To cite this publication, please use the final published version (if applicable).
Please check the document version above.

Copyright

Other than for strictly personal use, it is not permitted to download, forward or distribute the text or part of it, without the consent of the author(s) and/or copyright holder(s), unless the work is under an open content license such as Creative Commons.

Takedown policy

Please contact us and provide details if you believe this document breaches copyrights.
We will remove access to the work immediately and investigate your claim.

Deactivation pathways in methane upgrading catalysis

Robert Franz

Deactivation pathways in methane upgrading catalysis

Dissertation

for the purpose of obtaining the degree of doctor
at Delft University of Technology

by the authority of the Rector Magnificus Prof.dr.ir. T.H.J.J. van der Hagen,
chair of the Board for Doctorates

to be defended publicly on

Monday, 7 June 2021 at 10:00 o'clock

by

Robert Peter Michael FRANZ

Master of Science in Chemical and Process Engineering,
Karlsruhe Institute of Technology, Germany

born in Ludwigshafen am Rhein, Germany

This dissertation has been approved by the promoters:

Prof. dr. E.A. Pidko
Prof. dr. A. Urakawa

Composition of the doctoral committee:

Rector Magnificus	chairperson
Prof. dr. E.A. Pidko	Delft University of Technology, promotor
Prof. dr. A. Urakawa	Delft University of Technology, promotor

Independent members:

Prof. dr. A.A. Kiss	Delft University of Technology
Prof. dr. G. Rothenberg	University of Amsterdam
Prof. dr. L. Lefferts	University of Twente
Dr. N. Kosinov	Eindhoven University of Technology
Prof. dr. F. Mulder	Delft University of Technology, reserve member

The work described in this thesis was carried out in the Inorganic Systems Engineering group and the Catalysis Engineering section, Faculty of Applied Sciences, Delft University of Technology. The research was financed by the CatC1Chem consortium, a partnership of NWO, BASF, SABIC and Sasol.

Dissertation, Delft University of Technology
With a summary in Dutch
ISBN: 978-94-6384-212-9

Printed by Ipskamp Printing, Enschede

©2021 Robert Franz

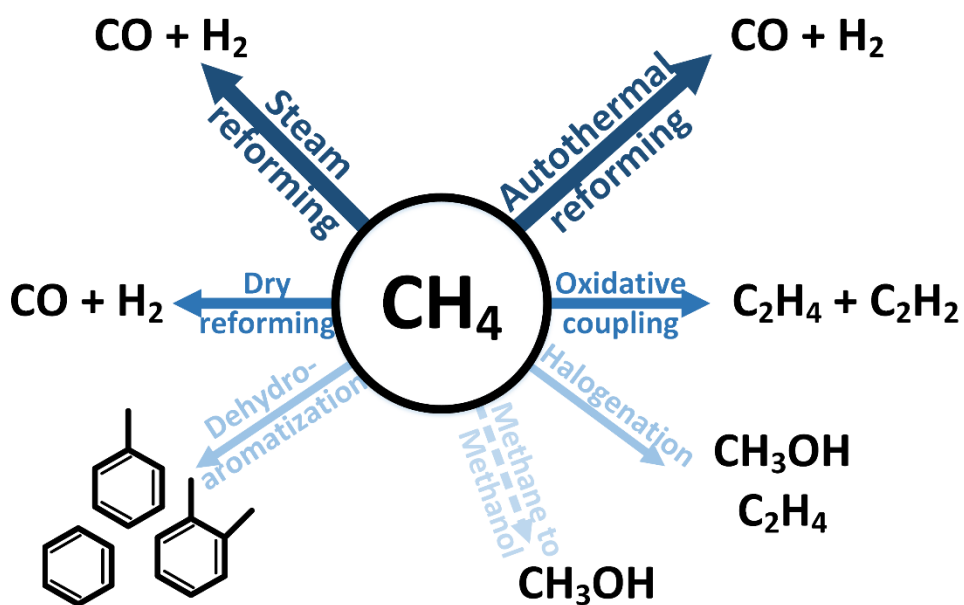
To my family

Table of contents

Chapter 1	Challenges for the usage of methane as a chemical feedstock	1
Chapter 2	Impact of small promoter amounts on coke structure in dry reforming of methane over Ni/ZrO ₂	31
Chapter 3	Dry reforming of methane to test passivation stability of Ni/Al ₂ O ₃ catalysts	59
Chapter 4	Impact of promoter addition on the regeneration of Ni/Al ₂ O ₃ dry reforming catalysts	83
Chapter 5	Potential for false positive in methane to methanol conversion experiments due to MOF contamination and the impact on apparent productivity	119
	Summary and outlook	141
	Samenvatting en vooruitzicht	145
	Acknowledgements	151
	List of publications and presentations	155
	CV	159

Chapter 1

Challenges for the usage of methane as a chemical feedstock



The abundance of methane has led to a strong interest to use methane as a feedstock in the chemical industry. One of the main challenges is the initial activation of the methane molecule. This has resulted in the development of several different approaches to utilize methane, some more developed than others. In this chapter the status of the different approaches is discussed and the main issues for industrial utilization described. A special focus of this work is the status of catalyst development.

This chapter is based on the following publication:
R. Franz, and E. A. Pidko, *in preparation*.

1.1 Motivation

Methane (CH_4) is both the simplest hydrocarbon and one of the hydrocarbons with the largest supply available. Methane concentration in natural gas is typically in the range of 70-90%.¹ At the end of 2018 the total proven reserves of natural gas amounted to 196.9 trillion m^3 .² This represents reserves sufficient to fulfill human demands for the next 50 years if gas consumption remains on 2018 levels. Furthermore, methane is the main component of biogas, making up more than 50% in almost all cases.³ Despite this abundance of methane, the usage of methane in the chemical industry is still limited. More than 90% of the methane used worldwide is burned to generate electricity, heat (for cooking) or similar.¹

Methane is not only burned to generate energy. Significant quantities of methane are burned or flared in the extraction of oil. Methane is a common by-product in oil extraction (so-called associated gas). The common options available to operators of oil extraction operations are to burn the gas, re-inject it into the ground or release it into the atmosphere. On a molar basis the contribution of methane to the greenhouse effect is 25 times greater than that of CO_2 .⁴ Flaring the associated gas is therefore preferable over releasing methane into the atmosphere. As a result, in 2017 a total of 140 bcm of methane (corresponding to 270 Mt of CO_2) were flared but an even larger amount of methane was released into the atmosphere.⁵

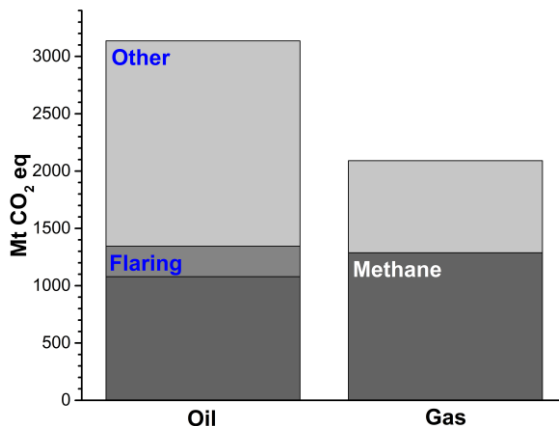


Figure 1.1: Greenhouse gas emissions in 2017 from oil and gas operations, modified from 5.

Methane is sparingly used as a feedstock in the chemical industry due to various issues related to methane activation. In a methane molecule, the carbon atom is surrounded by four hydrogen atoms, forming a regular tetrahedron (bond angle of 109.471°). The carbon atom is thus symmetrically protected by four identical bonds. Also, the C-H bonds are highly stable

and only weakly polarized. The first challenge of methane usage in the chemical industry is to activate the C-H bond. The second challenge is to maintain a high selectivity, since many theoretically possible products are less symmetrical and stable and thus more reactive than methane.

These challenges have almost always proven to be too great to allow for industrial use of methane as a feedstock. The main example of methane usage in the chemical industry is methane reforming to syngas (CO and H₂). The enormous heat requirements of this reaction only allow for profitable operation on a large scale. To convert smaller amounts of methane, other processes would be necessary. Therefore, significant research efforts have been undertaken to develop new methane conversion routes. In the following we will give an overview of the different reactions, their status on the path to industrial implementation and the biggest challenges on this road.

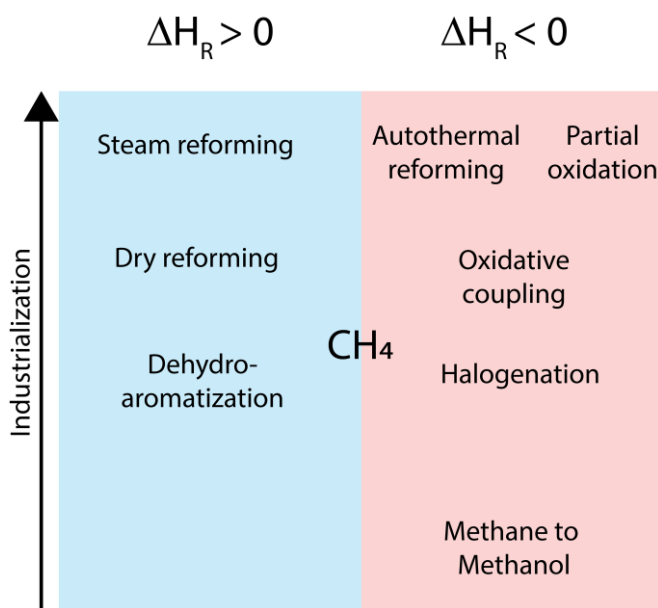


Figure 1.2: Schematic overview of the different possibilities for methane conversion

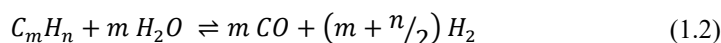
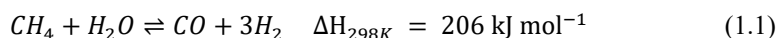
In Figure 1.2 an overview of the different reactions for methane conversion is given. The reactions are subdivided into the two categories of endo- and exothermic reactions. This subdivision was used as it allows us to highlight the two main challenges typically encountered in methane conversion: coke formation (for endothermic reactions) and stabilization of the intermediate products (exothermic reactions). The endothermic reactions will be discussed first, starting with the most advanced process – steam reforming (SR). Likewise, for the exothermic reactions, the processes with the most industrial applicability,

autothermal reforming (ATR) and partial oxidation (POX), will be discussed first followed by a brief overview of the less developed processes.

1.2 Methane steam reforming

1.2.1 Overview

Steam reforming is the most well-known example of hydrocarbon reforming reactions. This process should not be confused with catalytic reforming. The latter refers to the conversion of paraffinic hydrocarbons to isoalkanes and aromatics (i.e. hydrocarbons with high octane numbers). Steam reforming is the reaction of methane or other hydrocarbons with steam to produce a mixture of CO and H₂ that is commonly referred to as syngas:



This reaction has been used in industry since the 1930s.⁶ It is the key process in the supply of both synthesis gas and hydrogen for the chemical industry. In view of its enormous economic and technological importance, methane steam reforming has been a subject of intense research both in industry and in academia for almost a century.⁶⁻⁸ This process is so popular in industry due to its flexibility. It can be adapted to a wide range of hydrocarbons, for example from methane to naphtha.⁹⁻¹¹ The reaction is catalyzed and a large variety of different typically Ni-based catalysts are commercially available, optimized for the possible hydrocarbons.⁶ Additionally, the desired H₂/CO ratio in the product stream varies depending on the intended process, e.g. hydroformylation or methanol synthesis. This can also be taken into account by adjusting the process parameters (T, p, H₂O to carbon ratio, etc.). For steam reforming of methane, typical H₂/CO values are in the range of 2.8-4.7.¹¹

The process conditions are set according to the compromise between thermodynamics and operational cost considerations typical of industry. The temperature of the reformer is set at 700-900 °C, while the pressure is normally kept at 20 bar or higher.⁶ This high temperature is necessary due to the strongly endothermic nature of the reaction.¹ Operation at low pressures would be thermodynamically preferable, since the total amount of molecules increases with conversion. However, typical downstream applications, such as NH₃-synthesis or the Fischer-Tropsch process, require the supply of hydrogen and synthesis gas at elevated pressures. Consequently, operation at elevated pressures is economically preferable to operation at low pressures with ensuing compression of the increased gas volumes.⁶

Operation under such conditions is costly with regard to both capital and operational expenses. As a result, steam reforming is typically not feasible for the valorization of smaller or highly remote gas reserves¹² and it is usually combined with immediate consumption of the syngas in another reaction on-site. Even in this context, the costs of syngas production are considerable. For an industrial-scale Gas to Liquids (GtL) plant, it represents the lion's share of the capital expenditure.¹³ A typical process example of a facility incorporating steam reforming can be seen in Figure 1.3.

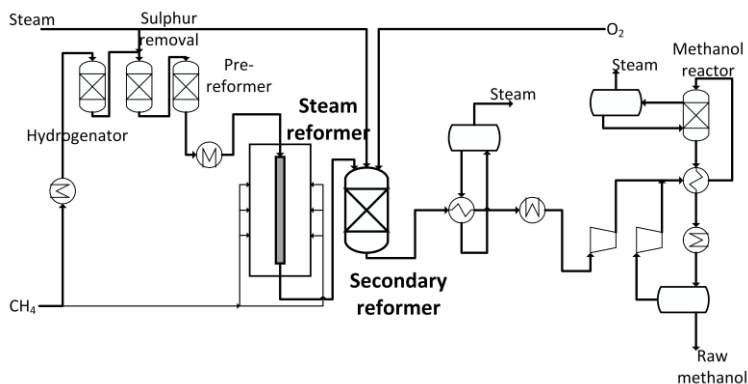


Figure 1.3: Simplified flow scheme of a methanol plant utilizing Topsøe two-step reforming, modified from 14.

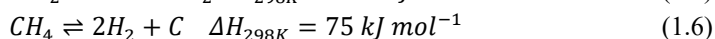
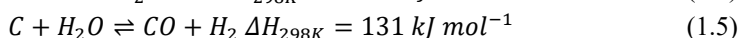
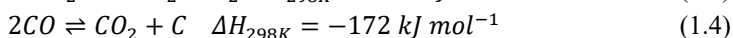
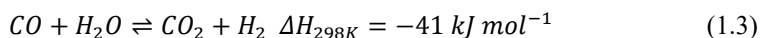
1.2.2 Principles of catalyst design in steam reforming

As mentioned previously, the thermodynamics of steam reforming requires temperatures that can approach $1000\text{ }^\circ\text{C}$. Above $1000\text{ }^\circ\text{C}$ the formation of radicals from methane cracking becomes more and more relevant. However, only at around $1500\text{ }^\circ\text{C}$ is the conversion achievable through this gas-phase reaction pathway sufficiently high.¹⁵ Thus, heterogeneous catalysts are necessary to keep the reaction temperature sufficiently low for a profitable operation. The goal for a company operating such an energy-intensive bulk process is to limit the downtime of a steam reforming plant to the scheduled maintenance intervals. Thus, an industrial catalyst must allow for stable operation in the timescale of years rather than months or weeks.¹⁶ Regeneration procedures or similar would reduce the profitable operation period of an already quite expensive process. If catalyst stability over a period of years is the main goal, a good overview of potential problems is necessary. According to literature, a catalyst can deactivate due to one or several of the reasons shown in Table 1.1.

Table 1.1: Mechanisms of catalyst deactivation¹⁷

Mechanism	Type	Brief description
Poisoning	Chemical	Strong chemisorption of species on catalytic sites which block sites for catalytic reaction
Fouling, coking	Mechanical, chemical	Physical deposition of species from fluid phase onto the catalytic surface and in catalyst pores
Thermal degradation, sintering	Thermal, chemical	Thermally induced loss of catalytic surface area, support area, and active phase-support reactions
Vapor formation	Chemical	Reaction of gas with catalyst phase to produce volatile compound
Vapor-solid and solid-solid reactions	Chemical	Reaction of vapor, support, or promoter with catalytic phase to produce inactive phase
Attrition/ crushing	Mechanical	Loss of catalytic material due to abrasion; loss of internal surface area due to mechanical-induced crushing of the catalyst particle

In steam reforming of hydrocarbons, the main challenges in designing a stable catalyst are sulfur poisoning, catalyst coking and sintering.⁶ As already mentioned previously, the typical steam reforming catalysts employ nickel as an active metal.¹⁸ This is due to the low cost of Ni compared to other catalytically active metals such as Rh. Therefore, in the following descriptions, we will assume Ni-based catalysts. In a reformer, the main reaction is typically accompanied by the following side reactions:



The principles of coke formation have been reviewed extensively in literature.^{16, 19} Depending on the feedstock used, the operating conditions in the reactor and the characteristics of the catalyst, different species of coke can be generated. For the conditions typical of steam reforming, two species of carbon deposits are the most common: carbon filaments and pyrolytic carbon.¹⁹ Carbon filaments are whisker-like structures that can be compared to carbon nanotubes.^{20, 21} Their geometry does not allow them to block the catalyst surface. However, a continued growth of carbon fibers can lead to breakage of catalyst particles and blockage of the entire reactor in severe cases.^{19, 22} Pyrolytic carbon on the other hand grows on the catalyst surface and thus deactivates the active sites. However, an excessive growth of pyrolytic carbon will also increase the pressure drop over the reactor.¹⁹

These carbon structures do not appear randomly over the Ni surface. Coke formation can be traced to two distinct structural configurations of the Ni surface: defects in the Ni surface and large surfaces in general. In a first step, coke nuclei must be formed and then stabilized on a Ni surface for coke growth to proceed. Nucleation preferentially takes place on Ni defect sites, with step sites being the prime example.^{11, 23} Step sites are more reactive than close-packed Ni surfaces, since they allow for methane to interact with more Ni atoms simultaneously. This increased activation of methane also means that a reaction like methane decomposition will take place more easily on at a step site. This fresh coke nucleus must be stabilized in order to grow. Literature has clearly established that this stabilization of coke nuclei proceeds much better on large Ni surfaces than small ones.^{11, 23-25} Thus, the bigger and more defect-rich a Ni surface, the easier carbon formation is initiated.

Carbon deposits are not the sole cause for the blockage and deactivation of the active sites on the catalyst surface. The deactivation of catalytic sites due to strong adsorption of reactants, products or impurities is so common that it even has its own name: catalyst poisoning.¹⁹ Group VIII metals are quite susceptible to reactions with sulfur and natural hydrocarbon sources are typically contaminated with H₂S in sufficiently high concentrations.²⁶ Under steam-reforming conditions, a group VIII metal will react with H₂S to form hydrogen and chemisorbed sulfur, making this the main route of catalyst poisoning:



Nickel is more sensitive to the formation of sulfide than the other group VIII metals.¹¹ The regeneration of a deactivated catalyst poisoned by sulfur is possible but labor and energy intensive.²⁶ Therefore, the best and most commonly practiced solution for this problem is to carefully desulfurize the feed upstream of the reactor.^{16, 27} Interestingly, the deactivating effect of the sulfur can be used to combat the formation of carbon deposits on the excessively reactive sites at the catalyst surface and increase the lifetime of the catalyst. This is the concept of the so-called SPARG process, where well-controlled low concentrations of co-fed H₂S are used to selectively deactivate the excessively reactive Ni sites on which the most coke is formed. The result is a significantly enhanced catalyst lifetime.²⁵

The last significant deactivation mechanism is sintering of the catalyst, i.e. a reduction in surface area caused by particle growth at elevated temperature. Sintering of both the support and the active phase has been extensively reviewed in literature.^{16, 19, 28} Possible mechanisms include solid-state diffusion, surface diffusion and phase changes.²⁷ Two important thresholds for the onset of sintering are the Hüttig temperature and the Tamman temperature. The prior signifies the mobility of atoms near defects. The Tamman temperature on the other hand is seen as the point at which the bulk atoms become mobile. Empirical correlations for both were given by *Moulijn et al.* as:²⁹

$$T_{Hüttig} = 0.3 T_{melt} \quad (T \text{ in K}) \quad (1.8)$$

$$T_{Tamman} = 0.5 T_{melt} \quad (T \text{ in K}) \quad (1.9)$$

Metallic bulk nickel melts at 1455 °C. Thus, the nickel particles on the surface are highly susceptible to sintering in the temperature range of 700-900 °C typical of steam reforming ($T_{Hüttig} = 518$ °C, $T_{Tamman} = 863$ °C).¹⁷ Sintering can be accelerated by the presence of impurities in the feed. The feeding of Cl₂ for example leads to the formation of NiCl₂, which sinters at lower temperatures ($T_{Hüttig} = 384$ °C, $T_{Tamman} = 641$ °C). Traces of CO in the feed during heating or cooling of the reactor are similarly dangerous as Ni(CO)₄ has a boiling point of 43 °C.^{19, 30, 31} This is not a problem at during steam reforming itself, since Ni(CO)₄ is no longer stable at typical operating temperatures.

Catalyst supports typically consist of metal oxides, such as MgO, Al₂O₃ or MgAl₂O₄.⁶ The higher melting points of metal oxides compared to reduced metals means that the agglomeration of nickel particles is the main sintering problem. However, supports can easily sinter because of a thermally induced phase-change. The prime example for this behavior is Al₂O₃ with its plethora of metastable phases.

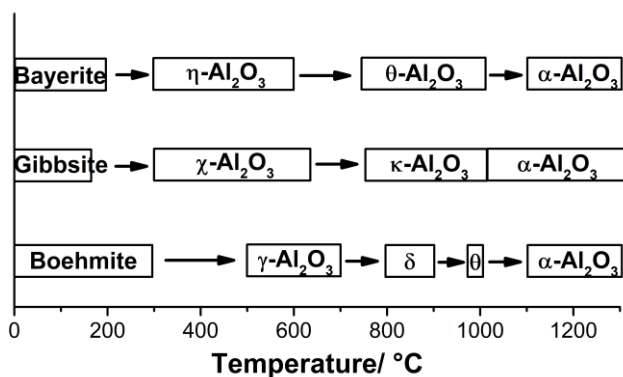


Figure 1.4: Al₂O₃ phase changes from the hydroxides to $\alpha\text{-Al}_2\text{O}_3$ as a function of temperature³².

The packing density of Al₂O₃ increases, when the temperature is increased and phase change occurs. The most stable modification ($\alpha\text{-Al}_2\text{O}_3$) exists in hexagonal close-packed configuration.³³ Thus, a structural change in the support at elevated temperature can decrease the total surface area and the available number of active sites drastically. Besides phase changes, the sintering of the support is also governed by diffusion processes, just as the sintering of the active metal.¹⁷ Similarly, the presence of other elements can accelerate or inhibit the sintering of the support. Using Al₂O₃ as an example again, the following statements can be found in literature: alkali metals and steam enhance sintering, whereas

metals such as Ca or Ni form spinel phases with Al_2O_3 , reducing sintering.¹⁷ Alternatively, a treatment with sulfuric acid can also improve the stability of Al_2O_3 .²⁸

To sum up, the main challenge in catalyst design for steam reforming is the engineering of the nickel particles. These must be dispersed to provide a high Ni surface area. At the same time the highly reactive nickel ensembles that generate the most coke must be deactivated to guarantee stable operation. The minimum requirements for the support are relatively simple by comparison. The typical support is a metal oxide that can be pretreated to increase the sintering resistance even further. Additionally, support materials such as MgO or Al_2O_3 tend to stabilize Ni particles and thus contribute to the catalyst stability.

1.2.3 Commercial catalysts and reformers

The parameters for successful catalyst design mentioned above are not sufficient as they only consider the catalyst in isolation and ignore issues such as the reactor design. The specifics of large-scale steam reforming lead to further requirements for a successful catalyst. The most typical process design for a steam reformer is the so-called tubular reformer.⁶ The catalyst is placed in a multitude of narrow (i.e. 10 – 15 cm) tubes, which in turn are located in a furnace. In such an arrangement, the catalyst must be shaped to provide for maximum external surface area on large particles/ pellets with the lowest possible pressure drop. Too small pellets would lead to an unacceptable pressure drop over the bed.³¹ This problem is especially relevant for steam reforming due to the operating temperatures and the ensuing mass transport limitations. Under industrial conditions, catalyst effectiveness is around 10% with the activity roughly proportional to the external surface area.¹¹

Industrial catalysts are often shaped into rings and extrudates with multiple holes but foams and monoliths have also been reported.¹¹ The simultaneous usage of several tube reactors also means that a good catalyst shape and thus good packing must be guaranteed. Otherwise, an uneven flow distribution of the reactants through the different tubes causes temperature variations throughout the reactor, shortening the lifetime.⁶ The typical commercial catalyst consists of supported nickel but the nature of the support varies significantly. “Standard” supports that can be found in industry are $\alpha\text{-Al}_2\text{O}_3$, MgO and spinels like MgAl_2O_4 .⁶ At the same time, support optimization appears to be a major focus of industrial R&D leading to novelties such as supports with “built-in promoter reservoirs” to ensure stable operation even during attrition.³⁴

Besides improvement of the catalyst, research is also being undertaken at the moment, to enhance the overall process. One example that can be mentioned here is to improve the heating mechanism of the reformer itself. Instead of the classical heat transfer, supported CoNi nanoparticles can in principle be heated by other methods such as magnetic induction or microwave heating.³⁵⁻³⁷ While this is still early-stage research it shows that steam reforming is continuously being adapted to be the workhorse of the chemical industry in the coming decades.

1.3 Dry reforming of methane

Dry reforming of methane (DRM) is a reaction closely related to steam reforming and under extensive investigation at the moment. Methane or other hydrocarbons are reacted with carbon dioxide instead of steam:

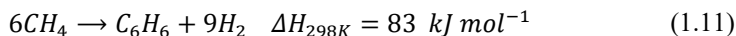


This process in principle has several advantages over the steam reforming of methane. Firstly, it allows for the direct chemical utilization of CO₂, which is the most abundant greenhouse gas, making CO₂ valorization a globally pressing issue. Secondly, the resulting product gas has a significantly lower H₂/CO ratio than in steam reforming, which can be very beneficial for specific downstream chemical conversion processes.³⁸ The biggest downside of dry reforming is the noticeably more pronounced endothermic nature of the reaction compared to SR or ATR, due to the higher stability of CO₂. At the same time the usage of CO₂ means an increase in the overall carbon levels and thus an elevated risk of coke formation.

The combination of elevated coke levels and high purity requirement for CO₂ has delayed the industrial implementation of DRM.^{39, 40} Especially the former of the two challenges has stimulated considerable research activity. The basics of catalyst design are similar for dry and steam reforming of methane. Countless different approaches have been and are being investigated to obtain a catalyst that is sufficiently resistant to coke formation in dry reforming of methane. Nevertheless, the closest existing applications in industry is so-called tri-reforming of methane, in which both CO₂ and H₂O are fed together with methane.^{6, 38}

1.4 Non-oxidative methane upgrading

Methane can also be converted to higher hydrocarbons without the necessity to add additional gases. The best example for this is the so-called methane dehydroaromatization (MDA):



Due to the endothermic nature of this reaction, it is also carried out at elevated temperatures, with typical values being 650 – 800 °C.⁴¹ In contrast to the reforming reactions described earlier, the conversion values at thermodynamic equilibrium in this temperature range are rather low. At 800 °C, the equilibrium conversion of methane is only around 25%.⁴¹ Additionally, the issue of coke management is even more essential than it is in methane reforming reactions due to the absence of an oxidant such as H₂O or CO₂ in the feed. At

thermodynamic equilibrium the benzene yield is effectively zero with the selectivity to coke being almost 100%.⁴² In real-life tests, such results typically do not set in because of the kinetic control over the reaction pathways provided by the catalyst. Nevertheless, the selectivity towards useable aromatics, such as BTX over other products such as naphthalene or coke still requires further optimization.

Significant effort has been invested into catalyst design and mechanistic understanding in order to optimize the product yields. The most commonly investigated catalyst type is a zeolite with added extraframework metals (e.g. refs. 43, 44). Among different modified zeolites, Mo-containing Mo/ZSM-5 and Mo/MCM-22 were found to provide the best results in the non-oxidative methane conversion to aromatics.^{42, 45} The production of aromatics proceeds via a complex reaction network.⁴⁶ The overall mechanism is still unclear but a two-step mechanism with ethane and ethylene as intermediates is generally accepted.^{41, 47} In this mechanism methane is first activated over the Mo species to form C2 intermediates which then react over the Brønsted acid sites (BAS) of the zeolite. Furthermore, it has been proposed that MDA proceeds via a carbon pool mechanism, similar to methanol to hydrocarbons (MTH).⁴⁸ The pore structure of the zeolite is key to provide shape selectivity with regard to the product distribution.^{41, 45}

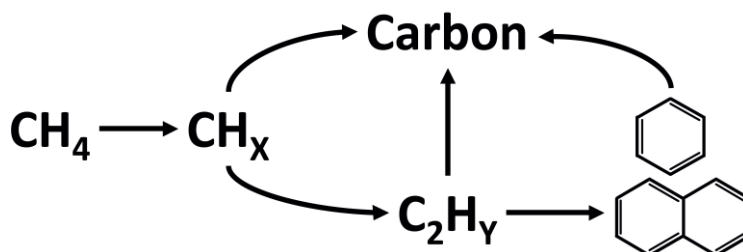


Figure 1.5: Simplified reaction mechanism for MDA⁴⁹.

Deactivation of MDA catalysts is typically a result of the accumulation of polyaromatic coke inside the zeolite pores, which blocks the access to the confided carbidic Mo species and, simultaneously, enhances their sintering and the formation of bulk Mo-carbide.⁵⁰ Therefore, any industrial process must periodically regenerate the catalyst. The most straightforward regeneration procedure would be the removal of coke via oxidation with air. Indeed, cycled operation of methane and oxygen can significantly increase catalyst lifetime.⁵¹ The oxidation periods should be limited to short pulses of oxidant, to optimize the results.⁵² The challenge of a reactor that allows such operation on a larger scale has yet to be addressed, however. Although different reactor concepts have been investigated in literature (e.g. in refs. 53-56), no breakthroughs in terms of industrial implementation have been reported so far.

Despite a lot of research on this topic, cost-effective MDA on an industrial scale is still elusive.

In 2014, a new approach to nonoxidative methane upgrading was developed in the group of Bao.⁵⁷ Through a combination of ball-milling and high temperature treatment, an Fe/SiO₂ catalyst was synthesized with isolated Fe sites in the SiO₂ lattice. Conversion of methane at 950 °C and higher was reported to exclusively yield ethylene, benzene and naphthalene. It has been proposed, that the isolated Fe sites generate methyl radicals which then react to longer hydrocarbons in homogeneous gas-phase reactions.⁴⁵ Coke formation, i.e. C-C coupling on the catalyst surface would require clusters of Fe sites according to this theory.

This already shows two of the biggest problems in this reaction concept: the very high temperatures necessary and the synthesis of a catalyst with sufficient Fe dispersion. *Sakbodin et al.* combined this catalyst with an H₂-permeable membrane to improve yields.⁵⁸ While they achieved the same products, the conversion was significantly lower than reported previously by *Guo et al.* (23% at 1050 °C and 3.2 L g⁻¹ h⁻¹ vs. 42% at 1030 °C and 14.5 L g⁻¹ h⁻¹).⁵⁷ Additionally, no TGA data was provided to guarantee the absence of coking. This is relevant, as in a later publication, the same group reported a 10% selectivity to coke for this system at 1000 °C, both in powdered form and when coated to the reactor wall.⁵⁹ Thus, this approach is still at the stage where catalyst synthesis optimization is necessary before any final statement can be made on the industrial feasibility of the process.

1.5 Partial oxidation and catalytic partial oxidation

In contrast to the previously described reactions, partial oxidation of methane (POX) is an exothermic reaction that proceeds according to the following equation:



This reaction can proceed uncatalyzed and the typical operation parameters are then 1150-1500 °C and 25-80 bar.⁶⁰ The high temperatures are the result of the exothermic nature of the reaction and are also necessary to overcome the high barriers for uncatalyzed gas-phase reactions. Operation with air as the oxidant is theoretically possible, but the use of pure oxygen is more attractive as it reduces the required downstream gas separation. Despite the use of pure oxygen, POX can be economically attractive in certain scenarios. POX units can be used for virtually all hydrocarbon feedstocks and are thus employed in refineries to generate hydrogen from residual oil.^{60, 61} The selectivity issues typical of partial oxidation reactions can be controlled in two manners. Firstly, working with substoichiometric amounts of oxygen automatically reduces the chance of CO₂ production. Secondly, the formation of

H₂ and CO over CO₂ is thermodynamically advantageous at the temperatures of over 1000 °C typical for POX.⁶²

Research is also undergoing to develop a catalytic version of this process, which could operate at lower reaction temperatures (so-called catalytic partial oxidation or CPOX) decreasing the operation and capital costs of the overall process.²⁷ The catalytically active metals for CPOX are, in principle, the same as for steam reforming but the even higher temperatures of CPOX appear to make noble metals such as Rh more attractive than Ni.⁶⁰ The reaction proceeds in different steps over the catalyst with the oxygen rapidly being consumed in the upstream part of the catalyst followed by steam reforming and WGS in the downstream section of the bed.^{60, 63}

1.6 Autothermal reforming of methane

There is a process that is closely related to catalytic partial oxidation but is already being used commercially, namely the so-called autothermal reforming (ATR). Essentially, ATR consists of a combination of POX and steam reforming being carried out in the same reactor. Thus, the feed contains significant amounts of steam besides methane and oxygen. The advantage of such a process is that it yields syngas with a H₂/CO ratio of around 2, which is very favorable for Fisher-Tropsch and methanol syntheses.⁶⁰ Operating conditions can range between 900-1150 °C and 1-80 bar.⁶⁰ Two possible modes of operation have been established. Firstly, the reactant mixture can be fed directly to a catalyst bed. Alternatively, the mixing section at the inlet of the reactor doubles as a burner, discharging into an empty portion of the reactor. The catalyst is then placed further downstream in the reactor as illustrated in Figure 1.6.⁶¹ The second option has proven to be more versatile and is thus commonly used in industry, for example in the SynCORTM process of Haldor Topsøe.⁶⁴

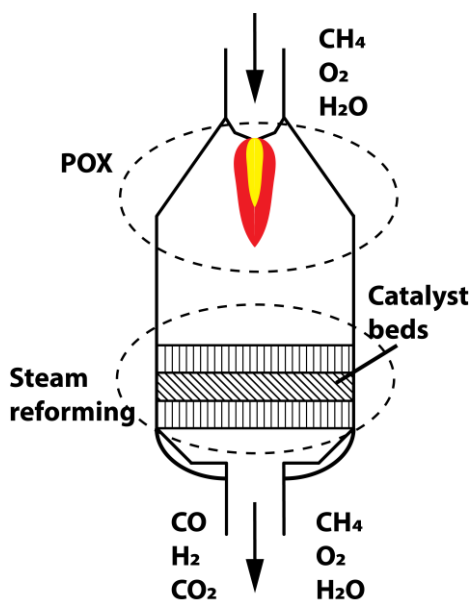
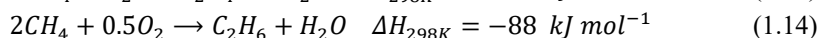


Figure 1.6: A schematic of an ATR reactor, modified from 64.

The main advantages of ATR are the absence of elements such as heat exchangers (allowing for a more compact design) and the cold reactor walls (internal methane combustion provides the necessary heat for steam reforming). The latter allows for higher operating pressures than pure steam reforming. Therefore, ATR is typically employed in “secondary” reformers downstream of the primary steam reformer. Alternatively, ATR is also being investigated as a hydrogen source for fuel cells.^{65, 66}

1.7 Oxidative coupling of methane

Oxidative coupling of methane (OCM) refers to the conversion of methane with oxygen to C₂ hydrocarbons at temperatures in the range of 500-1000 °C:



The first reports on this reaction were published in the early 1980s.^{67, 68} Despite extensive research on potential catalytic systems since then, no industrially feasible process has been developed yet.⁶⁹ In the context of product gas separation and purification, a single-pass yield

of 30% is typically seen as the critical value for an industrially competitive process.⁷⁰ This value has proven challenging due to the nature of the reaction mechanism. The reaction proceeds via a heterogeneous-homogeneous mechanism.^{1, 71} In a first step, methane is activated on the catalyst surface and a C-H bond cleaved, yielding a $\cdot\text{CH}_3$ radical. This radical can then participate in a number of reactions. The recombination of two $\cdot\text{CH}_3$ radicals yields ethane, which can then be dehydrogenated to form ethylene. Figure 1.7 shows a simplified reaction scheme that illustrates the selectivity problem. The methyl radicals are highly reactive and carbon oxides can be formed at any point during the reaction. Thus, the higher the conversion of methane becomes, the lower the selectivity towards C_2 .

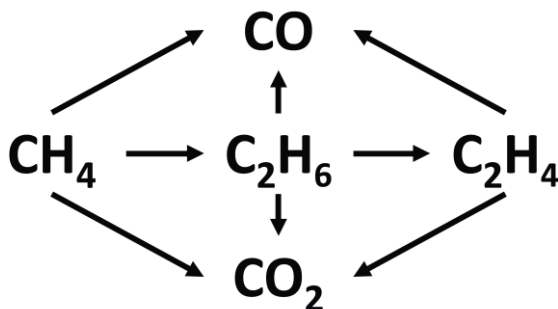


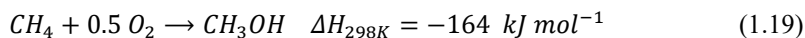
Figure 1.7: Simplified schematic of the OCM process⁷¹.

The catalysts investigated in literature can typically be classified into four different categories⁷¹. These are reducible metal oxides^{72, 73}, non-reducible metal oxides⁷⁴, halogen-containing oxide materials⁷⁵ and solid electrolytes.⁷⁶ Recently, a fifth category has been added. The California-based company Siluria Technologies has reported to have developed a novel nanowire catalyst.¹ Apart from this description, further information on the catalytic system is difficult to obtain. The patent on nanowire catalyst synthesis is valid for both common reducible and non-reducible metal oxides typically used as OCM catalysts.⁷⁷ It has been claimed that the nanowire catalyst can operate at lower temperatures than conventional bulk catalysts.⁷⁸ Coupled with a short contact time over a nanowire catalyst, this could explain a superior performance of such a system. In 2018 Saudi Aramco licensed Siluria's technology to implement on a larger scale.⁷⁹ Therefore, it can be assumed, that the yield and product separation challenges are close to being solved.

Besides the inherent risks of working with halogens, this approach faces a second challenge. Any industrial process would be a multistep process with corresponding separation and purification steps, increasing the costs.¹ On the other hand, the entire halogen cycle can run at temperatures below 500 °C and at atmospheric pressure compared to the harsher conditions necessary for methane steam or dry reforming.⁸⁵ Halogenation and oxyhalogenation have been evaluated for methane upgrading before.⁸⁶ At the time of publishing (1996), the actual hydrocarbon synthesis via methyl halides was considered competitive compared to partial methane oxidation coupled with Fischer-Tropsch (FT) synthesis. However, the costs of separation and purification in the halide approach were considered prohibitive. In the 25 years since this comparison was carried out, the available Gas to Liquids (GtL) technologies have undoubtedly been improved. Unless the separation costs in the halogenation process are drastically reduced or external parameters shift significantly (e.g. the price of emissions), an industrial implementation of the halogenation approach appears unlikely.

1.9 Methane to methanol

The selective low-temperature conversion of methane to methanol and other oxygenates is a “dream reaction” investigated for more than a century. The theoretical advantages of such an approach are undeniable. In an ideal scenario, even small reserves of methane could be exploited and converted to methanol with air as an oxidant. The reaction product would then be a liquid at room temperature and thus easy to separate, transport and implement in a wide range of down-stream chemical conversion processes. The extensive research undertaken on the conversion of methanol to hydrocarbons (MTH) further emphasizes the fact that methanol is an industrially attractive chemical intermediate.



The oxidative upgrading of methane has been investigated in three different regimes so far: at temperatures above 300 °C and temperatures below 300 °C using either heterogeneous or homogeneous catalysts. Similar to the oxidative coupling of methane, the desired product is less stable than either CH₄ or CO₂. Thus, the main challenge is that higher degrees of methane conversion typically result in poor selectivity to methanol.

The oxidative upgrading of methane at temperatures above 300 °C can proceed both non-catalytically and using catalysts. Typically, the reaction is carried out with a considerable excess of methane to improve the selectivity. For the non-catalytic reaction, ambient pressure operation favors the formation of formaldehyde, while methanol is generated at elevated pressures.⁸⁷ The reaction proceeds via a radical mechanism.⁸⁷⁻⁸⁹ The yields achievable in this manner can be relatively high, such as $Y_{MeOH} = 10\%$ reported by *Feng et al.* at 330 °C and

50 bar.⁸⁹ The main problem with this approach is the rather long residence time necessary for such results.⁹⁰

The residence time can be reduced considerably by the use of heterogeneous catalysts, which are typically $\text{MoO}_3/\text{SiO}_2$ or $\text{V}_2\text{O}_5/\text{SiO}_2$ or derivatives thereof.⁹¹⁻⁹⁵ Despite research on these systems the yields reported so far are too low for any industrial consideration.⁹⁰ Additionally, the Mo-based systems have been reported to experience significant stability issues due to Mo-volatilization.⁹⁶

At the same time, the naturally occurring enzyme methane monooxygenase (MMO) is capable of oxidizing methane to methanol. Two known variations of MMO have been extensively studied in literature. Soluble MMO (sMMO) is known to contain a dinuclear Fe cluster.⁹⁷⁻⁹⁹ Particulate MMO (pMMO) on the other hand contains Cu but the exact nature of the active site is still a topic of discussion.^{97, 100} This provided the inspiration for the attempt to convert methane to methanol over well-defined metal clusters in zeolites and Metal-Organic Frameworks (MOFs) resembling the structures of the enzymatic reactive ensembles. For zeolites the focus has been on Cu (e.g. refs. 101-106) and Fe (e.g. refs. 107-111), but Ni¹¹² and Co¹¹³⁻¹¹⁵ have also shown to be active. Catalytically active Metal-Organic Frameworks have also been reported but focused exclusively on Fe and Cu as active metals so far.¹¹⁶⁻¹¹⁹

These studies focused on the elucidation of the active site nature. For a better overview of the different proposed active sites, we refer to reviews on this topic.^{96, 120} Different reaction modes have been tested such as batch reactions^{106, 121-123} or continuous operation.^{105, 124, 125} Regardless of the testing conditions, the yields of methane are several orders of magnitude from any industrial applicability. The research projects on zeolite catalysts were carried out to gain insight into the nature of the active site, meaning yield was not a priority. Nevertheless, these tiny methanol yields at the edges of detectability nicely emphasize the previously mentioned issue of conversion vs. selectivity in partial oxidation reactions. The pronounced difference in stability between methanol and methane compounds the problem for this reaction.

The increased interest in the direct conversion of methane to methanol in recent years has led to growing awareness of this issue of product stability.^{96, 126} Using nature (and thus MMO) as an inspiration again, it is obvious that the activity and selectivity of MMO are only achievable through the combination of two factors: a well-designed active site and a gating mechanism that prevents methanol from reaching the active site to be oxidized further.¹²⁷

A gating mechanism is challenging to achieve in a synthetic catalyst. The existing work on homogeneous catalysis provides insight into how the yield can be increased nevertheless. A plethora of different homogeneous systems has been reported so far. The most promising results so far are based on the work of *Shilov* and *Shul'pin*.¹²⁸ Typically, complexes of transition metals such as Pt^{II} , Pd^{II} or $\text{Au}^{\text{I/III}}$ in highly acidic media are capable of oxidizing methane to methanol derivatives.^{12, 96} The most famous example is the so-called Periana system. It consists of a bypyridimine- PtCl_2 complex that can oxidize methane using oleum

both as a solvent and as an oxidant.¹²⁹ At reaction conditions of greater than 200 °C and 30 bar, single-pass yields of greater than 70 % were reported.

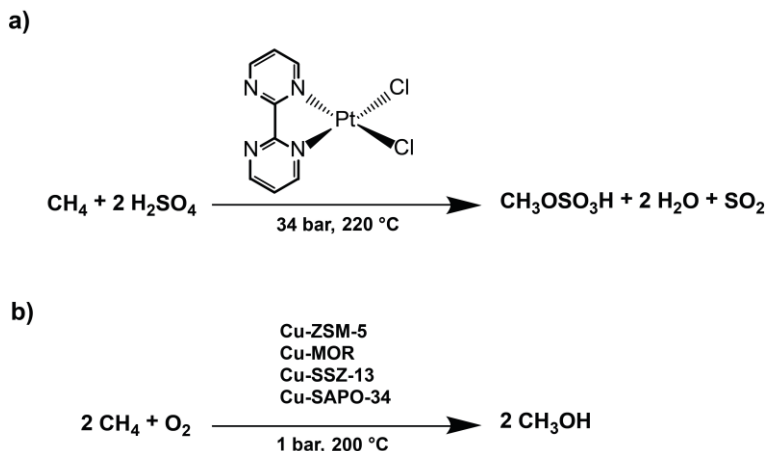


Figure 1.9: Examples of methane oxidation strategies with a protective group for methanol (Periana catalyst – a)) or without any protective group (direct oxidation over Cu-exchanged zeolites – b)).

The key is that methanol is present as methyl bisulfate and thus protected against further oxidation.¹³⁰ This concept of a “scavenger molecule” that reacts with methanol and prevents overoxidation has been labelled as essential to make this reaction industrially relevant.¹²⁶ Besides sulfuric acid-based systems, fluorine-based acids such as trifluoroacetic acid are also known to be a good reaction medium.^{131, 132} The group of *van Bokhoven* has published excellent reviews giving an extensive overview of the different systems, in which methanol is protected by such a “scavenger molecule”.^{96, 133} Coordination of the Periana catalyst to solid supports has been reported in literature.^{134, 135} Beyond such conversion of homogeneous to heterogeneous catalysts there is little information available on heterogeneous systems that increase the yield by employing “scavenger molecules”. While the use of protective groups leads to higher yields of methanol derivatives, numerous challenges still exist on the path to industrial application. These range from corrosion due the strong acids used over catalyst stability in the presence of water or methanol to product purification.⁹⁶ Industrial implementation of methane to methanol is consequently still far away. However, the growing admission amongst researchers that yield is essential can be a basis for optimism.

1.10 Scope of this thesis

As could be seen in the previous sections, there is a wide variety of options available in theory to utilize methane as a chemical feedstock. However, most of these options are still in various stages of development. The growing importance of sustainability greatly increases the importance of implementing large-scale processes that allow for the further utilization of methane. In many of the above-mentioned processes the catalyst performance is still a critical stumbling block. Therefore, the aim of this thesis is to provide insight into parameters affecting catalyst activity. This is done for two different processes, separating the thesis into two parts.

The first of these processes is the dry reforming of methane. The two main issues encountered in this process are coke formation and catalyst sintering. Coke formation during dry reforming is the topic of discussion of **Chapter 2**. Using Ni/ZrO₂ as a model system, the most active coke-forming Ni sites are deactivated by promoters. While this mechanism is well-known, the exact impact on the carbon structure has not been investigated before. Therefore, K, Cs, Na and Mn are compared as promoters, with the latter being used as a reference to judge the impact of alkali-catalyzed carbon gasification on the coke content. This comparison shows, that in contrast to the superior performance of Cs and K in coal gasification, only Cs and Na show additional gasification activity during dry reforming. The latter is explained by the superior interactions of Na₂O with the ZrO₂ support. Additionally, ¹³C-NMR shows that the alkali metals are more effective at suppressing the growth of carbon fibers than Mn.

In **Chapter 3** the focus shifts to a specific subcategory of catalyst sintering, namely sintering during catalyst passivation. Literature has highlighted, that passivation of supported Ni catalysts, especially Ni/Al₂O₃ systems, can quickly induce sintering of the Ni particles. However, these studies are typically done with sample sizes of several 100 mg or even on a scale of several grams. In this chapter, the impact of passivation is instead measured by testing the catalytic activity in the dry reforming of methane, keeping the overall scale below 30 mg. This is possible, since larger Ni particles are known to form more carbon and less Ni surface should also reduce the overall activity. The comparison of four Ni/Al₂O₃ samples with different Ni-loadings shows, that even on this scale Ni sintering very quickly sets in, especially for higher Ni loadings.

Building on the results of the previous two chapters, the effect of promoters on catalyst regeneration is studied in **Chapter 4**. The effect of the three promoter metals Cr, Mn and Fe on Ni/Al₂O₃ catalysts is investigated, using two different regeneration protocols. Firstly, the samples are exposed to diluted flows of CO₂ and of H₂ for 30 minutes each. While this redox cycle is shown to restore the initial catalytic activity, the coke content does increase substantially. Secondly, the catalysts are exposed to a flow of diluted CO₂ for only a few minutes. In this case, the effectivity of the regeneration procedure depends greatly on the

promoter in question. For promoters that cause enhanced interaction with CO₂, noticeable deactivation can already be noticed after this regeneration protocol.

Chapter 5 deals with the direct gas-phase oxidation of methane to methanol. The focus of this chapter is Metal-Organic Frameworks. MOF synthesis allows for a wide range of options to modify the final framework structure. This in turn would allow the close study of the influence of several parameters on the catalytic activity. The work on bimetallic frameworks presented in this chapter highlights the considerable risk of false positive detection of catalytic activity within MOFs. All tested samples lead to the detection of methanol under reaction conditions. The data imply that this is due to impurities of methanol present during the syntheses, the remainders of which can only be removed with a great deal of effort. To ensure clean data, any synthesis would then require the exclusive use of solvents completely free of methanol traces. These considerations greatly limit the applicability of MOFs.

Note that the chapters 1-4 have been written as individual publications and can be read separately. Therefore, they may overlap to a minor degree.

1.11 References

1. R. Horn and R. Schlögl, *Catal. Lett.*, 2015, **145**, 23-39.
2. BP Statistical Review of World Energy, 68th Edition, <https://www.bp.com/content/dam/bp/business-sites/en/global/corporate/pdfs/energy-economics/statistical-review/bp-stats-review-2019-natural-gas.pdf>, (accessed May 4th, 2020).
3. S. Rasi, A. Veijanen and J. Rintala, *Energy*, 2007, **32**, 1375-1380.
4. H. Rodhe, *Science*, 1990, **248**, 1217-1219.
5. IEA, Tracking Fuel Supply, <https://www.iea.org/data-and-statistics/charts/sources-of-greenhouse-gas-emissions-from-oil-and-gas-operations-in-2017>, (accessed May 4, 2020).
6. J. R. Rostrup-Nielsen, in *Handbook of Heterogeneous Catalysis*, eds. G. Ertl, H. Knözinger, F. Schüth and J. Weitkamp, 2008, DOI: 10.1002/9783527610044.hetcat0146, pp. 2882-2905.
7. J. Rostrup-Nielsen, in *Stud. Surf. Sci. Catal.*, eds. X. Bao and Y. Xu, Elsevier, 2004, vol. 147, pp. 121-126.

8. C. Murkin and J. Brightling, *Johnson Matthey Technology Review*, 2016, **60**, 263-269.
9. S. P. S. Andrew, *Product R&D*, 1969, **8**, 321-324.
10. J. R. Rostrup-Nielsen, T. S. Christensen and I. Dybkjaer, in *Stud. Surf. Sci. Catal.*, eds. T. S. R. P. Rao and G. M. Dhar, Elsevier, 1998, vol. 113, pp. 81-95.
11. J. R. Rostrup-Nielsen, J. Sehested and J. K. Nørskov, in *Adv. Catal.*, Academic Press, 2002, vol. 47, pp. 65-139.
12. C. Hammond, S. Conrad and I. Hermans, *ChemSusChem*, 2012, **5**, 1668-1686.
13. A. Holmen, *Catal. Today*, 2009, **142**, 2-8.
14. *Nitrogen + Syngas*, 2012, 38.
15. J. R. Rostrup-Nielsen and J. B. Hansen, in *Fuel Cells: Technologies for Fuel Processing*, eds. D. Shekhawat, J. J. Spivey and D. A. Berry, Elsevier, Amsterdam, 2011, DOI: <https://doi.org/10.1016/B978-0-444-53563-4.10004-5>, pp. 49-71.
16. J. A. Moulijn, A. E. van Diepen and F. Kapteijn, in *Handbook of Heterogeneous Catalysis*, eds. G. Ertl, H. Knözinger, F. Schüth and J. Weitkamp, 2008, DOI: 10.1002/9783527610044.hetc0098, pp. 1829-1845.
17. M. D. Argyle and C. H. Bartholomew, *Catalysts*, 2015, **5**, 145-269.
18. A. Iulianelli, S. Liguori, J. Wilcox and A. Basile, *Catal Rev*, 2016, **58**, 1-35.
19. C. H. Bartholomew, *Appl. Catal., A*, 2001, **212**, 17-60.
20. C. Wang, N. Sun, N. Zhao, W. Wei, J. Zhang, T. Zhao, Y. Sun, C. Sun, H. Liu and C. E. Snape, *ChemCatChem*, 2014, **6**, 640-648.
21. R. Franz, T. Kuhlewind, G. Shterk, E. Abou-Hamad, A. Parastaev, E. Uslamin, E. J. M. Hensen, F. Kapteijn, J. Gascon and E. A. Pidko, *Catal. Sci. Tech.*, 2020, **10**, 3965-3974.
22. J. R. Rostrup-Nielsen, *Catal. Today*, 1997, **37**, 225-232.
23. H. S. Bengaard, J. K. Nørskov, J. Sehested, B. S. Clausen, L. P. Nielsen, A. M. Molenbroek and J. R. Rostrup-Nielsen, *J. Catal.*, 2002, **209**, 365-384.
24. C. Vogt, J. Kranenborg, M. Monai and B. M. Weckhuysen, *ACS Catal.*, 2020, **10**, 1428-1438.
25. J. R. Rostrup-Nielsen, *J. Catal.*, 1984, **85**, 31-43.
26. C. H. Bartholomew, P. K. Agrawal and J. R. Katzer, in *Adv. Catal.*, eds. D. D. Eley, H. Pines and P. B. Weisz, Academic Press, 1982, vol. 31, pp. 135-242.
27. T. Roussière, PhD thesis, Karlsruhe Institute of Technology, 2013.
28. D. L. Trimm, in *Stud. Surf. Sci. Catal.*, eds. C. H. Bartholomew and J. B. Butt, Elsevier, 1991, vol. 68, pp. 29-51.
29. J. A. Moulijn, A. E. van Diepen and F. Kapteijn, *Appl. Catal., A*, 2001, **212**, 3-16.
30. O. Deutschmann, H. Knözinger, K. Kochloefl and T. Turek, in *Ullmann's Encyclopedia of Industrial Chemistry*, DOI: 10.1002/14356007.o05_o02.

31. J. Hagen, *Industrial Catalysis : A Practical Approach*, John Wiley & Sons, Incorporated, Berlin, GERMANY, 2015.
32. M. F. Peintinger, M. J. Kratz and T. Bredow, *J. Mater. Chem. A*, 2014, **2**, 13143-13158.
33. K. Wefers and C. Misra, *Oxides and Hydroxides of Aluminium Alcoa Technical Paper N°19*, Aluminium Company of America Pittsburgh, PA, 1987.
34. New steam reforming catalyst from Haldor Topsoe, <https://blog.topsoe.com/2013/09/new-steam-reforming-catalyst-haldor-topsoe>).
35. M. R. Almind, S. B. Vendelbo, M. F. Hansen, M. G. Vinum, C. Frandsen, P. M. Mortensen and J. S. Engbæk, *Catal. Today*, 2020, **342**, 13-20.
36. S. Hamzehlouia, S. A. Jaffer and J. Chaouki, *Sci. Rep.*, 2018, **8**, 8940.
37. P. M. Mortensen, J. S. Engbæk, S. B. Vendelbo, M. F. Hansen and M. Østberg, *Ind. Eng. Chem. Res.*, 2017, **56**, 14006-14013.
38. Technologies that do more with less, <https://www.linde-engineering.com/en/about-linde-engineering/success-stories/technologies-more-with-less.html>, (accessed Nov. 19, 2019).
39. N. A. K. Aramouni, J. G. Touma, B. A. Tarboush, J. Zeaiter and M. N. Ahmad, *Renew. Sustain. Energy Rev.*, 2018, **82**, 2570-2585.
40. S. Arora and R. Prasad, *RCS Adv.*, 2016, **6**, 108668-108688.
41. I. Vollmer, I. Yarulina, F. Kapteijn and J. Gascon, *ChemCatChem*, 2019, **11**, 39-52.
42. J. J. Spivey and G. Hutchings, *Chem. Soc. Rev.*, 2014, **43**, 792-803.
43. P. L. Tan, C. T. Au and S. Y. Lai, *Catal. Lett.*, 2006, **112**, 239-245.
44. B. M. Weckhuysen, D. Wang, M. P. Rosynek and J. H. Lunsford, *J. Catal.*, 1998, **175**, 347-351.
45. P. Schwach, X. Pan and X. Bao, *Chem. Rev.*, 2017, **117**, 8497-8520.
46. K. S. Wong, J. W. Thybaut, E. Tangstad, M. W. Stöcker and G. B. Marin, *Microporous Mesoporous Mater.*, 2012, **164**, 302-312.
47. L. Y. Chen, L. W. Lin, Z. S. Xu, X. S. Li and T. Zhang, *J. Catal.*, 1995, **157**, 190-200.
48. N. Kosinov, A. S. G. Wijkema, E. Uslamin, R. Rohling, F. J. A. G. Coumans, B. Mezari, A. Parastayev, A. S. Poryvaev, M. V. Fedin, E. A. Pidko and E. J. M. Hensen, *Angew. Chem. Int. Ed.*, 2018, **57**, 1016-1020.
49. R. Ohnishi, S. Liu, Q. Dong, L. Wang and M. Ichikawa, *J. Catal.*, 1999, **182**, 92-103.
50. C. H. L. Tempelman and E. J. M. Hensen, *Appl. Catal. B*, 2015, **176-177**, 731-739.
51. M. T. Portilla, F. J. Llopis and C. Martínez, *Catal. Sci. Tech.*, 2015, **5**, 3806-3821.

52. N. Kosinov, F. J. A. G. Coumans, E. Uslamin, F. Kapteijn and E. J. M. Hensen, *Angew. Chem. Int. Ed.*, 2016, **55**, 15086-15090.
53. Y. Xu, J. Lu, J. Wang, Y. Suzuki and Z.-G. Zhang, *Chem. Eng. J.*, 2011, **168**, 390-402.
54. M. P. Gimeno, J. Soler, J. Herguido and M. Menéndez, *Ind. Eng. Chem. Res.*, 2010, **49**, 996-1000.
55. S. H. Morejudo, R. Zanón, S. Escolástico, I. Yuste-Tirados, H. Malerød-Fjeld, P. K. Vestre, W. G. Coors, A. Martínez, T. Norby, J. M. Serra and C. Kjøseth, *Science*, 2016, **353**, 563-566.
56. S. Natesakhawat, N. C. Means, B. H. Howard, M. Smith, V. Abdelsayed, J. P. Baltrus, Y. Cheng, J. W. Lekse, D. Link and B. D. Morreale, *Catal. Sci. Tech.*, 2015, **5**, 5023-5036.
57. X. Guo, G. Fang, G. Li, H. Ma, H. Fan, L. Yu, C. Ma, X. Wu, D. Deng, M. Wei, D. Tan, R. Si, S. Zhang, J. Li, L. Sun, Z. Tang, X. Pan and X. Bao, *Science*, 2014, **344**, 616-619.
58. M. Sakbodin, Y. Wu, S. C. Oh, E. D. Wachsman and D. Liu, *Angew. Chem. Int. Ed.*, 2016, **55**, 16149-16152.
59. S. C. Oh, E. Schulman, J. Zhang, J. Fan, Y. Pan, J. Meng and D. Liu, *Angew. Chem. Int. Ed.*, 2019, **58**, 7083-7086.
60. K. Liu, C. Song and V. Subramani, *Hydrogen and Syngas Production and Purification Technologies*, American Institute of Chemical Engineers, Hoboken, UNITED STATES, 2010.
61. R. Reimert, F. Marschner, H.-J. Renner, W. Boll, E. Supp, M. Brejc, W. Liebner and G. Schaub, in *Ullmann's Encyclopedia of Industrial Chemistry*, Wiley-VCH Verlag GmbH & Co. KGaA, 2011, DOI: 10.1002/14356007.o12_o01.
62. A. P. E. York, T. Xiao and M. L. H. Green, *Top. Catal.*, 2003, **22**, 345-358.
63. R. Schwiedernoch, S. Tischer, C. Correa and O. Deutschmann, *Chem. Eng. Sci.*, 2003, **58**, 633-642.
64. H. T. S/A, SynCOR™ - Autothermal Reformer (ATR), <https://www.topsoe.com/products/equipment/syncortm-autothermal-reformer-atr>, (accessed Mar. 19, 2020).
65. T. Giroux, S. Hwang, Y. Liu, W. Ruettinger and L. Shore, *Appl. Catal. B*, 2005, **56**, 95-110.
66. V. Palma, A. Ricca and P. Ciambelli, *Chem. Eng. J.*, 2012, **207-208**, 577-586.
67. W. Hinsen and M. Baerns, *Chem.-Ztg.*, 1983, **107**, 223-226.
68. G. E. Keller and M. M. Bhasin, *J. Catal.*, 1982, **73**, 9-19.
69. U. Zavyalova, M. Holena, R. Schlögl and M. Baerns, *ChemCatChem*, 2011, **3**, 1935-1947.
70. L. Hu, D. Pinto and A. Urakawa, in *Catalysis: Volume 32*, The Royal Society of Chemistry, 2020, vol. 32, pp. 203-223.

71. E. V. Kondratenko and M. Baerns, in *Handbook of Heterogeneous Catalysis*, 2008, DOI: 10.1002/9783527610044.hetcat0152, pp. 3010-3023.
72. US Patent 4443644, 1984.
73. A. I. Bostan, Y. I. Pyatnitskii, L. N. Raevskaya, V. G. Pryanikova, S. A. Nedil'ko, A. G. Dzyaz'ko and E. G. Zen'kovich, *Theor. Exp. Chem.*, 2005, **41**, 32-36.
74. T. Ito, J. Wang, C. H. Lin and J. H. Lunsford, *J. Am. Chem. Soc.*, 1985, **107**, 5062-5068.
75. C. T. Au, X. P. Zhou, Y. W. Liu, W. J. Ji and C. F. Ng, *J. Catal.*, 1998, **174**, 153-163.
76. K.-i. Machida and M. Enyo, *J. Chem. Soc., Chem. Commun.*, 1987, DOI: 10.1039/C39870001639, 1639-1640.
77. 2013.
78. A. Galadima and O. Muraza, *Journal of Industrial and Engineering Chemistry*, 2016, **37**, 1-13.
79. C. Joe, Saudi Aramco Taps Silicon Valley Startup in Plastics Push, <https://www.bloomberg.com/news/articles/2018-06-13/saudi-aramco-taps-silicon-valley-startup-in-oil-to-plastics-push>, (accessed Dec. 4, 2019).
80. US3894107A, 1973.
81. C. E. Taylor, R. P. Noceti and R. R. Schehl, in *Stud. Surf. Sci. Catal.*, eds. D. M. Bibby, C. D. Chang, R. F. Howe and S. Yurchak, Elsevier, 1988, vol. 36, pp. 483-489.
82. S. Svelle, S. Aravinthan, M. Bjørgen, K.-P. Lillerud, S. Kolboe, I. M. Dahl and U. Olsbye, *J. Catal.*, 2006, **241**, 243-254.
83. M. H. Nilsen, S. Svelle, S. Aravinthan and U. Olsbye, *Appl. Catal., A*, 2009, **367**, 23-31.
84. V. Paunović, R. Lin, M. Scharfe, A. P. Amrute, S. Mitchell, R. Hauert and J. Pérez-Ramírez, *Angew. Chem. Int. Ed.*, 2017, **56**, 9791-9795.
85. V. Paunović, G. Zichittella, M. Moser, A. P. Amrute and J. Pérez-Ramírez, *Nature Chem.*, 2016, **8**, 803-809.
86. J. P. Lange and P. J. A. Tijm, *Chem. Eng. Sci.*, 1996, **51**, 2379-2387.
87. H. D. Gesser, N. R. Hunter and C. B. Prakash, *Chem. Rev.*, 1985, **85**, 235-244.
88. G. A. Foulds and B. F. Gray, *Fuel Process. Technol.*, 1995, **42**, 129-150.
89. W. Feng, F. C. Knopf and K. M. Dooley, *Energy Fuels*, 1994, **8**, 815-822.
90. A. I. Olivos-Suarez, Á. Szécsényi, E. J. M. Hensen, J. Ruiz-Martinez, E. A. Pidko and J. Gascon, *ACS Catal.*, 2016, **6**, 2965-2981.
91. Y. Barbaux, A. R. Elamrani, E. Payen, L. Gengembre, J. P. Bonnelle and B. Grzybowska, *Appl. Catal.*, 1988, **44**, 117-132.
92. J. A. Barbero, M. C. Alvarez, M. A. Bañares, M. A. Peña and J. L. G. Fierro, *Chem. Commun.*, 2002, DOI: 10.1039/B202812N, 1184-1185.

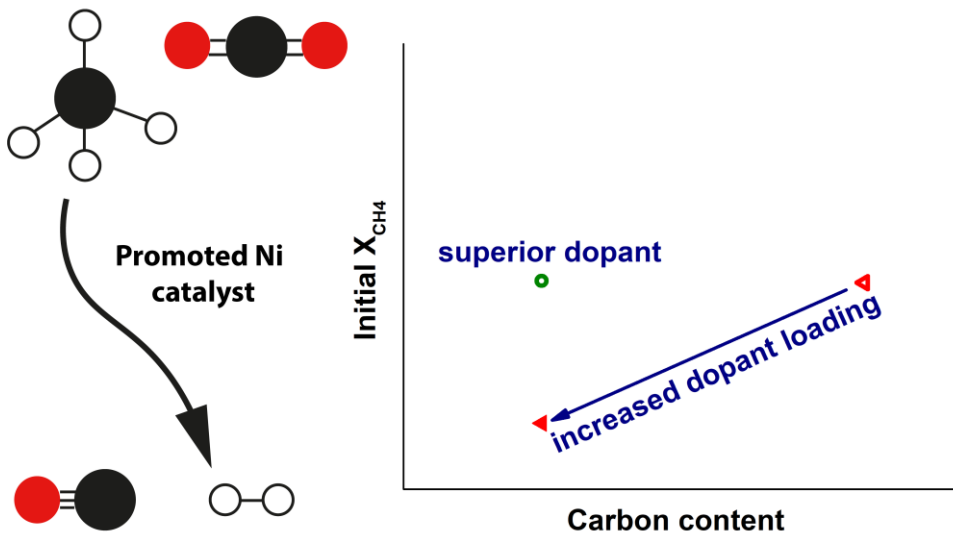
93. S. Y. Chen and D. Willcox, *Ind. Eng. Chem. Res.*, 1993, **32**, 584-587.
94. N. D. Spencer, *J. Catal.*, 1988, **109**, 187-197.
95. N. D. Spencer and C. J. Pereira, *J. Catal.*, 1989, **116**, 399-406.
96. M. Ravi, M. Ranocchiari and J. A. van Bokhoven, *Angew. Chem. Int. Ed.*, 2017, **56**, 16464-16483.
97. S. Friedle, E. Reisner and S. J. Lippard, *Chem. Soc. Rev.*, 2010, **39**, 2768-2779.
98. S. K. Lee, B. G. Fox, W. A. Froland, J. D. Lipscomb and E. Munck, *J. Am. Chem. Soc.*, 1993, **115**, 6450-6451.
99. A. A. Shteinman, *FEBS Lett.*, 1995, **362**, 5-9.
100. L. Cao, O. Caldararu, A. C. Rosenzweig and U. Ryde, *Angew. Chem. Int. Ed.*, 2018, **57**, 162-166.
101. K. T. Dinh, M. M. Sullivan, K. Narsimhan, P. Serna, R. J. Meyer, M. Dincă and Y. Román-Leshkov, *J. Am. Chem. Soc.*, 2019, **141**, 11641-11650.
102. M. H. Grootaert, P. J. Smeets, B. F. Sels, P. A. Jacobs and R. A. Schoonheydt, *J. Am. Chem. Soc.*, 2005, **127**, 1394-1395.
103. S. Grundner, W. Luo, M. Sanchez-Sanchez and J. A. Lercher, *Chem. Commun.*, 2016, **52**, 2553-2556.
104. G. Li, P. Vassilev, M. Sanchez-Sanchez, J. A. Lercher, E. J. M. Hensen and E. A. Pidko, *J. Catal.*, 2016, **338**, 305-312.
105. K. Narsimhan, K. Iyoki, K. Dinh and Y. Román-Leshkov, *ACS Cent. Sci.*, 2016, **2**, 424-429.
106. P. Tomkins, A. Mansouri, S. E. Bozbag, F. Krumeich, M. B. Park, E. M. C. Alayon, M. Ranocchiari and J. A. van Bokhoven, *Angew. Chem. Int. Ed.*, 2016, **55**, 5467-5471.
107. K. A. Dubkov, N. S. Ovanesyan, A. A. Shteinman, E. V. Starokon and G. I. Panov, *J. Catal.*, 2002, **207**, 341-352.
108. C. Hammond, N. Dimitratos, J. A. Lopez-Sanchez, R. L. Jenkins, G. Whiting, S. A. Kondrat, M. H. ab Rahim, M. M. Forde, A. Thetford, H. Hagen, E. E. Stangland, J. M. Moulijn, S. H. Taylor, D. J. Willock and G. J. Hutchings, *ACS Catal.*, 2013, **3**, 1835-1844.
109. E. V. Kondratenko and J. Pérez-Ramírez, *Catal. Today*, 2007, **119**, 243-246.
110. N. S. Ovanesyan, K. A. Dubkov, A. A. Pyalling and A. A. Shteinman, *J. Radioanal. Nucl. Chem.*, 2000, **246**, 149-152.
111. V. I. Sobolev, K. A. Dubkov, O. V. Panna and G. I. Panov, *Catal. Today*, 1995, **24**, 251-252.
112. J. Shan, W. Huang, L. Nguyen, Y. Yu, S. Zhang, Y. Li, A. I. Frenkel and F. Tao, *Langmuir*, 2014, **30**, 8558-8569.
113. N. V. Beznis, A. N. C. van Laak, B. M. Weckhuysen and J. H. Bitter, *Microporous Mesoporous Mater.*, 2011, **138**, 176-183.

114. N. V. Beznis, B. M. Weckhuysen and J. H. Bitter, *Catal. Lett.*, 2010, **136**, 52-56.
115. M. C. Kung, S. S.-Y. Lin and H. H. Kung, *Top. Catal.*, 2012, **55**, 108-115.
116. J. Baek, B. Rungtaweevoranit, X. Pei, M. Park, S. C. Fakra, Y.-S. Liu, R. Matheu, S. A. Alshimri, S. Alshehri, C. A. Trickett, G. A. Somorjai and O. M. Yaghi, *J. Am. Chem. Soc.*, 2018, **140**, 18208-18216.
117. T. Ikuno, J. Zheng, A. Vjunov, M. Sanchez-Sanchez, M. A. Ortuño, D. R. Pahls, J. L. Fulton, D. M. Camaioni, Z. Li, D. Ray, B. L. Mehdi, N. D. Browning, O. K. Farha, J. T. Hupp, C. J. Cramer, L. Gagliardi and J. A. Lercher, *J. Am. Chem. Soc.*, 2017, **139**, 10294-10301.
118. D. Osadchii, A. I. Olivos Suarez, Á. Szécsényi, G. Li, M. A. Nasalevich, A. I. Dugulan, P. Serra-Crespo, E. J. M. Hensen, S. L. Veber, M. V. Fedin, G. Sankar, E. A. Pidko and J. Gascon, *ACS Catal.*, 2018, DOI: 10.1021/acscatal.8b00505.
119. J. Zheng, J. Ye, M. A. Ortuño, J. L. Fulton, O. Y. Gutiérrez, D. M. Camaioni, R. K. Motkuri, Z. Li, T. E. Webber, B. L. Mehdi, N. D. Browning, R. L. Penn, O. K. Farha, J. T. Hupp, D. G. Truhlar, C. J. Cramer and J. A. Lercher, *J. Am. Chem. Soc.*, 2019, **141**, 9292-9304.
120. P. Tomkins, M. Ranocchiari and J. A. van Bokhoven, *Acc. Chem. Res.*, 2017, **50**, 418-425.
121. S. Grundner, M. A. C. Markovits, G. Li, M. Tromp, E. A. Pidko, E. J. M. Hensen, A. Jentys, M. Sanchez-Sanchez and J. A. Lercher, 2015, **6**, 7546.
122. M. J. Wulfers, S. Teketel, B. Ipek and R. F. Lobo, *Chem. Commun.*, 2015, **51**, 4447-4450.
123. M. A. C. Markovits, A. Jentys, M. Tromp, M. Sanchez-Sanchez and J. A. Lercher, *Top. Catal.*, 2016, **59**, 1554-1563.
124. B. Ipek and R. F. Lobo, *Chem. Commun.*, 2016, **52**, 13401-13404.
125. M. V. Parfenov, E. V. Starokon, L. V. Pirutko and G. I. Panov, *J. Catal.*, 2014, **318**, 14-21.
126. K. T. Dinh, M. M. Sullivan, P. Serna, R. J. Meyer, M. Dincă and Y. Román-Leshkov, *ACS Catal.*, 2018, **8**, 8306-8313.
127. S. J. Lee, M. S. McCormick, S. J. Lippard and U.-S. Cho, *Nature*, 2013, **494**, 380-384.
128. A. E. Shilov and G. B. Shul'pin, *Russ. Chem. Rev.*, 1987, **56**, 442-464.
129. R. A. Periana, D. J. Taube, S. Gamble, H. Taube, T. Satoh and H. Fujii, *Science*, 1998, **280**, 560-564.
130. M. Ahlquist, R. J. Nielsen, R. A. Periana and W. A. Goddard Iii, *J. Am. Chem. Soc.*, 2009, **131**, 17110-17115.
131. M. N. Vargaftik, I. P. Stolarov and I. I. Moiseev, *J. Chem. Soc., Chem. Commun.*, 1990, DOI: 10.1039/C39900001049, 1049-1050.
132. L. C. Kao, A. C. Hutson and A. Sen, *J. Am. Chem. Soc.*, 1991, **113**, 700-701.

133. M. Ravi, V. L. Sushkevich, A. J. Knorpp, M. A. Newton, D. Palagin, A. B. Pinar, M. Ranocchiari and J. A. van Bokhoven, *Nat. Catal.*, 2019, **2**, 485-494.
134. A. V. Bavykina, A. I. Olivos-Suarez, D. Osadchii, R. Valecha, R. Franz, M. Makkee, F. Kapteijn and J. Gascon, *ACS Appl. Mater. Interfaces*, 2017, **9**, 26060-26065.
135. R. Palkovits, M. Antonietti, P. Kuhn, A. Thomas and F. Schüth, *Angew. Chem. Int. Ed.*, 2009, **48**, 6909-6912.

Chapter 2

Impact of small promoter amounts on coke structure in dry reforming of methane over Ni/ZrO₂



Coke deposition is one of the main challenges in the commercialization of dry reforming of methane over supported Ni catalysts. Besides the coke quantity, the structure of the deposits is also essential for the catalyst lifetime. Accordingly, in this study, we analyzed the effect of Na, K, and Cs promoters on both these variables over Ni/ZrO₂ catalysts. Besides blocking the most active coke-forming sites already at low loading, the promoting effect of the alkali metals is also contributed to by their coke gasification activity. To evaluate the additional impact of the latter, the behavior of alkali-doped catalysts was compared to that for Mn-doped catalysts, exclusively featuring the site-blocking promotion mechanism. While the conversion is barely affected by the type of promoter, it has a profound effect on the amount and the composition of carbon deposits formed during the reaction. Promoting with K or Mn reduces the coke content to a similar degree but with less carbon fibers observed in the case of K. The promotion by Cs and Na results in the lowest coke content. The superior performance of Cs and Na-doped Ni/ZrO₂ catalysts is attributed to the enhanced coke gasification via carbonate species on top of the site blocking effects.

This chapter is based on the following publication:

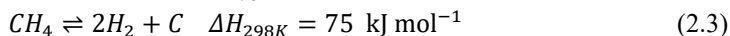
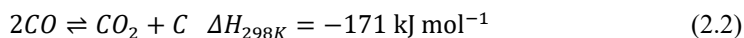
R. Franz, T. Kuhlewind, G. Shterk, E. Abou-Hamad, A. Parastayev, E. Uslamin, E. J. M. Hensen, F. Kapteijn, J. Gascon and E. A. Pidko, *Catal. Sci. Tech.*, 2020, **10**, 3965-3974.

2.1 Introduction

Current prognoses for worldwide energy consumption predict an increase in global CO₂ emissions for all except the most optimistic scenarios. At the same time, the demand for various chemical products, especially plastics, will keep increasing and thereby also the consumption of fossil fuels.¹ Recycling CO₂ as a raw material for the chemical industry would lead to a reduction of CO₂ emissions and at the same time help to meet growing customer demands. The so-called dry reforming of methane (2.1), in which carbon dioxide and methane react to synthesis gas or syngas at elevated temperatures, is a potential route to achieve this.



The extensive experience of the (petro)chemical industry with the related process of methane steam reforming is a considerable advantage of dry reforming. However, one of the significant drawbacks of this process over steam reforming is the more extensive carbon formation, causing rapid deactivation of the catalyst during operation.² The main coking reactions are the Boudouard reaction (2.2) and methane decomposition (2.3):



The comparison of thermodynamic equilibrium constants for the target dry reforming and the undesirable side-reactions shown in Figure 2.1 highlights the fundamental challenges of this process, especially when aiming for large-scale industrial application. Ideally, the reaction temperature should be low to reduce energy consumption and thus costs. High-pressure operation would also be economically preferable to a compression of the more voluminous syngas for use in syntheses at elevated pressure (e.g., Fischer-Tropsch (FT)⁴ or methanol⁵ syntheses).⁶ At low temperature and high pressure, the side-reactions producing coke are thermodynamically most favorable, however (Figure 2.1). According to thermodynamics, high temperature and low pressure operation is desired, if coke formation is to be minimized. A compromise of high temperature and pressure would lead to additional issues. Under such conditions, gas-phase reactions start becoming relevant, which also lead to coke formation.⁷

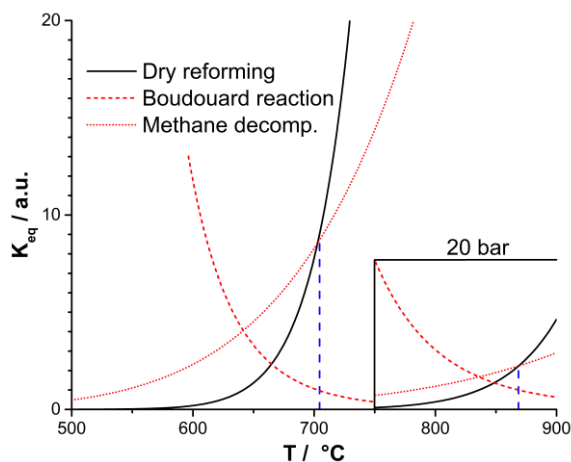


Figure 2.1: Equilibrium constants of the dry reforming and the two main coking reactions as a function of temperature at 1 bar and 20 bar (insert); calculated using ASPEN V8.8, amended from³.

Coke formation appears, therefore, inevitable under practical conditions, which implies that a successful dry reforming catalyst should be highly resistant to coking.⁸ To develop a coke-resistant catalyst, both support and active phase need to be optimized. Precious metals such as Ru exhibit good performance but are scarce and expensive, shifting the research focus to alternative catalyst formulations based on earth-abundant *3d* transition metals.⁹ Amongst these, nickel is the most studied element due to its wide availability and high catalytic activity in dry reforming.¹⁰⁻¹² The downside of nickel is its considerable susceptibility to coking. Depending on the reaction temperature, Ni catalysts can promote the formation of various types of coke, such as surface graphite, graphene as well as carbon fibers.¹³⁻¹⁵ The latter represent the most critical challenge as the growth of carbon fibers in the course of the catalytic process breaks catalyst particles and results in reactor plugging.⁹

A popular approach to improve the coke resistance of Ni-based dry reforming catalysts is to deactivate the highly reactive sites on the surface by promoter addition. This approach has been earlier investigated in detail for various support-promoter combinations.¹⁶⁻²⁰ A representative example is the Sulphur PAssivated ReforminG (SPARG) process developed by Haldor Topsøe, in which the feed contains a controlled amount of H₂S poison.²¹ The H₂S chemisorbs on the Ni catalyst, deactivating the most active sites, which are also responsible for most of the coke formation. As a result, the catalyst operates with reduced activity but in a much more stable fashion over extended periods of time.²²

Single-crystal studies of methane decomposition on Ni have shown that a similar effect is achieved with Au and K.^{23, 24} Step sites on Ni clusters are the most active sites for coke formation and all above-mentioned promoters preferentially occupy these sites.²⁵ Site blocking with alkaline and earth-alkaline oxides has already been investigated.^{18-20, 26, 27.}

Other additives such as Mn or Sn are also reported to reduce coking by blocking the Ni surface.^{28, 29} For the earth-alkaline metals and manganese a caveat must be added. Besides blocking the Ni surface, these promoters are also assumed to increase the CO₂ affinity of the catalyst, additionally reducing the coking. Although the site-sensitivity of the Boudouard reaction has been studied less extensively, the literature points to similar trends as for methane decomposition for this process with a higher reactivity of the step-edge sites.³⁰ Furthermore, it has been proposed that promoter ions may also affect the electronic structure of the neighboring Ni centers, reducing their activity towards dissociative methane chemisorption.²³ At the same time, alkali addition can enhance Ni sintering in select cases, meaning that a fine balance must be struck during synthesis.³¹⁻³⁴

However, a detailed quantitative analysis of the effect on the coke structure of several different promoters operating through a similar mechanism has not been reported until now. Even small decreases in coking activity can have a significant cumulative effect over the runtime of several years for an industrial reforming catalyst. Consequently, the alkali elements Na, K and Cs were selected as the first batch of promoters. Potassium has been one of the prime examples of this site-blocking behavior. Other alkali metals should thus represent a rather moderate change of promoter characteristics, allowing to probe the electronic effects mentioned previously.²³ Amongst metal oxides, MnO_x has been reported as a promoter in dry reforming literature.^{29, 35} As mentioned above, at high loadings of manganese, an increased CO₂-affinity of the catalyst is noticeable. For low loadings, the physical blocking of Ni sites dominates. This apparent similarity in function made MnO_x an interesting comparison. MnO_x is typically reported to have little to no activity in the gasification of carbon.^{36, 37} In contrast, alkali metals are well-known for their activity in carbon gasification.^{38, 39} Thus, manganese as the fourth promoter should also clarify, if this reaction contributes to the reduced coke content. All samples were supported on ZrO₂ since it is less prone to forming mixed phases with Ni or the promoters, as is the case for Al₂O₃ or SiO₂ (e.g. refs. 31, 40). To avoid possible interference of additional species, pure ZrO₂ without any stabilizing additives was used. Additives such as CaO would be necessary to stabilize cubic ZrO₂,⁴¹ which has been reported to be the superior ZrO₂ phase for use as a catalyst support.⁴² In contrast to other supports ZrO₂-based catalysts also tend to form more coke, which is desirable in the analysis of the impact of the promoters on the coke structure.^{43, 44}

2.2 Experimental

2.2.1 Chemicals

Ethylenediaminetetraacetic acid (EDTA, Thermo Fisher 99%), NH_3 solution (VWR, 25%), ZrO_2 (Alfa Aesar, 51 m^2/g), $\text{Ni}(\text{NO}_3)_2 \cdot 6\text{H}_2\text{O}$ (Merck, analysis quality), KNO_3 (Acros, 99%+), NaNO_3 (Riedel-De Haen, 99.5%), CsNO_3 (Alfa Aesar 99.5%), $\text{Mn}(\text{NO}_3)_2 \cdot 4\text{H}_2\text{O}$ (Thermo Fisher, analysis quality).

All materials were used without further modification except for NH_3 (aq), which was diluted with demineralized water in a volumetric ratio of 1:1 before usage, and ZrO_2 . ZrO_2 extrudates were ground to a fine powder before impregnation.

2.2.2 Catalyst synthesis

All catalysts were synthesized via incipient wetness impregnation on commercial ZrO_2 support. A solution of the required concentration was prepared in the following fashion: In a first step EDTA was dissolved in a solution of 12.5% NH_3 . Afterwards, the required amount of $\text{Ni}(\text{NO}_3)_2$ and either KNO_3 , NaNO_3 , CsNO_3 or $\text{Mn}(\text{NO}_3)_2$ were added to the solution. After the dissolution of all components, the required amount of liquid (0.4 mL g^{-1}) was impregnated onto the dry ZrO_2 powder. This was followed by thorough mixing, drying for 5 h at $80 \text{ }^\circ\text{C}$ and then calcination at $700 \text{ }^\circ\text{C}$ for 5 h (heating rate of $10 \text{ }^\circ\text{C min}^{-1}$). For all samples the loading of Ni was set at $0.02 \text{ g}_{\text{Ni}} \text{ g}_{\text{Support}}^{-1}$. The amount of the promoter was calculated to achieve molar ratios of promoter: Ni = 1:10 or 1:5. In all syntheses a ratio of EDTA: Ni = 1 was maintained. An overview of the different catalysts is given in Table 2.1.

Table 2.1: Overview of the tested catalysts

Promoter metal	Molar ratio promoter/Ni	Abbreviation
--	--	REF
K	1/10	1K
K	2/10	2K
Cs	1/10	1Cs
Cs	2/10	2Cs
Na	1/10	1Na
Mn	1/10	1Mn

2.2.3 Catalyst characterization

Temperature programmed reduction (TPR) was carried out in a fixed-bed reactor system. 100 mg of freshly prepared sample was pelletized, crushed and sieved to a particle size of 212-355 μm and filled into a quartz reactor (I.D. 6 mm). The quartz reactor was placed into a furnace and a flow of 10% H₂/Ar (30 mL min⁻¹) started. The furnace was then heated from room temperature to 900 °C with a rate of 5 °C min⁻¹. At the outlet, the hydrogen signal was monitored with a thermal conductivity detector (TCD). Peak deconvolution of the TPR data was carried by the superposition of three Gaussian functions for each profile.

H₂-Chemisorption was measured on a Micromeritics ASAP 2020C. Approx. 130 mg of sample were loaded into the setup and reduced at 650 °C for 2 h in 20% H₂ in N₂, thus mimicking the reduction conditions of the reactivity tests. Afterwards the sample was cooled down to 30 °C, at which H₂ chemisorption was measured with a static-volumetric method.

Electron microscopy was carried out on different instruments. ADF-STEM analysis and EELS elemental mapping of the samples were carried out with an FEI Titan G² 80–300 kV electron microscope operated at 300 kV. For the TEM analysis of the coked samples, a Jeol JEM 1400 plus TEM was used. The high resolution images were obtained on a JEM3200-FSC.

1D ¹³C MAS NMR was measured using a known amount of sample filled into zirconia rotors and recorded on a Bruker AVANCE III spectrometer. The system operated at resonance frequencies of 600 MHz (¹H frequency), and a conventional double resonance 3.2 mm CPMAS probe was used. The spinning frequency was set to 10-15 kHz. NMR chemical shifts are reported with respect to TMS as the external reference. Spectra were recorded by a spin echo pulse sequence (pulse length 3.4 μs) with four-phase alternation synchronized with the spinning rate for the MAS experiments to delete all background signals from the probe. The interscan delay was set to 15 s to allow complete relaxation, and 5,000-30,000 scans were performed. An apodization function (exponential) corresponding to a line broadening of 80 Hz was applied prior to the Fourier transformation.

X-ray diffraction (XRD) measurements were carried out in a Bruker D8 Advance Diffractometer with monochromatic Co *K* α radiation ($\lambda=0.179026$ nm) at room temperature.

Raman spectra were obtained with a Renishaw Via Reflex confocal spectrometer using a 532 nm laser excitation. The laser power was set to 100% and the sample was irradiated for 10 s with 6 accumulations. The laser has a maximum power of 30 mW.

2.2.4 Reactivity tests

The system used for catalytic testing has been described in detail in previous publications.⁴⁵ In short, it consists of a parallel fixed-bed reactor system with six reactors (quartz tubes with 4 mm I.D.). The quartz tubes are inserted into steel tubes mounted within the furnace to provide for better heat conduction. For each experiment the reactors were filled in the following manner (top to bottom): quartz wool plug, a 15 cm SiC bed (212–425 μm), a thin quartz layer, the catalytic bed, a thin quartz wool layer, a 10 cm SiC bed, a quartz wool plug. For the standard catalytic experiments, the catalyst bed consisted of 30 mg of catalyst (212–355 μm) mixed with 70 mg of SiC (300–355 μm). These two components were mixed as described in literature to ensure proper distribution of the sample.⁴⁶ For a detailed coke content analysis, catalytic runs were carried out with a catalytic bed of 75 mg of undiluted catalyst (212–355 μm), to allow for a full recovery of coked catalyst without SiC contamination. In all experiments the correct placement of the catalytic bed within the isothermal zone of the reactor was ensured.

The catalytic setup allowed for premixing the reaction mixture in a separate mixing section upstream of the reactors. The custom mixture was then fed to each reactor individually through separate mass flow controllers (MFCs). Activity testing was carried out as follows. To reduce the catalysts, the reactors were heated under a flow of 40 mL min⁻¹ (20% H₂ in N₂) to 650 °C with a rate of 10 °C min⁻¹, followed by an isothermal period of 2 h. Next, the feed was switched to the reaction mixture. For the catalytic activity tests, the feed consisted of 20% CO₂, 20% CH₄ and 60% N₂. For the separate coking runs 50% CO₂ and 50% CH₄ were used. In both cases, the flow of gas per reactor was 80 mL min⁻¹, keeping the reactant to catalyst ratio identical between the two sets of experiments (32 L_{CH₄} g⁻¹ h⁻¹). All runs were carried out for a total of 12 hours. The coke content was determined with the aid of a TGA-MS (Mettler Toledo TGA/DSC1 connected to a Pfeiffer Vacuum OmniSTAR) by quantifying the CO₂ signal while heating the sample using synthetic air as an oxidant. Product analysis was carried out by a GC equipped with both an FID and a TCD. The TCD was used for the analysis of all gases (columns: 0.3 m Hayesep Q 80–100 mesh with back-flush, a Porabond Q of 25 m (length) \times 0.53 mm(I.D.) \times 10 μm (film thickness) and a molsieve 5A (15 m \times 0.53 mm \times 10 μm) with bypass option) with N₂ as the internal standard. The FID signal provided a quality check for the TCD signal.

2.3 Results and discussion

2.3.1 Catalyst characterization

In STEM analysis of the synthesized catalysts Ni particles smaller than 20 nm were detected in all samples, with a major fraction smaller than 10 nm, again for all samples. The low loading of Ni and the low number of detected particles (14 for Ni/ZrO₂ (REF) and the 1/10 Na-promoted sample (1Na), around 30 for all other samples) did not allow for a proper statistical analysis, especially when the possible variation of the particle size distribution (PSD) on the Ni/ZrO₂ system is considered. For example, *Charisiou et al.* report a PSD from 20 nm to 80 nm for an 8 wt.% Ni/ZrO₂ catalyst characterized via STEM-HAADF.⁴⁷ The different particles observed in STEM have irregular shapes, similar to previously published literature.⁴⁸ Previous studies revealed that the nature of the support and the synthesis method have a strong impact on the observed Ni particle shapes.^{49, 50} Another primary characterization tool for the Ni-PSD of Ni/ZrO₂ catalysts is H₂ chemisorption. While this method allows estimating an averaged diameter, the exact ZrO₂ morphology can also strongly impact the average Ni size.⁵¹ In contrast to frequent literature reports of successful H₂ chemisorption, no H₂ uptake at 30 °C was observed. It is possible for metal particles to be partially covered by the support after prolonged reduction at high temperatures, which significantly reduces H₂ uptake.⁵²⁻⁵⁴ *Steib et al.* have observed ZrO_x clusters on Ni particles in a Ni/ZrO₂ system.⁵⁵ Therefore, the chemisorption results can be seen as proof of a partial coverage of the Ni particles by the support. The low loading of Ni prevented its detection in the XRD measurements and thus the determination of the Ni particle size via line broadening. XRD established that in all cases ZrO₂ is present in the monoclinic phase.

Temperature-programmed reduction (TPR) has been used in the past to compare the particle size of supported Ni catalysts. Deconvolution of the TPR profiles leads to three peaks in all cases with the maxima at 350 °C, 456 °C and 510 °C for pure Ni/ZrO₂ (Figure 2.2 and Table A1). When considering the positions of peaks 1 and 3, no general statement can be made. The peak positions are shifted to higher or lower temperatures depending on the promoter with no visible systematic effect. Only the position of the intermediate peak 2 is shifted to lower temperatures for all promoted catalysts. 1Mn must be mentioned separately, since here the positions of peaks 2 and 3 shift more substantially than for the catalysts promoted with alkali metals.

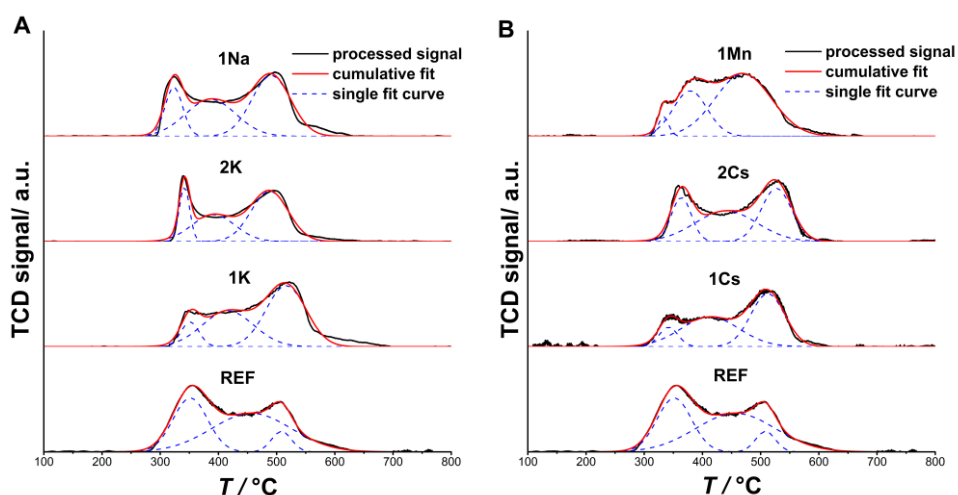


Figure 2.2: TPR curves with peak deconvolution for K-promoted and Na-promoted (A) and Cs-promoted and Mn-promoted (B) catalysts.

A more interesting effect can be noted when analyzing the relative peak area of the three reduction peaks. In short, all promoters increase the area of the highest temperature peak at the expense of the two others. Except for 1Mn, this increase comes mainly at the cost of the lowest temperature peak. Increasing the loading of Cs or K once again increases the lowest temperature peak, as seen in Figure 2.3.

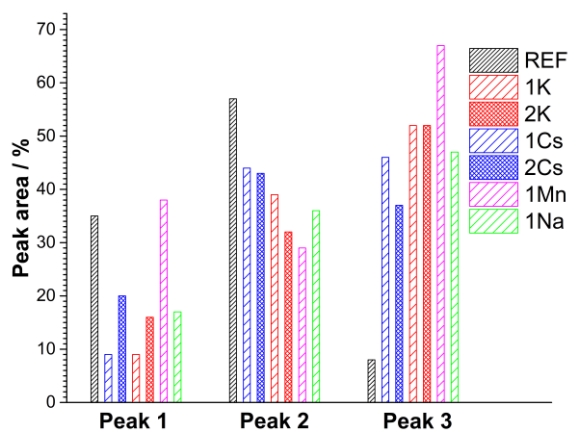


Figure 2.3: Relative distribution of peak areas observed in TPR.

Previous studies indicate that in TPR analysis of supported Ni catalysts smaller NiO clusters are reduced at higher temperatures. In contrast, large NiO particles on the support

can be considered bulk NiO.⁵⁶⁻⁵⁸ This rule cannot be applied universally, however. Available literature on Mn-promoted Co and Ni catalysts shows that shifts in reduction temperature are not necessarily caused by changes in Ni particle size but can also be affected by the formation of solid solutions during synthesis.^{59, 60} The promoter itself can also decrease the reducibility of the Ni active phase. Mixed oxides of alkali metals and nickel have mainly been reported for Ni³⁺.⁶¹ However, we found no indication of Ni³⁺ in our samples and this is not expected after calcination at 700 °C.

Instead, the TPR curves are in good agreement with the results of *Peters et al.* for pure Ni/ZrO₂.⁵⁸ We propose that a correlation between reducibility and particle size is also appropriate for alkali-promoted Ni/ZrO₂. Thus, we attribute here peak 1 to bulk NiO and peaks 2 and 3 to dispersed Ni species with different degrees of interaction with the support.⁵⁸

To summarize, our TPR data show, that the addition of alkali promoters reduces the amount of “bulk” nickel (peak 1). All alkali promoters increase the highest temperature peak also at the expense of the intermediate peak. However, an increase in alkali loading again increases the percentage of “bulk” nickel. It depends on the promoter in question, which of the two “dispersed nickel” peaks is affected by this readjustment. This concept of an optimal promoter loading for nickel distribution mirrors the TEM analyses of *Park et al.*⁶² When adding various alkali metals to Ni/SiO₂, they also noticed a smaller average Ni particle size for low promoter loadings and an growth in particle size with increased promoter loading.

2.3.2 Catalytic activity

The catalytic runs were carried out with very low loadings of the active metal under conditions at which coking is thermodynamically favorable. This allowed us to observe a significant deactivation for all catalysts during the 12 h activity test. The results of the catalytic runs are summarized in Figure 2.4, in which the methane conversion is shown for all samples over the time on stream (TOS). For the CO₂ conversion, we refer to Appendix A4. For all catalysts, the increase in the promoter loading gave rise to a decreased conversion. Interestingly, at identical loadings, the catalysts with different promoters show similar levels of conversion (Figure 2.4). These data suggest that regardless of the choice of promoter, a similar number of active sites in the catalyst was blocked by promoter addition.

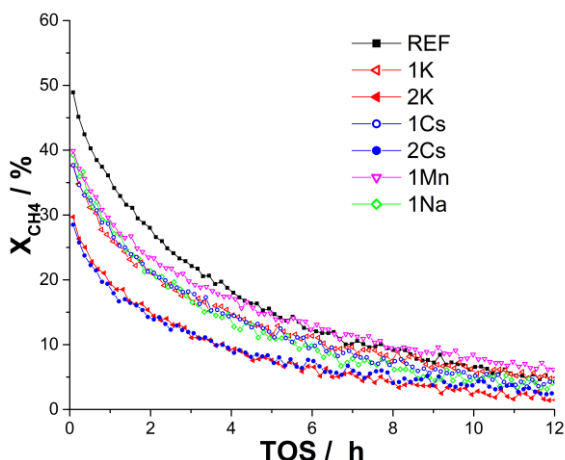


Figure 2.4: Methane conversion over promoted and non-promoted Ni/ZrO₂ as a function of time-on-stream at 650 °C, 30 mg sample, 80 mL min⁻¹ (20% CH₄, 20% CO₂ in N₂).

Following this line of thought, samples with higher promoter loadings should be more resistant to coking and deactivate less. Yet, in all cases the conversion decreases considerably within 12 h TOS and after 6-8 h the measured values differ only marginally between the samples. Catalyst deactivation in dry reforming is frequently caused by coke formation, but sintering can also play a significant role. For example, the weak interactions between ZrO₂ and Ni have been proposed to accelerate Ni sintering and thus catalyst deactivation during dry reforming.⁴³ Pronounced sintering would thus be a credible explanation for the observed behavior.

A strong impact of sintering may obscure differences between the different promoters. The different promoters do appear to block a similar amount of active sites. The question that remains is, if the effect on the catalyst stability is the same or if differences exist between the promoters. For example, one promoter may be more effective at blocking the most coke forming sites. To elucidate these potential differences, the coke contents on the spent catalysts was analyzed and quantified.

2.3.3 Coke characterization

The carbon content of spent samples was analyzed with TGA-MS. The data are summarized in Figure 2.5. In short, the non-promoted REF contains 53 mg_C g⁻¹_{cat} and the coke loading of all promoted samples was substantially lower. In this group, samples 1Mn and 1K contain the most coke with 9 and 10 mg_C g⁻¹_{cat} respectively. Using cesium and sodium as promoters instead reduces the coke content by around 50% to 3 or 5 mg_C g⁻¹_{cat}. Increasing the loading of potassium reduces the coke content further (3 mg_C g⁻¹_{cat} for 2K). 2Cs is on a similar level with 4 mg_C g⁻¹_{cat}. As mentioned previously, the increased promoter loadings of 2Cs and 2K

also reduce the initial methane conversion substantially. The coke contents in REF sample is already rather low compared to the values commonly reported for different Ni-based catalyst systems.^{18, 63} We attribute this to a low Ni loading and the short runtime of 12 h TOS used in this study. Experiments at higher Ni loadings and longer reaction times have indicated, that ZrO₂-based systems commonly form more coke than those based on Ce_{1-x}Zr_xO₂.⁴⁴ Supports such as MgO or SiO₂ have also been reported to lead to less carbon formation.⁴³

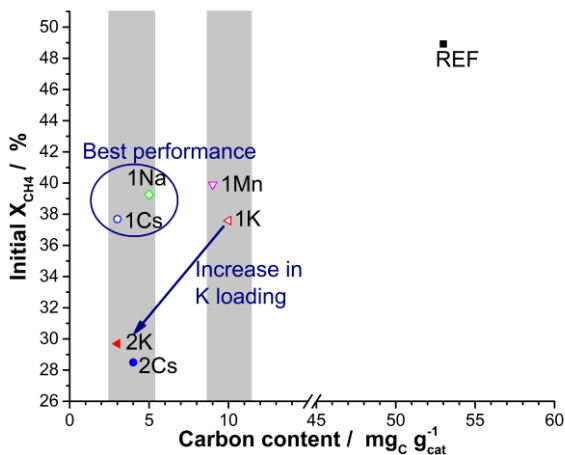


Figure 2.5: Initial methane conversion of the samples plotted over the carbon content after 12 hours of coking.

Published literature shows that increasing the loading of alkali metal promoter reduces both the conversion and the amount of coke deposits.¹⁸ For the K-promoted samples, this correlation holds. Increasing the K/Ni ratio from 1/10 (1K) to 2/10 (2K) further reduces the coke, albeit only by small overall amounts when comparing the drop in coke content from REF to 1K. This is in line with the previously proposed concept of site blocking by the promoters, which implies that the most active coke forming sites are quickly blocked by the promoter.^{23, 25} The remaining coke is not formed on step-edge sites but on Ni ensembles of a minimal size.^{21, 64} Larger quantities of the promoter are then necessary to cover all such ensembles sufficiently to prevent further coke formation. For Cs the situation is slightly different as a Cs/Ni ratio of 1/10 (1Cs) is already enough to reduce the carbon content to 3 mg_C g_{cat}⁻¹. In our work we were not able to obtain a catalyst that coked less.

The TPR analysis indicated an increase of the average Ni diameter when increasing the promoter loading from 1/10 to 2/10. The further decrease of the coke content when increasing the promoter loading from 1/10 to 2/10 shows that the effect of these changes in the Ni particle size are negligible compared to the site blocking effects. Otherwise, the coke content should not decrease so noticeably.

To summarize, in our work cesium and sodium were more effective at reducing the overall coke content than manganese and potassium at low promoter loadings. At higher promoter loadings, the low total coke content prevents any differentiation between the samples. Literature has already hinted at Cs being more effective at reducing the carbon formation than K.²⁰ *Horiuchi et al.* compared the relative effectiveness of sodium and potassium in suppressing coke formation but their data do not establish a clear trend.²⁶ Alkali metals are well-known coke gasification catalysts (e.g. refs. 65, 66) and typically outperform manganese oxides in this respect.^{36, 67} Thus, the comparable coke content of 1Mn and 1K implies the site-blocking mechanism dominating in these cases. The superior performance of 1Cs and 1Na may well be due to an increased gasification activity.

A different effectivity at reducing the coke content could result in different coke structures for the individual promoters. Besides the presence of carbon fibers (Fig. A1), TEM analysis revealed carbon agglomerates of initially unclear structure. HRTEM analysis indicated that these agglomerates are composed at least partially of overlapping and intertwining fibers (Fig. A2). Additionally, at high resolution, non-hollow coke structures could be identified on the catalyst surface (Figure 2.6 and A3). This structure also appears ordered when contrasted with published TEM images of amorphous carbon deposits.⁴² Lastly, it must be mentioned, that the most carbon fibers were observed, when analyzing samples REF and 1Mn.

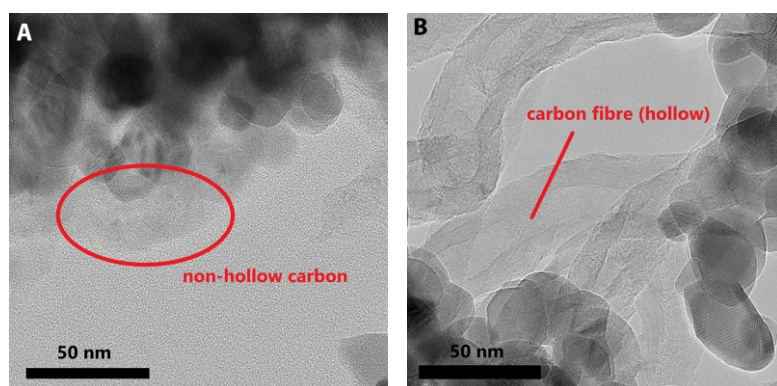


Figure 2.6: HRTEM images of non-hollow carbon (A – sample REF) and carbon filaments (B – sample 1K) after 12 h coking treatment.

Raman spectroscopy is a potential tool to probe the nature of the carbon species in dry reforming catalysts.⁶⁸ In particular the graphitic coke species are probed, since Raman spectra of carbons are typically dominated by the characteristic bands of sp^2 species.⁶⁹ Figure 2.7 shows the spectra for the pure Ni/ZrO₂ and all samples with a 1/10 promoter ratio. The only exception is 1Cs for which no Raman spectrum of the carbon could be obtained.

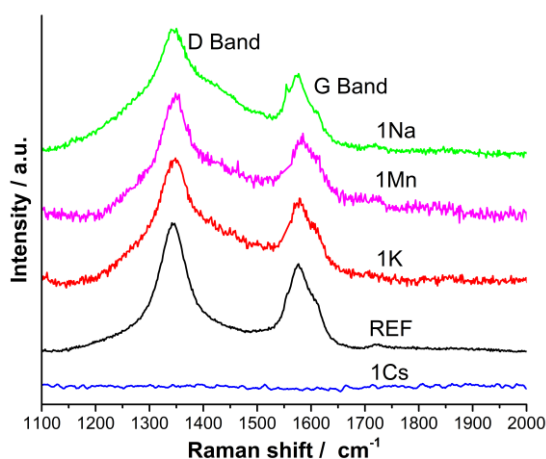


Figure 2.7: Raman spectra for coked catalysts.

sp² carbons typically display two different Raman bands: The D band (approx. 1360 cm⁻¹) and G band (approx. 1560 cm⁻¹). The latter has been correlated to the tangential vibrations of C-C bonds, while the D-band indicates the defect density within the graphitic structure.⁶⁸ In Figure 2.7 all samples exhibit these two bands. To further differentiate between the samples, the relative intensity of the D- and G-bands can be calculated for the different samples. A high value of the I_D/I_G is a sign of a graphitic carbon with high defect density or of nanocrystalline graphite.^{69, 70} Carbon nanotubes are highly structured graphitic species and should thus lead to a more pronounced G-band relative to the D-band.⁷⁰

The I_D/I_G values for all samples are in the range of 1.45-1.55, whereas *Stroud et al.* reported values between 0.8 and 2.0.⁶⁸ However, they also reported different ratios for measurements carried out on different regions of the same catalyst. These observations can be explained by considering the contribution of carbon fibers with their low defect density. During the TEM analysis described above a distinct clustering of carbon fibers was observed. *Stroud et al.* did not report coke quantification but the catalysts investigated contained roughly 5 times more Ni than the samples in this work and were tested for longer periods of time.⁶⁸ This ought to lead to a significantly higher coke contents and thus more clusters of carbon fibers. It is possible that the different ratios of I_D/I_G reported previously were caused by analyzing areas of coke containing vastly different percentages of carbon fibers. Less clusters of fibers make their contribution to the measured Raman spectra unlikely in this work. The calculated I_D/I_G values of approx. 1.5 are too low for only the presence of nanocrystalline graphite.^{69, 71} Instead they are indicative of the presence of amorphous carbon on all samples in addition to nanocrystalline graphite.

To check this hypothesis, the pure Ni/ZrO₂ and all samples with a promoter/Ni ratio of 1/10 were analyzed with ¹³C-NMR to investigate the character of the carbon species further. The presence of magnetic nickel on the catalysts required high spinning frequencies and short

relaxation times to obtain information on the carbon without interference. At the same time, the low carbon content required measurement periods of approx. 24 h per sample. As can be seen in Figure 2.8, the spectra of 1Cs, 1K and 1Na on the one hand and REF and 1Mn on the other hand are rather similar.

All samples clearly show a peak in the range of 0-50 ppm, typically associated with alkanes and sp^3 -hybridized carbons. Therefore, this proves the presence of amorphous carbon with its contributions to both the sp^2 and sp^3 -range of the NMR spectrum.^{72, 73} Pure amorphous carbon would consist of two peaks around 30 ppm and 120 ppm. Instead, REF and 1Mn contain a significant peak around 100 ppm. For 1K the main peak decreases slowly with increasing chemical shift and a smaller peak is visible at approx. 120 ppm. For 1Cs and 1Na, instead of a distinct peak at 120 ppm, a shoulder can still be identified in this range. Additionally, these two samples also display a comparatively sharp peak at 167 ppm.

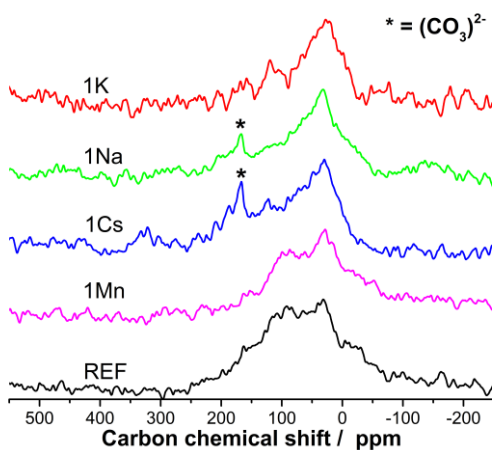


Figure 2.8: ^{13}C -NMR spectra of the non-promoted (REF) Ni/ZrO₂ sample and all catalysts with a promoter loading of 1/10.

The contribution between 50-100 ppm may be due to several reasons. Firstly, hydrogen-poor amorphous carbon has been observed to display clear peaks or shoulders in the sp^3 -peak at around 70 ppm.⁷³ The less hydrogen is present in the amorphous carbon, the clearer this peak at 70 ppm becomes. Secondly, the existence of carbon fibers was proven by TEM for almost all samples. These fibers are typically compared to carbon nanotubes. Pristine nanotubes display a chemical shift of 100-130 ppm, depending on their diameter.⁷⁴ At the same time, the encapsulation of hydrocarbons within carbon nanotubes typically reduces the chemical shift of these molecules in ^{13}C -NMR.^{74, 75} Sp^2 -hydrocarbons (typically 120-160 ppm) encapsulated in the fibers could then contribute in the range of 80-100 ppm.

Thus, we consider the carbon deposits to contain amorphous carbon with a noticeable sp^3 -contribution. For REF and 1Mn the NMR spectra further show the presence of significant

amounts of carbon fibers. For the alkali-promoted samples, the small peak or shoulder at 120 ppm is more in keeping with a small sp²-contribution in amorphous carbon. The comparison of the different spectra shows that while all promoters reduce overall carbon levels, alkali metals are more effective at preventing the formation of carbon fibers. This is in line with TEM analysis, where carbon fibers were easier to detect for REF and 1Mn than for the alkali-promoted samples.

The NMR results for all alkali-promoted samples are mostly comparable, especially since at such low coke contents contaminations could quickly influence the signal. The only exception is the peak mentioned above at approx. 167 ppm for 1Cs and 1Na, which is absent for 1K. The peak is attributed to carbonate species present in the spent catalyst in the form of either alkali carbonates or as Zr(CO₃)₂. A clear identification was not possible, since the chemical shift of the different carbonates differ only slightly.⁷⁶⁻⁷⁹ However, the coke contents of all three samples are in the same order of magnitude. If the peak were due to Zr(CO₂)₃ it should also be visible in the spectrum of 1K. This is a strong indication of the presence of Na₂CO₃ and Cs₂CO₃.

The detection of carbonates is in line with the previous proposal of enhanced coke gasification for the samples 1Cs and 1Na. Carbonate formation is commonly considered an important step in the (earth) alkali-catalyzed gasification of carbon with CO₂.^{39, 80, 81} The accepted order of catalytic activity in coal gasification of the alkali metals used in this work is Cs > K > Na.⁸¹ However, this relative activity is affected by the dispersion of the alkali metals on the carbon, since Na is known to agglomerate on carbon surfaces.³⁹ At the same time, the CO₂ absorption capacity of Na₂ZrO₃ has been reported previously.^{82, 83} For Na-promoted Ni/ZrO₂ a coke gasification cycle including Na₂ZrO₃ and Na₂CO₃ has already been proposed for dry reforming of methane.²⁷ Thus, whereas Cs itself is a very active gasification catalyst, the activity of Na may be increased through interaction with the support.

Summarizing, the coke quantification shows that all promoters reduce the coke content significantly compared to the non-promoted Ni/ZrO₂ catalyst (REF). However, 1Na and 1Cs only contain approx. 50% of the carbon deposited on 1Mn and 1K. Raman spectroscopy did not reveal any differences in the structure of the non-fibrous carbon on the different samples. At the same time TEM and ¹³C-NMR show a higher propensity of 1Mn and REF to form carbon fibers. The relative amount of the different carbon species and thus the overall carbon composition appear to be a function of the promoter. We did not observe any effect of the promoters on the structure of the individual carbon species. Additionally, NMR showed significant contributions of sp³-hybridized carbon in all samples, which is assumed to be amorphous carbon. Operation at temperatures such as 650 °C and higher is expected to produce coke with high levels of graphitization.^{14, 84} This is such an accepted assumption that in reviews on methane reforming, the words graphite and coke have been used interchangeably.¹³ The presence of sp³ signals shows, that, at least at 650 °C, full graphitization cannot yet be assumed.

Furthermore, the NMR spectra of 1Na and 1Cs show the presence of carbonates indicating the presence of Cs_2CO_3 and Na_2CO_3 and thus carbon gasification activity for the two samples with the lowest coke content. The results in this publication show that the same promoted catalyst can achieve site blocking and carbon gasification. However, the overall catalytic effectiveness is not directly correlated to the results of classical coal gasification. It appears that the superior interaction of Na and ZrO_2 compared to Na and coal cause 1Na to outperform 1K, despite K being reported to be the superior coal gasification catalyst.

2.4 Conclusion

A series of Ni/ ZrO_2 catalysts with different promoter metals and promoter ratios was synthesized. TPR studies led to the observation of different effects of the metal promoters on Ni reducibility, which indicates smaller Ni particles when adding small promoter amounts. STEM analysis reveals that for all samples the majority of the Ni particles is smaller than 10 nm before the reaction. Despite varying effects on the reducibility of Ni, the different promoters lead to almost identical conversion in the dry reforming of methane at 650 °C. A difference only becomes noticeable in the analysis of coked samples.

While all promoters strongly reduce the coke content compared to the pristine Ni/ ZrO_2 , the degree of coke reduction depends on the promoter. ^{13}C -NMR analysis shows the presence of sp^3 -hybridized carbon in all samples, despite literature frequently assuming full graphitization at these temperatures. In combination with TEM analysis it could be established that alkali metals are more effective at suppressing fiber growth than manganese. At the same time, samples promoted with sodium or cesium coked less than a sample coked with potassium. These two samples are also the only ones, for which carbonate species could be detected in NMR. Therefore, it is proposed that the lower coke content is caused by coke gasification. Comparison with literature indicates that the higher than expected activity of the Na-promoted sample can be attributed to superior interactions between Na and the ZrO_2 support compared to Na on carbon in typical coal gasification.

2.5 References

1. BP Energy Outlook 2019 edition, <https://www.bp.com/content/dam/bp/business-sites/en/global/corporate/pdfs/energy-economics/energy-outlook/bp-energy-outlook-2019.pdf>, (accessed Apr. 17, 2020).
2. T. L. Roussière, PhD thesis, Karlsruhe Institute of Technology, 2013.
3. J. Zhang, H. Wang and A. K. Dalai, *J. Catal.*, 2007, **249**, 300-310.
4. I. K. van Ravenhorst, C. Vogt, H. Oosterbeek, K. W. Bossers, J. G. Moya-Cancino, A. P. van Bavel, A. M. J. van der Eerden, D. Vine, F. M. F. de Groot, F. Meirer and B. M. Weckhuysen, *Angew. Chem. Int. Ed.*, 2018, **57**, 11957-11962.
5. R. Gaikwad, A. Bansode and A. Urakawa, *J. Catal.*, 2016, **343**, 127-132.
6. L. Tillmann, J. Schulwitz, A. van Veen and M. Muhler, *Catal. Lett.*, 2018, **148**, 2256-2262.
7. L. C. S. Kahle, T. Roussière, L. Maier, K. Herrera Delgado, G. Wasserschaff, S. A. Schunk and O. Deutschmann, *Ind. Eng. Chem. Res.*, 2013, **52**, 11920-11930.
8. J. A. Moulijn, A. E. van Diepen and F. Kapteijn, *Appl. Catal., A*, 2001, **212**, 3-16.
9. N. A. K. Aramouni, J. G. Touma, B. A. Tarboush, J. Zeaiter and M. N. Ahmad, *Renew. Sustain. Energy Rev.*, 2018, **82**, 2570-2585.
10. H. Düdler, K. Kähler, B. Krause, K. Mette, S. Kühn, M. Behrens, V. Scherer and M. Muhler, *Catal. Sci. Tech.*, 2014, **4**, 3317-3328.
11. B. AlSabban, L. Falivene, S. M. Kozlov, A. Aguilar-Tapia, S. Ould-Chikh, J.-L. Hazemann, L. Cavallo, J.-M. Basset and K. Takanebe, *Appl. Catal. B*, 2017, **213**, 177-189.
12. S. A. Theofanidis, V. V. Galvita, H. Poelman and G. B. Marin, *ACS Catal.*, 2015, **5**, 3028-3039.
13. J. R. Rostrup-Nielsen, J. Sehested and J. K. Nørskov, in *Adv. Catal.*, Academic Press, 2002, vol. 47, pp. 65-139.
14. C. H. Bartholomew, *Appl. Catal., A*, 2001, **212**, 17-60.
15. R. T. K. Baker, P. S. Harris, J. Henderson and R. B. Thomas, *Carbon*, 1975, **13**, 17-22.
16. I. Chen and F. L. Chen, *Ind. Eng. Chem. Res.*, 1990, **29**, 534-539.
17. F. Frusteri, F. Arena, G. Calogero, T. Torre and A. Parmaliana, *Catal. Commun.*, 2001, **2**, 49-56.
18. J. Juan-Juan, M. C. Román-Martínez and M. J. Illán-Gómez, *Appl. Catal., A*, 2006, **301**, 9-15.

19. T. Osaki and T. Mori, *J. Catal.*, 2001, **204**, 89-97.
20. C. Ping, H. Zhao-Yin and Z. Xiao-Ming, *Chin. J. Chem.*, 2005, **23**, 847-851.
21. J. R. Rostrup-Nielsen, *J. Catal.*, 1984, **85**, 31-43.
22. S. Arora and R. Prasad, *RCS Adv.*, 2016, **6**, 108668-108688.
23. H. S. Bengaard, I. Alstrup, I. Chorkendorff, S. Ullmann, J. R. Rostrup-Nielsen and J. K. Nørskov, *J. Catal.*, 1999, **187**, 238-244.
24. F. Besenbacher, I. Chorkendorff, B. S. Clausen, B. Hammer, A. M. Molenbroek, J. K. Nørskov and I. Stensgaard, *Science*, 1998, **279**, 1913-1915.
25. H. S. Bengaard, J. K. Nørskov, J. Sehested, B. S. Clausen, L. P. Nielsen, A. M. Molenbroek and J. R. Rostrup-Nielsen, *J. Catal.*, 2002, **209**, 365-384.
26. T. Horiuchi, K. Sakuma, T. Fukui, Y. Kubo, T. Osaki and T. Mori, *Appl. Catal., A*, 1996, **144**, 111-120.
27. M. Németh, D. Srankó, J. Károlyi, F. Somodi, Z. Schay, G. Sáfrán, I. Sajó and A. Horváth, *Catal. Sci. Tech.*, 2017, **7**, 5386-5401.
28. Z. Hou, O. Yokota, T. Tanaka and T. Yashima, *Appl. Surf. Sci.*, 2004, **233**, 58-68.
29. S.-H. Seok, S. H. Han and J. S. Lee, *Appl. Catal., A*, 2001, **215**, 31-38.
30. D. W. Flaherty, W.-Y. Yu, Z. D. Pozun, G. Henkelman and C. B. Mullins, *J. Catal.*, 2011, **282**, 278-288.
31. A. Diaz, D. R. Acosta, J. A. Odriozola and M. Montes, *J. Phys. Chem. B*, 1997, **101**, 1782-1790.
32. W. D. Mross, *Catal Rev*, 1983, **25**, 591-637.
33. A. Parmaliana, F. Arena, F. Frusteri, N. Mondello and N. Giordano, in *Stud. Surf. Sci. Catal.*, eds. C. H. Bartholomew and J. B. Butt, Elsevier, 1991, vol. 68, pp. 489-492.
34. A. Ehrmaier, L. Löbber, M. Sanchez-Sanchez, R. Bermejo-Deval and J. Lercher, *ChemCatChem*, 2020, **n/a**.
35. P. Littlewood, X. Xie, M. Bernicke, A. Thomas and R. Schomäcker, *Catal. Today*, 2015, **242**, 111-118.
36. M. Keller, H. Leion and T. Mattisson, *Energy Technol-Ger*, 2013, **1**, 273-282.
37. D. W. McKee, *Carbon*, 1974, **12**, 453-464.
38. J. A. Moulijn and F. Kapteijn, in *Carbon and Coal Gasification: Science and Technology*, eds. J. L. Figueiredo and J. A. Moulijn, Springer Netherlands, Dordrecht, 1986, DOI: 10.1007/978-94-009-4382-7_6, pp. 181-195.
39. J. A. Moulijn and F. Kapteijn, *Carbon*, 1995, **33**, 1155-1165.
40. J. L. Rogers, M. C. Mangarella, A. D. D'Amico, J. R. Gallagher, M. R. Dutzer, E. Stavitski, J. T. Miller and C. Sievers, *ACS Catal.*, 2016, **6**, 5873-5886.
41. R. H. Nielsen and G. Wilfing, in *Ullmann's Encyclopedia of Industrial Chemistry*, 2010, DOI: 10.1002/14356007.a28_543.pub2.

42. C. Wang, N. Sun, N. Zhao, W. Wei, J. Zhang, T. Zhao, Y. Sun, C. Sun, H. Liu and C. E. Snape, *ChemCatChem*, 2014, **6**, 640-648.
43. R.-j. Zhang, G.-f. Xia, M.-f. Li, Y. Wu, H. Nie and D.-d. Li, *J. Fuel Chem. Technol.*, 2015, **43**, 1359-1365.
44. A. Wolfbeisser, O. Sophephun, J. Bernardi, J. Wittayakun, K. Föttinger and G. Rupprechter, *Catal. Today*, 2016, **277**, 234-245.
45. C. Nederlof, V. Zarubina, I. Melián-Cabrera, H. J. Heeres, F. Kapteijn and M. Makkee, *Catal. Sci. Tech.*, 2013, **3**, 519-526.
46. R. J. Berger, J. Pérez-Ramírez, F. Kapteijn and J. A. Moulijn, *Chem. Eng. Sci.*, 2002, **57**, 4921-4932.
47. N. D. Charisiou, S. L. Douvartzides, G. I. Siakavelas, L. Tzounis, V. Sebastian, V. Stolojan, S. J. Hinder, M. A. Baker, K. Polychronopoulou and M. A. Goula, *Catalysts*, 2019, **9**, 676.
48. P. M. Mortensen, D. Gardini, H. W. P. de Carvalho, C. D. Damsgaard, J.-D. Grunwaldt, P. A. Jensen, J. B. Wagner and A. D. Jensen, *Catal. Sci. Tech.*, 2014, **4**, 3672-3686.
49. W. L. Vrijburg, E. Moioli, W. Chen, M. Zhang, B. J. P. Terlingen, B. Zijlstra, I. A. W. Filot, A. Züttel, E. A. Pidko and E. J. M. Hensen, *ACS Catal.*, 2019, **9**, 7823-7839.
50. W. L. Vrijburg, J. W. A. van Helden, A. Parastaev, E. Groeneveld, E. A. Pidko and E. J. M. Hensen, *Catal. Sci. Tech.*, 2019, **9**, 5001-5010.
51. R. K. Singha, A. Shukla, A. Yadav, S. Adak, Z. Iqbal, N. Siddiqui and R. Bal, *Appl. Energy*, 2016, **178**, 110-125.
52. E. Taglauer, in *Handbook of Heterogeneous Catalysis*, eds. G. Ertl, H. Knözinger, F. Schüth and J. Weitkamp, 2008, DOI: 10.1002/9783527610044.hetcat0051, pp. 1014-1029.
53. G. Marcelin and J. E. Lester, *J. Catal.*, 1985, **93**, 270-278.
54. D. M. Stockwell, A. Bertucco, G. W. Coulston and C. O. Bennett, *J. Catal.*, 1988, **113**, 317-324.
55. M. Steib, Y. Lou, A. Jentys and J. A. Lercher, *ChemCatChem*, 2017, **9**, 3809-3813.
56. C. Li and Y.-W. Chen, *Thermochim. Acta*, 1995, **256**, 457-465.
57. B. Mile, D. Stirling, M. A. Zammitt, A. Lovell and M. Webb, *J. Mol. Catal.*, 1990, **62**, 179-198.
58. A. Peters, F. Nouroozi, D. Richter, M. Lutecki and R. Gläser, *ChemCatChem*, 2011, **3**, 598-606.
59. F. Morales, D. Grandjean, A. Mens, F. M. F. de Groot and B. M. Weckhuysen, *J. Phys. Chem. B*, 2006, **110**, 8626-8639.

60. W. L. Vrijburg, E. Moioli, W. Chen, M. Zhang, B. J. P. Terlingen, B. Zijlstra, I. A. W. Filot, A. Züttel, E. A. Pidko and E. J. M. Hensen, *ACS Catalysis*, 2019, DOI: 10.1021/acscatal.9b01968, 7823-7839.
61. L. D. Dyer, B. S. Borie and G. P. Smith, *J. Am. Chem. Soc.*, 1954, **76**, 1499-1503.
62. C. Park and M. A. Keane, *J. Colloid Interface Sci.*, 2002, **250**, 37-48.
63. H.-S. Roh, H. S. Potdar, K.-W. Jun, J.-W. Kim and Y.-S. Oh, *Appl. Catal., A*, 2004, **276**, 231-239.
64. N. T. Andersen, F. Topsøe, I. Alstrup and J. R. Rostrup-Nielsen, *J. Catal.*, 1987, **104**, 454-465.
65. F. Kapteijn, O. Peer and J. A. Moulijn, *Fuel*, 1986, **65**, 1371-1376.
66. D. W. McKee, *Fuel*, 1983, **62**, 170-175.
67. M. Arjmand, H. Leion, T. Mattisson and A. Lyngfelt, *Appl. Energy*, 2014, **113**, 1883-1894.
68. T. Stroud, T. J. Smith, E. Le Saché, J. L. Santos, M. A. Centeno, H. Arellano-Garcia, J. A. Odriozola and T. R. Reina, *Appl. Catal. B*, 2018, **224**, 125-135.
69. A. C. Ferrari, *Solid State Commun.*, 2007, **143**, 47-57.
70. M. S. Dresselhaus, G. Dresselhaus, A. Jorio, A. G. Souza Filho and R. Saito, *Carbon*, 2002, **40**, 2043-2061.
71. A. C. Ferrari and J. Robertson, *Phys Rev B*, 2000, **61**, 14095-14107.
72. R. H. Jarman, G. J. Ray, R. W. Standley and G. W. Zajac, *Appl. Phys. Lett.*, 1986, **49**, 1065-1067.
73. J. Braddock-Wilking, S. H. Lin and B. J. Feldman, *Solid State Commun.*, 2001, **119**, 19-21.
74. E. Abou-Hamad, M. R. Babaa, M. Bouhrara, Y. Kim, Y. Saih, S. Dennler, F. Mauri, J. M. Basset, C. Goze-Bac and T. Wågberg, *Phys Rev B*, 2011, **84**, 165417.
75. N. A. Besley and A. Noble, *J. Chem. Phys.*, 2008, **128**, 101102.
76. F. Takasaki, K. Fujiwara, Y. Nakajima, T. Nishikawa, H. Masu, M. Imanari, Y. Hidaka and N. Ogawa, *Dalton Trans.*, 2015, **44**, 645-652.
77. National Center for Biotechnology Information. PubChem Database. Sodium carbonate, CID=10340, <https://pubchem.ncbi.nlm.nih.gov/compound/Sodium-carbonate>, (accessed Feb. 5, 2020).
78. National Center for Biotechnology Information. PubChem Database. Cesium carbonate, CID=10796, <https://pubchem.ncbi.nlm.nih.gov/compound/Cesium-carbonate>, (accessed Feb. 5, 2020).
79. National Center for Biotechnology Information. PubChem Database. Potassium carbonate, ID=11430, <https://pubchem.ncbi.nlm.nih.gov/compound/Potassium-carbonate>, (accessed Feb. 5, 2020).

80. D. Cazorla-Amorós, A. Linares-Solano, F. H. M. Dekker and F. Kapteijn, *Carbon*, 1995, **33**, 1147-1154.
81. S. G. Chen and R. T. Yang, *Energy Fuels*, 1997, **11**, 421-427.
82. H. G. Jo, H. J. Yoon, C. H. Lee and K. B. Lee, *Ind. Eng. Chem. Res.*, 2016, **55**, 3833-3839.
83. G. G. Santillan-Reyes and H. Pfeiffer, *Int J Greenh Gas Con*, 2011, **5**, 1624-1629.
84. J. M. Ginsburg, J. Piña, T. El Solh and H. I. de Lasa, *Ind. Eng. Chem. Res.*, 2005, **44**, 4846-4854.

Appendix A

A1 TPR analysis

Table A1: Reduction peaks observed during TPR profile deconvolution.

Sample	Peak 1 [°C]	Peak 2 [°C]	Peak 3 [°C]
REF	350 °C	460 °C	510 °C
1K	350 °C	420 °C	520 °C
2K	340 °C	400 °C	490 °C
1Na	320 °C	390 °C	490 °C
1Cs	340 °C	410 °C	510 °C
2Cs	370 °C	440 °C	530 °C
1Mn	330 °C	380 °C	470 °C

A2 STEM images

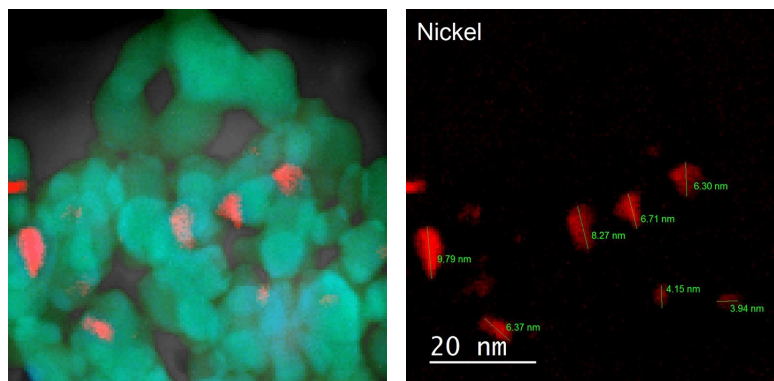


Fig. A1: Example of Ni particles visible on sample 2Cs.

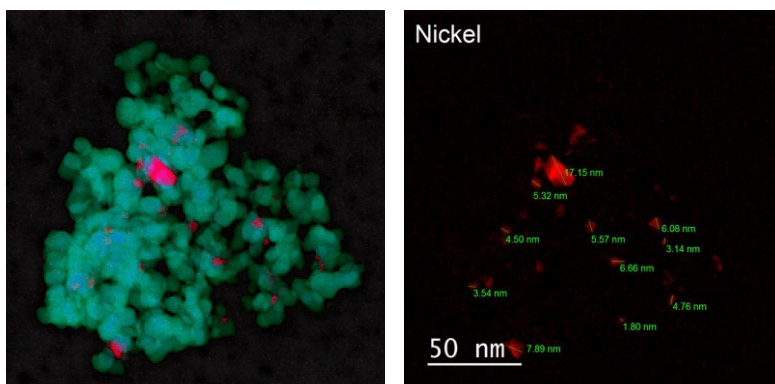


Fig. A2: Example of Ni particles visible on 2K.

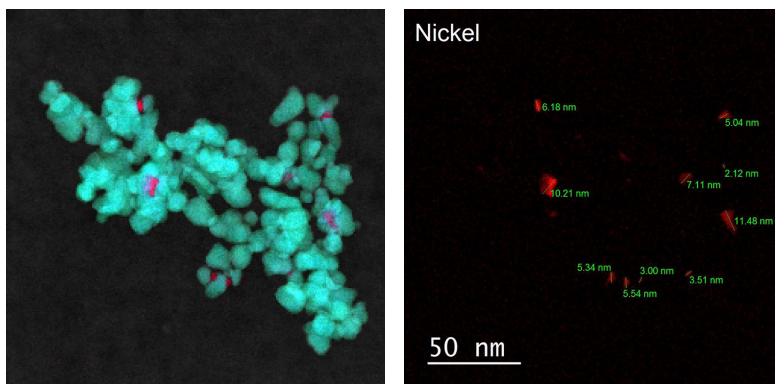


Fig. A3: Example of Ni particles visible on 1Mn.

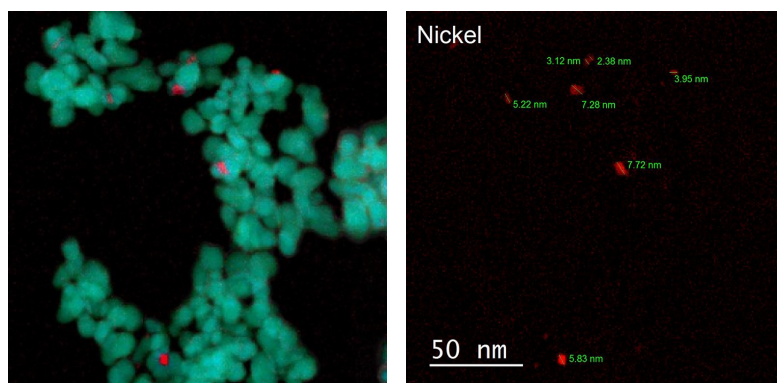


Fig. A4: Example of Ni particles visible on REF.

A3 TEM images

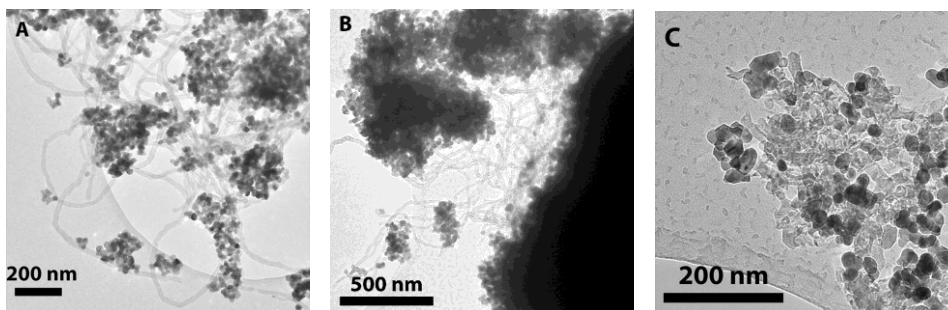


Fig. A5: Carbon structures visible after 12 h of coking treatment in TEM (A - REF, B - 1Mn, C - REF).

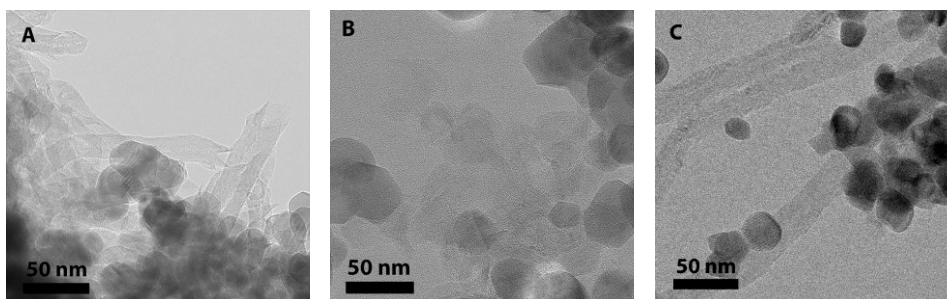


Fig. A6: HRTEM images of carbon fibers (A, C) and graphitic carbon (B) visible on REF (A) and 1Mn (B, C) after 12 h of coking treatment.

A4 Catalytic activity

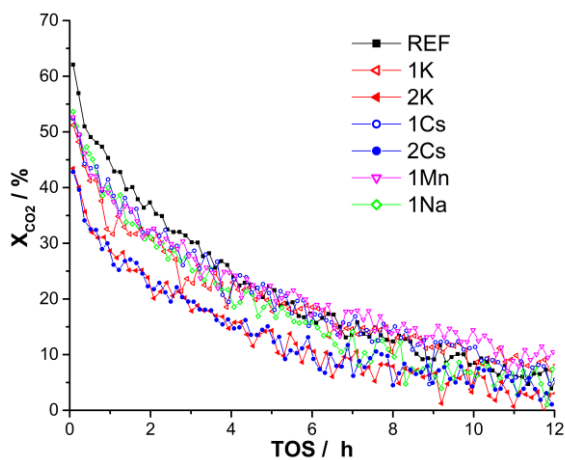


Fig. A7: CO₂ conversion over promoted and non-promoted Ni/ZrO₂ as a function of time-on-stream; 650 °C, 1 bar, 30 mg catalyst, 80 mL min⁻¹ (20%CH₄, 20% CO₂ in N₂).

A5 TGA-MS data

The CO₂ signals obtained during TGA-MS analysis did not allow for further insight into the carbons structure. For samples with more than 5 mg_C g⁻¹_{cat}, the TPO profile is dominated by a peak at 450-500 °C. On the other samples, the development of this peak is already partially observable. We attribute this to the use of undiluted synthetic air during TGA, which prevents sufficient separation of the oxidation temperatures of the different carbon species.

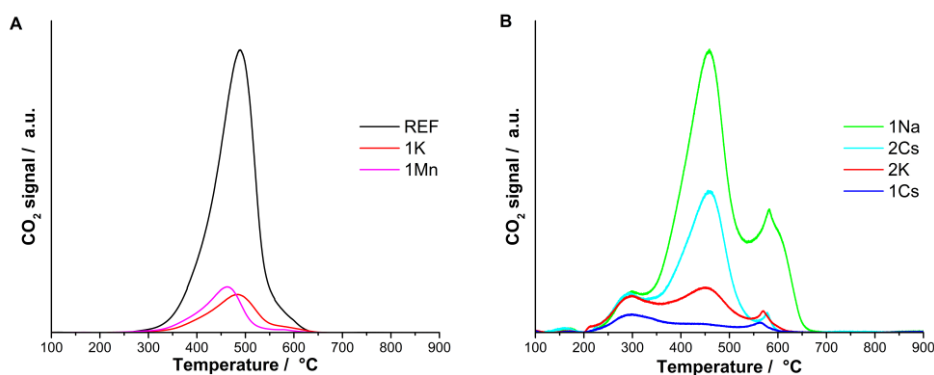


Fig. A8: CO₂ signals measured during the TGA-MS analyses as a function of the sample temperature.

A6 XRD data

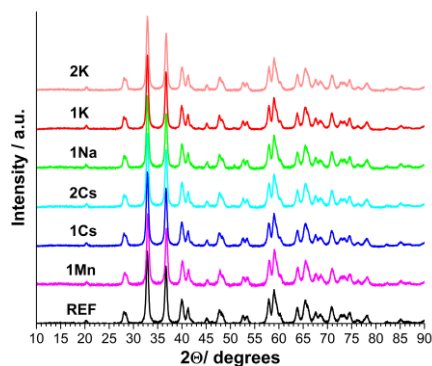
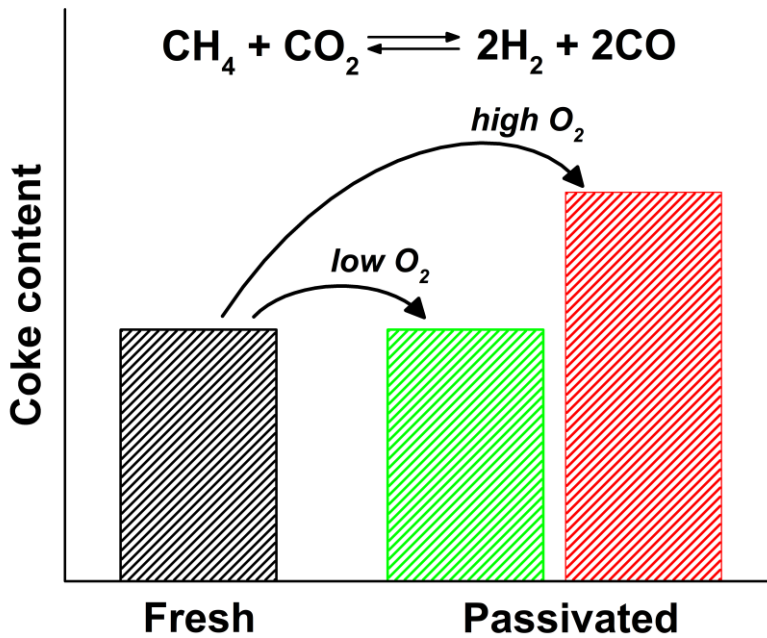


Fig. A9: CO₂ signals measured during the TGA-MS analyses as a function of the sample temperature.

Chapter 3

Dry reforming of methane to test passivation stability of Ni/Al₂O₃ catalysts



Catalyst passivation refers to the formation of a protective oxide layer on the active metal particles that prevents their oxidation when exposed to air. Common passivation procedures, when applied to Ni/Al₂O₃ catalysts, typically result in a significant decrease of the overall Ni surface area and, accordingly, the catalytic activity. Nevertheless, the combination of passivation and reactivation is an attractive pre-treatment option for this system. Ni/Al₂O₃ typically requires reduction temperatures much higher than the desired reaction temperature, whereas reactivation of passivated samples is a low-temperature reduction. This can be used to avoid temperature limitations of existing systems. Thus, more insight into the passivation process of this system is desirable. In this work we analyzed the impact of passivation on the catalytic performance of a series of Ni/Al₂O₃ catalysts in dry reforming of methane. This approach allows for the elimination of scale effects during passivation. We show that changes in conversion and especially of the coke content can be used to track sintering of Ni particles. This in turn highlights, that when working with too high oxygen concentrations during passivation local overheating (and thereby Ni sintering) sets in rapidly, even when working with less than 30 mg of sample. Consequently, the problems of this system are not limited to scaling issues and sufficient care must be taken even on a lab-scale when passivating Ni/Al₂O₃ catalysts.

This chapter is based on the following publication:

R. Franz, F. D. Tichelaar, E. A. Uslamin and E. A. Pidko, *Appl. Catal., A*, 2021, **612**, 117987.

3.1 Introduction

Supported nickel catalysts are a common subset of heterogeneous catalysts for various industrial applications. Both the high inherent catalytic activity of nickel as well as the abundance make it an attractive active metal. Consequently, nickel-based catalysts have been investigated and employed for such reactions as methane/ hydrocarbon reforming,¹⁻³ CO₂ methanation⁴⁻⁸ and other hydrogenation reactions.⁹⁻¹³ In hydrogenation and reforming reactions, the catalytically active substance is metallic nickel, requiring a dedicated reduction step. The most straightforward solution would be to reduce the catalyst in the reactor system directly prior to the catalytic process. However, such a one-pot activation-reactivation scheme may be prohibited by the large temperature gap between the two procedures.

While many catalysts can be reduced at moderate temperatures (200 – 600 °C),^{14, 15} Ni supported on materials such as Al₂O₃ or MgAl₂O₄ can require temperatures of 800 °C or higher, to achieve full reduction of the active phase.¹⁶⁻¹⁹ Most hydrogenation reactions such as CO₂ or alkene hydrogenation proceed at temperatures well below 500 °C. A reactor suitable for high temperatures only for in-place reduction would not be cost-effective, especially on an industrial scale. Instead, a passivated catalyst can be used.²⁰ In this approach the catalyst is first activated in a dedicated setup via high-temperature reduction, followed by cooling the activated catalyst and exposing it to low levels of oxidant. This treatment enables the formation of a protective superficial layer of metal oxide on the reduced metal particles. The surface oxide layer acts as a barrier for deep bulk oxidation of surface nanoparticles allowing thus for safe transport to the catalytic reactor. The reduction of this surface oxide layer can be accomplished under milder conditions than the bulk oxide reduction and therefore can be carried out directly in the catalytic reactor prior to the reaction or in situ.²¹ On an industrial scale, a shorter reduction period also reduces the downtime before production can be continued.²⁰

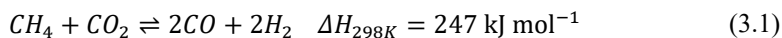
This approach is particularly useful for the cost-effective design of reactors. This is well reflected in the numerous patents incorporating catalyst passivation techniques.²²⁻²⁴ Many academic studies have been devoted to this topic as well.^{21, 25-32} Ni catalysts using either SiO₂ or Al₂O₃ supports are two of the most popular model systems.^{25-27, 29-31} For Ni/SiO₂ the general conclusion in literature is, that passivation treatments allows for full recovery of the metal surface area with marginal effects on the particle size distribution.^{26, 30} At the same time, the moderate reduction temperature of typical Ni/SiO₂ catalysts (usually less than 500 °C³³) limit the necessity of such a protocol in the first place.

For Al₂O₃-supported systems the situation is much more complex. While some authors mention a loss in metal surface area as a result of passivation and reactivation,^{26, 27} a preservation of total nickel surface area has also been reported.²⁵ Unfortunately, the only procedural detail mentioned for the latter was the oxygen concentration of 0.2%. Information

on the sample mass is critical, because of the scale-dependency of potential heat effects and the associated structural changes during passivation.²⁵

Heat management during the passivation procedure critically depends on the scale of the operation. Scaling effects will certainly play an important role in an industrial setting, but on a lab-scale the situation is less clear. Exothermic reactions at low temperatures (such as CO oxidation^{34,35}) have been noted to lead to overheating of catalytically active metallic particles on metal oxide supports. If such local overheating effects can cause substantial structural modifications of the supported catalysts, the passivation of small amounts of sample can already become challenging. The high reduction temperatures of Ni/Al₂O₃ compared to Ni/SiO₂ make the passivation particularly attractive for the former. Thus, further understanding of the process would be of help for the design and optimization of practical passivation procedures.

In the above-mentioned literature examples H₂ chemisorption is the method of choice to quantify the impact of passivation but this requires sample sizes of more than 100 mg. To reduce the catalyst amounts during passivation and thus eliminate scaling effects as far as possible, we chose dry reforming of methane as a probe reaction. Dry reforming of methane refers to the high-temperature conversion of methane and carbon dioxide to syngas (CO+H₂):



Several considerations have led to an active interest in dry reforming research in recent years. Firstly, a large scale reduction of CO₂ emissions is desirable to contain the effects of global warming.³⁶ Incorporating CO₂ into methane reforming represents a relatively moderate modification of a single process step in the chemical supply chain. Secondly, the use CO₂ as a feedstock in methane reforming provides syngas with a higher CO to H₂ ratio that can be desirable for the syntheses of bulk chemicals such as acetic acid.³⁷

In this work we systematically investigated the impact of passivation and reactivation on Ni/Al₂O₃-catalysts. The samples were prepared through conventional incipient wetness impregnation and thoroughly characterized. We were able to show how Ni loading affects the reducibility and surface area of Ni through a combination of TEM, N₂O titration, TPR and N₂ physisorption. The effects on the catalytic performance were evaluated using dry reforming of methane as a probe reaction. Dry reforming is a suitable probe reaction to investigate the effects of passivation and activation on the catalytic properties for several reasons. Firstly, 10 mg of catalyst are sufficient to achieve significant levels of conversion over extended periods of time.³⁸ This approach allows us to reduce, passivate and analyze on a scale of less than 30 mg, eliminating heat effects from neighboring catalyst particles as much as possible. Secondly, the elevated carbon levels compared to pure steam reforming lead to a higher susceptibility for coking.³⁹

Coke nuclei form preferentially at step-edge sites and on large facets of the Ni surface.^{1, 40} Small terrace sites on the other hand do not allow for the formation of stable nuclei.

Consequently, changes in conversion and different coke contents after dry reforming should allow the direct probing of the effects of catalyst passivation. Mild overheating with moderate sintering would yield slightly larger particles that produce more coke. Significant overheating and sintering on the other hand would give rise to a noticeable decrease in Ni surface area and thus of coke content and conversion as well.

Our analysis reveals that the oxygen concentration used during passivation has a pronounced effect on Ni dispersion. Non-ideal passivation parameters are reached very quickly and negatively affect the performance almost independently of the amount of catalyst mass used.

3.2 Experimental

3.2.1 Chemicals

Ethylenediaminetetraacetic acid (EDTA, ThermoFisher 99%), NH₃ solution (VWR, 25%), SAS90 Al₂O₃ catalyst support (BASF Nederland B.V.), Ni(NO₃)₂ · 6H₂O (Merck, analysis quality)

All materials were used as received except for NH₃ (aq), which was diluted with demineralized water in a volumetric ratio of 1:1 before usage, and SAS90. The SAS90 Al₂O₃ spheres were ground to a powder (< 212 μm) before impregnation.

3.2.2 Catalyst synthesis

All samples were synthesized via incipient wetness impregnation. In a typical synthesis, EDTA and Ni(NO₃)₂ with a Ni²⁺/EDTA molar ratio of 1 were dissolved in aqueous 12.5% ammonia solution. This solution was then immediately used for impregnation. Per impregnation step an amount of Ni(NO₃)₂ was used to increase the loading of Ni on the support by 0.04 g_{Ni} g_{support}⁻¹. After impregnation, the solid was dried at 80 °C for 5 h and calcined at 700 °C for 5 h (heating rate of 10 °C min⁻¹). For the samples with a loading of more than 0.04 g g⁻¹ this procedure of impregnation, drying and calcination was repeated as often as necessary. In total, four different loadings were synthesized: 0.04, 0.08, 0.12 and 0.24 g g⁻¹. All batches were synthesized in duplicate. ICP-OES was used to determine the final Ni loading.

3.2.3 Catalyst characterization

Temperature programmed reduction (TPR) was carried out in a dedicated setup equipped with thermal conductivity detector (TCD) and mass-spectrometer (MS). For TPR measurements, 100 mg of sample (particle size 212-355 μm) were filled into a quartz reactor (I.D. of 6 mm) and the reactor was placed into the furnace. Afterwards, a flow of 30 mL min^{-1} (10% H_2 in Ar) was started. The setup was heated to 950 $^\circ\text{C}$ with a ramp of 10 C min^{-1} . H_2 consumption was monitored with the TCD downstream of the reactor.

Total metal Ni surface was quantified by N_2O titration using the TPR setup described above. Per experiment 200 mg of sample (particle size 212-355 μm) were mixed with 300 mg SiC (particle size 212-355 μm) and filled in a quartz reactor (I.D. of 6 mm) and the reactor was placed into the furnace. In a first step, the sample was reduced using a flow of 30 mL min^{-1} at 800 $^\circ\text{C}$ for 1 h (heating rate of 10 C min^{-1}). Then, the sample was cooled in 27 mL min^{-1} of pure Ar to 75 $^\circ\text{C}$. At this temperature, a mixture of 20% N_2O in Ar was pulsed into the reactor. This was achieved with the help of a switching valve equipped with a 100 μL loop upstream of the reactor. The N_2O and N_2 signals were tracked using mass spectrometry. N_2O was pulsed into the system until no more N_2O consumption could be detected. The Ni surface area was calculated according to the method described by *Tada et.al.*⁴¹

$$S_{\text{Ni,cat}} = \frac{n_{\text{N}_2\text{O}} * N_A}{A * m_{\text{cat}}} \quad (3.2)$$

$$S_{\text{Ni,Ni}} = \frac{n_{\text{N}_2\text{O}} * N_A}{A * m_{\text{Ni}}} \quad (3.3)$$

where A is the number of Ni atoms per unit area ($1.54 * 10^{19} \text{ m}^{-2}$), $n_{\text{N}_2\text{O}}$ the molar N_2O consumption as measured with mass spectrometry, N_A Avogadro's constant and m_x the mass of either the catalyst or the reduced Ni on the catalyst. The latter was determined by integrating the TCD signal during the initial period of Ni reduction.

N_2 physisorption was carried out after drying all samples overnight at 150 $^\circ\text{C}$ under N_2 flow. Afterwards, the samples were loaded into a *micromeritics TriStar II*. The measurements proceeded at 77 K.

The chemical composition of the samples with regards to the Al and Ni content was determined via ICP-OES. Each sample was digested by dispersing 30 mg of solid in a mixture of 4.5 mL HCl and 1.5 mL 65% HNO_3 using a microwave. The microwave was set at 1000 W for 60 minutes. After digestion, each sample was diluted with 50 mL of MQ and analyzed with an ICP-OES 5300 DV.

TEM images were obtained using a FEI Tecnai TF20UT/STEM. The instrument was operated in STEM mode and in brightfield mode. Sample preparation before STEM-analysis consisted of a reduction of 30 mg at 800 °C in a flow of 10% H₂ in inert followed by passivation at room temperature. Two different procedures were used for the latter: The milder procedure was carried out in a reactor tube with an inner diameter of 1.5 cm. The O₂ concentration was increased every 20 minutes to the following levels: 0.2%, 1%, 3%, 10% and 20%. The harsher procedure was carried out in the same setup as the TPR measurements with steps of 3%, 10% and 20%.

3.2.4 Reactivity tests

Samples were tested for their catalytic activity in dry reforming of methane in a single-reactor system. In this system, a quartz reactor (I.D. of 4 mm) is placed in a furnace. Upstream of the reactor, mass flow controllers (Bronkhorst) regulate the flow of N₂, CH₄, CO₂ and H₂ to the reactor. Downstream of the reactor a compact GC equipped with a TCD was used for the online product analysis. Product separation was achieved using a micropacked column (ShinCarbon ST 80/100 2m, 0.53 mm I.D.). Conversion of methane and CO₂ was calculated using N₂ as the internal standard according to the following equation:

$$X_R = \frac{\left(\frac{A_R}{A_{N_2}}\right)_0 - \left(\frac{A_R}{A_{N_2}}\right)}{\left(\frac{A_R}{A_{N_2}}\right)_0} \quad (3.4)$$

where R is the reactant in question (either CH₄ or CO₂) and A is the peak area in the GC. In a typical catalytic experiment, 10 mg of sample (355-425 μm) were diluted in 140 mg of SiC (212-300 μm). This mixture was filled into the quartz reactor between two plugs of quartz wool and upstream of a 9 cm layer of SiC (212-425 μm). Upstream of the catalyst-SiC mixture, 7 cm of SiC (212-425 μm) provided pre-warming of the feed. For freshly calcined samples, the sample was heated in a stream of 10% H₂ in N₂ (50 mL min⁻¹) to 800 °C (10 °C min⁻¹) and reduced at this temperature for 1 h, before being cooled to 650 °C. At this point, the flow was switched to 100 mL min⁻¹ of 25% CH₄ and 25% CO₂ in N₂. Afterwards, dry reforming experiments were carried out for 12 h. If the sample was already pre-reduced and passivated, the sample was directly heated to 650 °C in 10% H₂ in N₂ (50 mL min⁻¹). Once the reaction temperature was reached, the dry reforming experiment started. After each catalytic experiment, the coke content of the sample was analyzed via TGA (Mettler-Toledo TGA/SDTA 851°). The catalytic activity of the freshly calcined sample was measured for two different batches of the same loading. The difference in catalytic activity was used to determine the experimental error. This allows for more accurate classification of the effects of passivation.

Pre-reduction and passivation were carried out in the same setup as used for the TPR and N_2O experiments. Here 25 mg of sample (355-425 μm) were used per run. The samples were reduced in 10% of H_2 in N_2 (30 mL min^{-1}) at 800 $^{\circ}C$ for 1 h (10 $^{\circ}C min^{-1}$) and then cooled to room temperature. An ensuing passivation procedure consisted of flowing 30 mL min^{-1} of Ar- O_2 mixtures over the catalyst. Each concentration of O_2 was maintained for 20 min. The concentrations of O_2 were either 1%, 3%, 10% and 20% or 3%, 10% and 20%. Alternatively, the passivation procedure could also be omitted and the freshly reduced sample was directly exposed to air.

3.3 Results and discussion

3.3.1 Catalyst characterization

To evaluate the effect of Ni loading on the physico-chemical properties of the synthesized materials, the samples were thoroughly characterized. The catalysts characterization data are summarized in Table 3.1. ICP data show that the metal content in the resulting samples corresponds well with the desired incipient wetness impregnation loading. This indicates that no Ni loss occurs during the consecutive calcination steps. The textural properties of the catalysts were characterized with N_2 physisorption. The isotherms presented in Figure B1 show similar behavior featuring adsorption on the surface. The adsorptive properties of alumina are not affected even by multiple calcination cycles (Figure B1). However, a slight decline in BET surface area is observed for the Ni/Al_2O_3 samples. This can be attributed to the formation of various Ni species on the surface of alumina.

Table 3.1: Ni/Al_2O_3 characterization data

Nominal loading [g g^{-1}]	Ni loading (ICP) [g g^{-1}]	Ni area [m ² g_{cat}^{-1}]	Ni area [m ² g_{Ni}^{-1}]	BET surface area [m ² g_{cat}^{-1}]
0.04	0.035	0.8	23.9	86
0.08	0.07	1.1	16.4	80
0.12	0.106	1.6	16.8	78
0.24	0.21	3.8	22.9	62

TPR experiments were carried out to study the dispersion and properties of the supported Ni species. The TPR data shown in Figure 3.1 indicate the presence of two features for all Ni/Al_2O_3 samples with maxima around 850 $^{\circ}C$ and 550 $^{\circ}C$. The high-temperature peak significantly dominates the TPR profiles for all catalysts. Increasing the loading of Ni does not affect the position of either peak, indicating a constant reduction temperature. However,

an increase in Ni loading from 0.04 to 0.12 g g⁻¹ leads to a significant increase in the intensity of the high temperature peak. A further increase in Ni loading to 0.24 g g⁻¹ does not lead to a further increase in peak intensity. In contrast, the TPR profile of the sample with 0.24 g g⁻¹ shows significantly higher reduction activity in the lower temperature range.

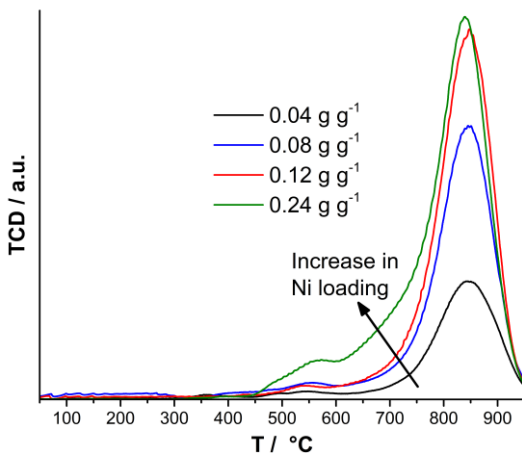


Figure 3.1: Temperature-programmed reduction of the as-prepared Ni/Al₂O₃ samples.

While the high temperature peak (850 °C) can be attributed to highly dispersed Ni particles, the low temperature reduction observed for higher Ni loadings is typically related to the bulk Ni phase.⁴²⁻⁴⁴ Indeed, with increasing quantities of bulk Ni, one would expect the Ni dispersion to decrease as well. However, the results of N₂O titration experiments reveal a rather different trend. While the overall Ni surface area increases with higher loadings (Table 3.1), the surface area per mass of Ni and thus the dispersion does not decrease monotonously. As can be seen from the results in Figure 3.2, the highest dispersion is indeed achieved at a Ni loading of 0.04 g g⁻¹ and increasing the loading to 0.08 g g⁻¹ does decrease the dispersion. However, a further increase in Ni content to 0.12 g g⁻¹ does not affect the dispersion noticeably, while at even higher loadings, the average Ni dispersion increases again.

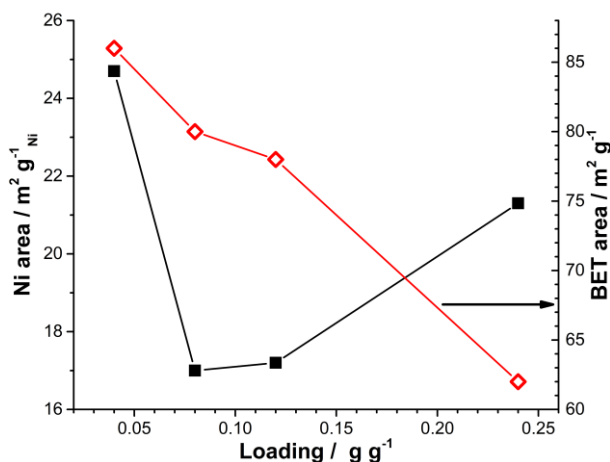


Figure 3.2: BET surface area and Ni dispersion obtained from N₂O titration (in m² g⁻¹_{Ni}) for Ni/Al₂O₃ catalyst samples.

At the same time, increasing the Ni loading reduces the BET area continuously from 86 m² g⁻¹ for 0.04 g g⁻¹ to 62 m² g⁻¹ for 0.24 g g⁻¹. Such a linear decrease in surface area with increasing Ni loading suggests that Ni particles are deposited on the external surface. The observed non-linearity of the Ni surface area per Ni mass can be attributed to several different factors. Firstly, the titration with N₂O is an exothermic reaction. Especially, for a Ni loading of 0.24 g g⁻¹ small temperature increases were observed during the initial pulses. It stands to reason that the local temperature around the titrated surface will have increased more than the overall bed temperature. Higher temperatures are known to lead to bulk oxidation in addition to surface titration.⁴¹ The total Ni surface increases disproportionately, when the loading is increased from 0.12 g g⁻¹ to 0.24 g g⁻¹ (see Table 3.1 and Figure B2). A certain percentage of this increase will be due to bulk oxidation contributing to the measured N₂O consumption.

Secondly, bimodal size distributions of metal particles on catalyst supports have frequently been reported in literature.⁴⁵⁻⁴⁸ Therefore, the development of a bimodal particle distribution could also contribute to the observed trend: At first the Ni particles are small and highly dispersed. A higher loading initially leads mainly to an increase of the average size. Adding more Ni to the support again causes the generation of smaller particles, which increases the average dispersion again.

To further elucidate the structure of the Ni on the surface, STEM-EDX measurements were carried out. To mimic the conditions before N₂O titration as best as possible, the samples underwent the same reduction procedure and were then passivated starting with an oxygen concentration of 0.2%, as described in the experimental section. At the same time, this opportunity was used to gauge the impact of passivation by also analyzing samples that were

passivated with an initial concentration of 3% O₂. The measured particle size distributions are shown in Figure 3.3.

Firstly, it must be noted, that the statistical uncertainty of these distributions cannot be neglected, because around 200 particles were measured for each sample. The observed distributions should be considered more as an indication. Nevertheless, the results of these measurements support the interpretation of the results of the N₂O titration. It can be observed, that for an initial O₂ concentration of 0.02% an increase in Ni loading from 0.04 to 0.08 g g⁻¹ leads to a significantly broader size distribution. Indeed, this is the only mildly treated sample with a considerable portion of particles of around 20 nm. For higher Ni loadings, the size distribution becomes more narrow and defined again.

When comparing the results for different initial O₂ concentrations, the higher loadings are more of interest, however. The samples with Ni loadings of 0.12 and 0.24 g g⁻¹ are the those, where an increase in the average Ni size is implied for higher initial O₂ concentrations during passivation. For the other two samples, no significant impact of the initial O₂ concentration was observed. Thus, noticeable sintering appears to be particularly problematic at elevated Ni loadings.

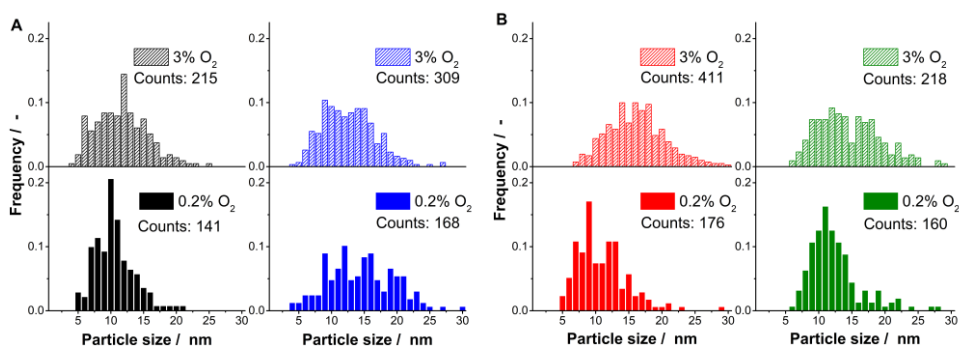


Figure 3.3: Observed Ni particle size distributions from STEM-EDX for initial O₂ concentrations of 0.2% (filled bars) and 3% (patterned bars). From left to right: 0.04, 0.08 (both A), 0.12 and 0.24 g g⁻¹ (both B).

3.3.2 Catalytic activity

Catalytic tests were carried out at a temperature of 650 °C. At this temperature coke formation is thermodynamically favored. This operating regime allows for a quicker identification of subtle differences in the morphology of the Ni surface between the different samples. In a first step, all four catalysts were tested in the standard procedure where the reduction takes place immediately prior to the catalytic run in the same reactor.

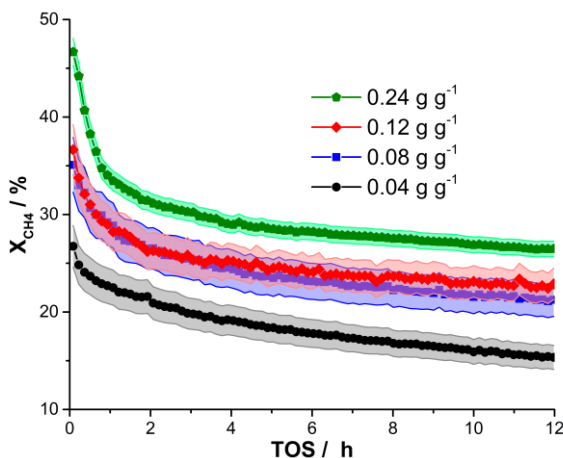


Figure 3.4: Methane conversion over TOS for Ni/Al₂O₃ catalysts pre-reduced in the reactor at 800 °C (Conditions: 10 mg sample, 650 °C, 100 mL min⁻¹ (25% CH₄, 25% CO₂ in N₂); highlighted areas represent the observed experimental error).

For these “baseline” measurements the conversion of methane as a function of time-on-stream during dry reforming over Ni/Al₂O₃ is shown in Figure 3.4. The catalytic activity of the samples increases with Ni loading. Interestingly though, increasing the loading of Ni from 0.08 g g⁻¹ to 0.12 g g⁻¹ has only a minor effect on the methane conversion. Somewhat faster deactivation at longer runtimes can be noted for the catalyst with 0.08 g g⁻¹ Ni loading. For higher Ni loadings the initial deactivation curve is steeper than that for 0.04 g g⁻¹. After the initial period of deactivation however (i.e. after 2-3 h TOS) the different curves can almost be seen as the same curve shifted vertically. It should also be noted that the catalyst particle size was varied during the initial phase of catalyst optimization (down to 100-150 μm). No signs of mass transport limitations could be observed.

The effect of passivation and reactivation depends substantially on the Ni loading of the catalyst (Figure 3.5). For the highest loading of 0.24 g g⁻¹ a reduction in conversion can be observed already after a passivation treatment starting with 1% O₂. Reducing the loading to 0.08 g g⁻¹ or 0.12 g g⁻¹ leads to no visible impact of the passivation on the conversion.

Interestingly, for the lowest loading of 0.04 g g⁻¹, passivation and reactivation lead to an increased conversion, comparable to that of the 0.08 g g⁻¹ sample.

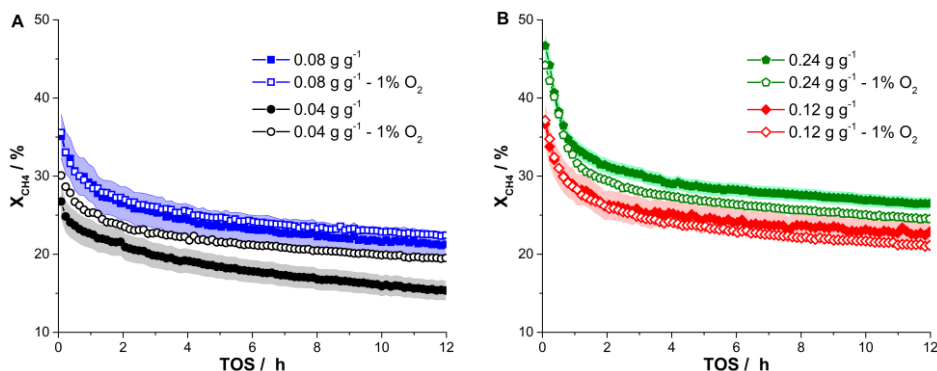


Figure 3.5: Methane conversion over TOS for catalysts purely reduced in the reactor (closed symbols) or with previous reduction and passivation starting with 1% O₂ (half-open symbols), separated for 0.04 and 0.08 g g⁻¹ (A) and 0.12 and 0.24 g g⁻¹ (B) (10 mg sample, 650 °C, 100 mL min⁻¹ (25% CH₄, 25% CO₂ in N₂)).

STEM-EDX analysis already indicated sintering of Ni particles during passivation for higher Ni loadings and higher initial O₂ concentrations. Consequently, the differences in the catalyst activity can be attributed to the overheating of metal particles during catalyst passivation. If the loading is high enough, such as for 0.24 g g⁻¹, enough heat is generated even on a 25 mg-scale to cause noticeable sintering of Ni particles and thus a reduction of catalytic activity. If the overall amount of Ni is lower, less heat is generated and little or no sintering takes place. The increase in catalytic activity for 0.04 g g⁻¹ has a different origin. Here the existence of less reducible Ni species such as NiAl₂O₄ needs to be taken into account.⁴⁹ While NiAl₂O₄ itself is not as easy to reduce as NiO, successive redox cycles have been shown to reduce such Ni species even below the nominal reduction temperature of NiAl₂O₄.⁵⁰ 0.04 g g⁻¹ is the system with the highest dispersion of Ni and consequently the largest Ni-Al₂O₃ interface. This explains a higher percentage of NiAl₂O₄ for 0.04 g g⁻¹ and a higher impact of a cyclic redox treatment.

The onset of sintering for 0.24 g g⁻¹ even with our mildest passivation procedure makes this sample a good starting point for further study. If a mild passivation procedure already causes overheating, a higher initial O₂ concentration should exacerbate local overheating even further. To verify this hypothesis, we performed catalytic experiments on 0.24 g g⁻¹ after reduction and passivation with different initial O₂ concentrations. However, when we increased the initial O₂ concentration during the passivation of 0.24 g g⁻¹, we noted no impact on the catalytic activity in the conversion plots. A further drop in activity was only

observable, when we increased the overall catalyst amount from 25 mg to 400 mg during reduction and passivation. This was done to increase the local peak temperatures during passivation further due to scale effects.

The conversion profiles and with the coke contents determined after the respective runs are shown in Figure 3.6. and Figure 3.7, respectively. The coke content after reaction is more sensitive to the exact conditions used during catalyst passivation. Compared to the reference measurement, a sample that underwent mild passivation contains more coke (61 wt.% vs. 52 wt.%). Increasing the initial O_2 concentration during passivation to 3% increases the coke content even further. Compared to this, a sample directly exposed to air after reduction contains a similar amount of coke (69 vs. 67 wt.%). However, when the overall catalyst amount was scaled to 400 mg, the direct exposure to air led to a significant drop in coke formation.

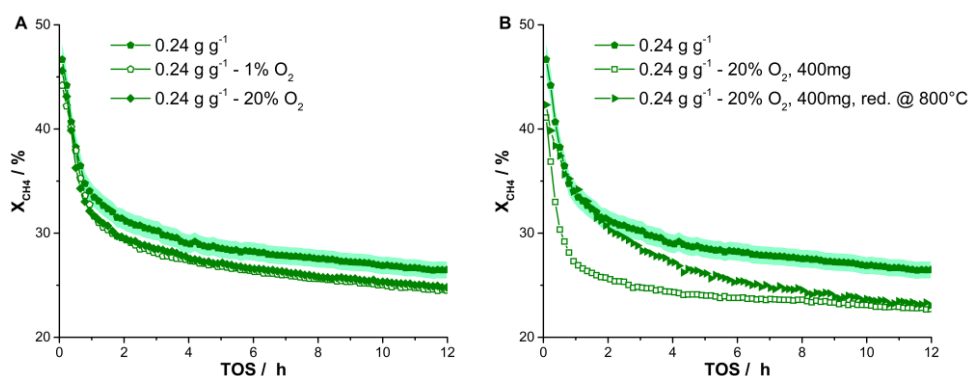


Figure 3.6: Impact of the initial O_2 concentration during passivation on a 25 mg scale on methane conversion (A) for 0.24 g g^{-1} and the effect of a 400 mg scale (B) (10 mg sample, $650 \text{ }^\circ\text{C}$, 100 mL min^{-1} , 25% CH_4 , 25% CO_2 in N_2).

This result on a 400 mg scale may not be discussed in isolation. If the catalyst is again reduced at $800 \text{ }^\circ\text{C}$ for 1 h before reaction (instead of heated in H_2 to $650 \text{ }^\circ\text{C}$), the catalytic activity is somewhat higher. However, the catalyst deactivation is more pronounced than when passivation is carried out on a smaller scale and after 12 h of reaction the conversion is comparable, regardless of the reduction temperature. At the same time a reduction at higher temperatures means that the coke content once again reaches almost 70 wt.%.

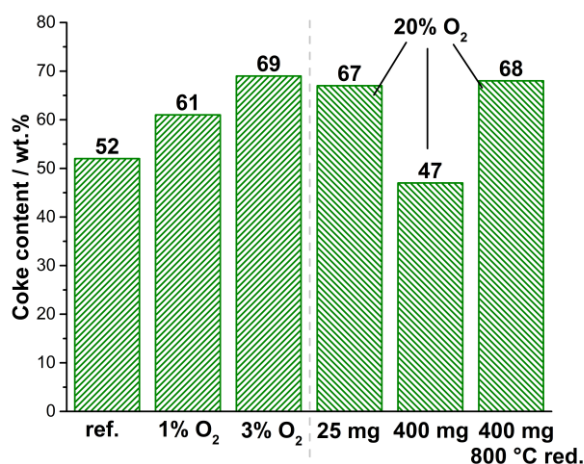


Figure 3.7: Impact of the different passivation procedures on the coke content after reaction (10 mg sample, 650 °C, 100 mL min⁻¹, 25% CH₄, 25% CO₂ in N₂).

These results fit nicely with the hypothesis of sintering due to local overheating. If the Ni particles sinter, the larger Ni particles cause more coke formation. The observations for the passivation on a 400 mg scale show that too much heat generation causes additional changes in the catalyst. It seems that then more stable oxidic Ni species are formed that need higher temperatures to reduce. The data on coke formation are not in agreement with the typical observations on NiAl₂O₄ catalysts. Different research groups reported highly stable methane reforming catalysts with little coke formation when reducing NiAl₂O₄.^{19, 51} If NiAl₂O₄ formation did take place, it was accompanied by considerable Ni sintering. The reduction of smaller Ni-containing species could not have caused an increase of the coke content by 20 wt.%.

This closer analysis of the sample 0.24 g g⁻¹ thus shows the effects that passivation can already have when operating on a scale of 25 mg. The samples with a lower overall Ni loading can be used to elucidate, how quickly overheating during passivation causes Ni sintering. We repeated the variation of the initial O₂ concentration during passivation for the remaining samples. As before, the initial O₂ concentration during passivation does not affect the conversion when passivating 25 mg (Figure B6). However, a closer analysis of the coke content after reaction provides more insight as can be seen in Figure 3.8.

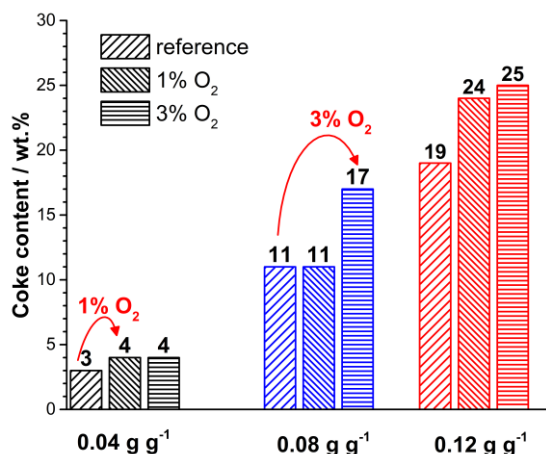


Figure 3.8: Coke content after reaction for Ni loadings (up to 0.12 g g^{-1}) and different passivation procedures, 10 mg sample, $650 \text{ }^\circ\text{C}$, 100 mL min^{-1} (25% CH_4 , 25% CO_2 in N_2).

If the loading of Ni is kept sufficiently low (0.04 g g^{-1}), passivation procedures starting at 1% or 3% do not lead to an increase in the coke content. If the Ni content is increased to 0.08 g g^{-1} , an initial O_2 concentration of 1% is still mild enough, while 3% lead to higher coke contents. For an overall loading of 0.12 g g^{-1} even 1% of O_2 is too harsh, causing an immediate increase in coking. To put this result into perspective, 25 mg of sample with a Ni loading of 0.12 g g^{-1} is equivalent to a total Ni amount of approx. 2.4 mg. The amount of Ni actually oxidized during passivation will be even smaller. Therefore, it can be said that the existence of overheating during the passivation of Ni/ Al_2O_3 systems is almost independent of scale. This must be taken into account when using passivation and reactivation during catalyst characterization to obtain relevant results.

At the same time, these results highlight the value of using dry reforming as a model reaction to check for sintering. Through this approach, sintering could already be observed for a loading of 0.08 g g^{-1} and an initial O_2 concentration of 3%. A STEM-EDX analysis of the same sample did not show any signs of sintering.

3.4 Conclusion

Four Ni/Al₂O₃ catalysts with different loadings of Ni were synthesized via incipient wetness impregnation. A high Ni dispersion for all catalysts was confirmed with TPR, BET, TEM and N₂O titration techniques. The impact of catalyst passivation and reactivation on the catalytic properties of the Ni/Al₂O₃ materials was evaluated in methane dry reforming. Despite the low catalyst amounts used for the experiments, a strong effect of the passivation conditions was observed. We suggest that this is mostly caused by a local overheating during the passivation and consequently sintering of the Ni particles. This in turn enhances the coking for higher Ni loadings and/or higher initial O₂ concentrations. Importantly, problems during the passivation of Ni/Al₂O₃ catalysts are almost independent of the catalyst bed volume and can occur even in low-volume lab scale reactors. Only for very low loadings or sufficiently mild passivation procedures can a constant Ni dispersion be achieved. Thus, even when working on a laboratory scale, an initial O₂ concentration during passivation of lower than 1% is advisable. For catalysts with high Ni loadings or in larger quantities, significantly lower O₂ concentrations may be necessary. Furthermore, this study highlights how dry reforming of methane can be used as a probe reaction to compare the Ni surface area of different samples. The amount of sample necessary is one order of magnitude lower than for classical measurement techniques such as H₂ chemisorption.

3.5 References

1. J. R. Rostrup-Nielsen, J. Sehested and J. K. Nørskov, in *Adv. Catal.*, Academic Press, 2002, vol. 47, pp. 65-139.
2. M. Akri, S. Zhao, X. Li, K. Zang, A. F. Lee, M. A. Isaacs, W. Xi, Y. Gangarajula, J. Luo, Y. Ren, Y.-T. Cui, L. Li, Y. Su, X. Pan, W. Wen, Y. Pan, K. Wilson, L. Li, B. Qiao, H. Ishii, Y.-F. Liao, A. Wang, X. Wang and T. Zhang, *Nat. Comm.*, 2019, **10**, 5181.
3. J. M. Ginsburg, J. Piña, T. El Solh and H. I. de Lasa, *Ind. Eng. Chem. Res.*, 2005, **44**, 4846-4854.
4. C. Vogt, M. Monai, G. J. Kramer and B. M. Weckhuysen, *Nat. Catal.*, 2019, **2**, 188-197.
5. W. L. Vrijburg, J. W. A. van Helden, A. Parastaev, E. Groeneveld, E. A. Pidko and E. J. M. Hensen, *Catal. Sci. Tech.*, 2019, **9**, 5001-5010.
6. Z. Zhang, T. Wei, G. Chen, C. Li, D. Dong, W. Wu, Q. Liu and X. Hu, *Fuel*, 2019, **250**, 176-193.

7. W. L. Vrijburg, E. Moioli, W. Chen, M. Zhang, B. J. P. Terlingen, B. Zijlstra, I. A. W. Filot, A. Züttel, E. A. Pidko and E. J. M. Hensen, *ACS Catal.*, 2019, **9**, 7823-7839.
8. W. L. Vrijburg, J. W. A. van Helden, A. J. F. van Hoof, H. Friedrich, E. Groeneveld, E. A. Pidko and E. J. M. Hensen, *Catal. Sci. Tech.*, 2019, **9**, 2578-2591.
9. M. J. F. M. Verhaak, A. J. van Dillen and J. W. Geus, *Catal. Lett.*, 1994, **26**, 37-53.
10. Y. Nakagawa, H. Nakazawa, H. Watanabe and K. Tomishige, *ChemCatChem*, 2012, **4**, 1791-1797.
11. E.-J. Shin and M. A. Keane, *Ind. Eng. Chem. Res.*, 2000, **39**, 883-892.
12. J. Xiong, J. Chen and J. Zhang, *Catal. Commun.*, 2007, **8**, 345-350.
13. K. Liu, J. Pritchard, L. Lu, R. van Putten, M. W. G. M. Verhoeven, M. Schmitkamp, X. Huang, L. Lefort, C. J. Kiely, E. J. M. Hensen and E. A. Pidko, *Chem. Commun.*, 2017, **53**, 9761-9764.
14. P. Andreas, N. Fatemeh, R. Dennis, L. Michal and G. Roger, *ChemCatChem*, 2011, **3**, 598-606.
15. C. Vogt, M. Monai, E. B. Sterk, J. Palle, A. E. M. Melcherts, B. Zijlstra, E. Groeneveld, P. H. Berben, J. M. Boereboom, E. J. M. Hensen, F. Meirer, I. A. W. Filot and B. M. Weckhuysen, *Nat. Comm.*, 2019, **10**, 5330.
16. K. Y. Koo, J. H. Lee, U. H. Jung, S. H. Kim and W. L. Yoon, *Fuel*, 2015, **153**, 303-309.
17. K. Y. Koo, H.-S. Roh, Y. T. Seo, D. J. Seo, W. L. Yoon and S. B. Park, *Appl. Catal., A*, 2008, **340**, 183-190.
18. Z. Mosayebi, M. Rezaei, A. B. Ravandi and N. Hadian, *Int. J. Hydrogen Energy*, 2012, **37**, 1236-1242.
19. J. L. Rogers, M. C. Mangarella, A. D. D'Amico, J. R. Gallagher, M. R. Dutzer, E. Stavitski, J. T. Miller and C. Sievers, *ACS Catal.*, 2016, **6**, 5873-5886.
20. L. Fratallocchi, G. Groppi, C. G. Visconti, L. Lietti and E. Tronconi, *Catal. Today*, 2020, **342**, 79-87.
21. A. L. Imbault and K. J. Smith, *Catal. Lett.*, 2016, **146**, 1886-1891.
22. US20060154813A1, 2002.
23. US9387463B2, 2013.
24. US6096790A, 1997.
25. C. H. Bartholomew and R. J. Farrauto, *J. Catal.*, 1976, **45**, 41-53.
26. A. Gil, A. Diaz and M. Montes, *J. Chem. Soc., Faraday Trans.*, 1991, **87**, 791-795.
27. B. W. Hoffer, A. Dick van Langeveld, J.-P. Janssens, R. L. C. Bonn e, C. M. Lok and J. A. Moulijn, *J. Catal.*, 2000, **192**, 432-440.

28. F. Huber, Z. Yu, S. Lögdberg, M. Rønning, D. Chen, H. Venvik and A. Holmen, *Catal. Lett.*, 2006, **110**, 211-220.
29. M. Popowicz, W. Celler and Treszcza.E, *Int Chem Eng*, 1966, **6**, 63-&.
30. J. T. Richardson and R. J. Dubus, *J. Catal.*, 1978, **54**, 207-218.
31. B. Vos, E. Poels and A. Blik, *J. Catal.*, 2002, **207**, 1-9.
32. M. Wolf, N. Fischer and M. Claeys, *Catal. Today*, 2016, **275**, 135-140.
33. C. Vogt, E. Groeneveld, G. Kamsma, M. Nachtegaal, L. Lu, C. J. Kiely, P. H. Berben, F. Meirer and B. M. Weckhuysen, *Nat. Catal.*, 2018, **1**, 127-134.
34. A. N. Subbotin, B. S. Gudkov, Z. L. Dykh and V. I. Yakerson, *React. Kinet. Catal. Lett.*, 1999, **66**, 97-104.
35. A. N. Subbotin, B. S. Gudkov and V. I. Yakerson, *Russ. Chem. Bull.*, 2000, **49**, 1373-1379.
36. S. Arora and R. Prasad, *RCS Adv.*, 2016, **6**, 108668-108688.
37. Technologies that do more with less, <https://www.linde-engineering.com/en/about-linde-engineering/success-stories/technologies-more-with-less.html>, (accessed Nov. 19, 2019).
38. H. Düdder, K. Kähler, B. Krause, K. Mette, S. Kühl, M. Behrens, V. Scherer and M. Muhler, *Catal. Sci. Tech.*, 2014, **4**, 3317-3328.
39. T. Roussi re, PhD thesis, Karlsruhe Institute of Technology, 2013.
40. H. S. Bengaard, J. K. Nørskov, J. Sehested, B. S. Clausen, L. P. Nielsen, A. M. Molenbroek and J. R. Rostrup-Nielsen, *J. Catal.*, 2002, **209**, 365-384.
41. S. Tada, M. Yokoyama, R. Kikuchi, T. Haneda and H. Kameyama, *J. Phys. Chem. C*, 2013, **117**, 14652-14658.
42. A. Peters, F. Nouroozi, D. Richter, M. Lutecki and R. Gläser, *ChemCatChem*, 2011, **3**, 598-606.
43. C. Li and Y.-W. Chen, *Thermochim. Acta*, 1995, **256**, 457-465.
44. B. Mile, D. Stirling, M. A. Zammitt, A. Lovell and M. Webb, *J. Mol. Catal.*, 1990, **62**, 179-198.
45. D. J. Lensveld, J. Gerbrand Mesu, A. Jos van Dillen and K. P. de Jong, *Microporous Mesoporous Mater.*, 2001, **44-45**, 401-407.
46. S. Sun, K. Fujimoto, Y. Zhang and N. Tsubaki, *Catal. Commun.*, 2003, **4**, 361-364.
47. P. Tabib Zadeh Adibi, V. P. Zhdanov, C. Langhammer and H. Grönbeck, *J. Phys. Chem. C*, 2015, **119**, 989-996.
48. Y. Zhang, Y. Liu, G. Yang, S. Sun and N. Tsubaki, *Appl. Catal., A*, 2007, **321**, 79-85.
49. T. Numaguchi, H. Eida and K. Shoji, *International Journal of Hydrogen Energy*, 1997, **22**, 1111-1115.
50. L. Silvester, D. Ipsakis, A. Antzara, E. Heracleous, A. A. Lemonidou and D. B. Bukur, *Energy Fuels*, 2016, **30**, 8597-8612.

51. L. Zhou, L. Li, N. Wei, J. Li and J.-M. Basset, *ChemCatChem*, 2015, **7**, 2508-2516.

Appendix B

B1 Surface characterization

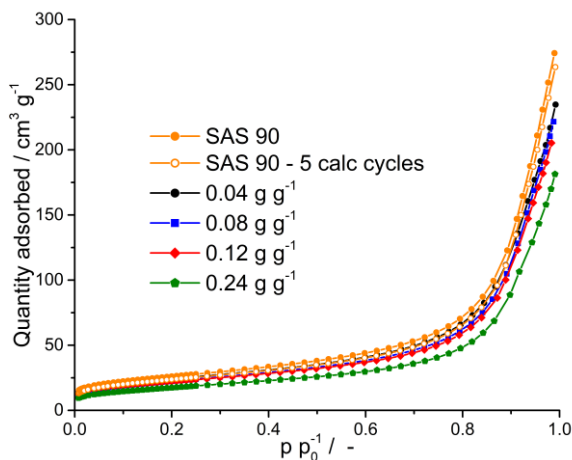


Figure B1: Adsorption branches of the N₂ isotherms of all tested catalysts, the bare support and the support after five cycles of calcination at 700 °C for 5 h each.

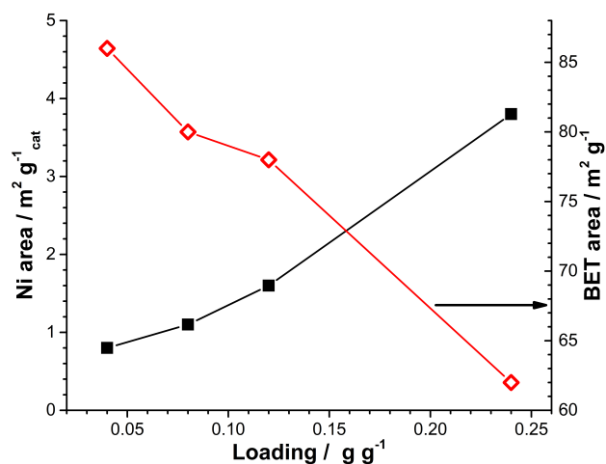


Figure B2: BET surface area and Ni surface area obtained from N₂O titration (in m² g⁻¹Ni) for Ni/ Al₂O₃ catalyst samples.

B2 TEM images

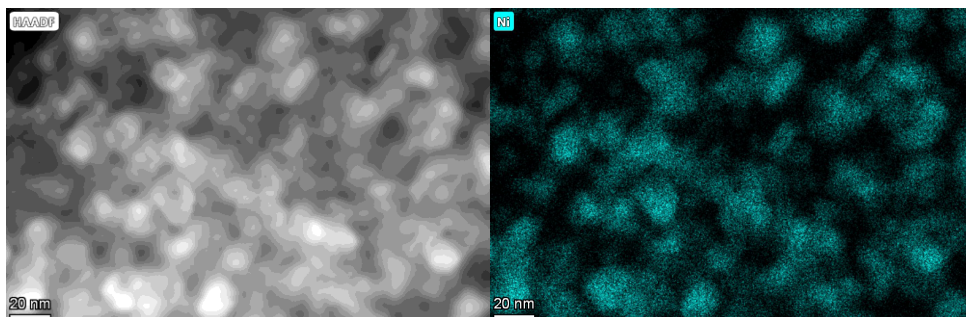


Figure B3: Representative STEM-EDX images for the sample with a Ni loading of 0.24 g g^{-1} , passivated with 0.2% O_2 .

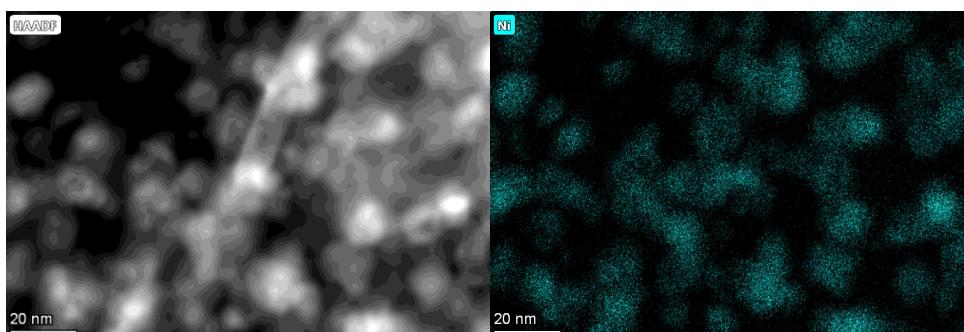


Figure B4: Representative STEM-EDX images for the sample with a Ni loading of 0.08 g g^{-1} , passivated with 0.2% O_2 .

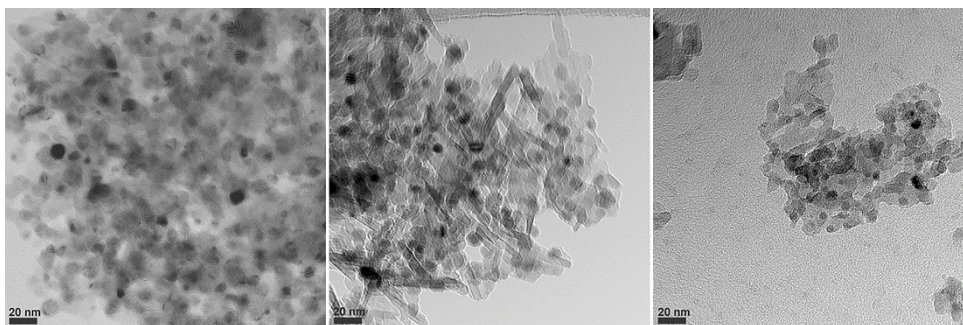


Figure B5: TEM bright field images of 0.24 g g⁻¹ (left), 0.12 g g⁻¹ (middle) and 0.04 g g⁻¹ (right) after reduction at 800 °C and passivation in 0.2% O₂.

B3 Catalytic activity

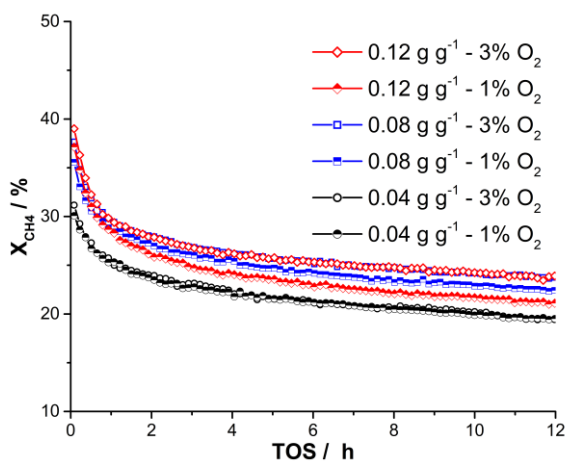


Fig. B6: Comparison of the catalytic activity after passivation starting with 1% O₂ vs. 3% O₂

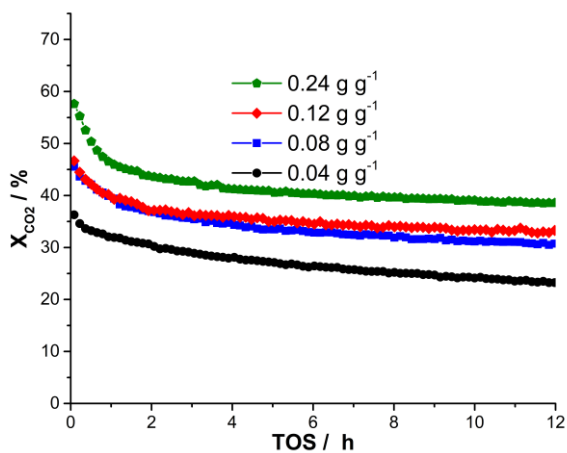
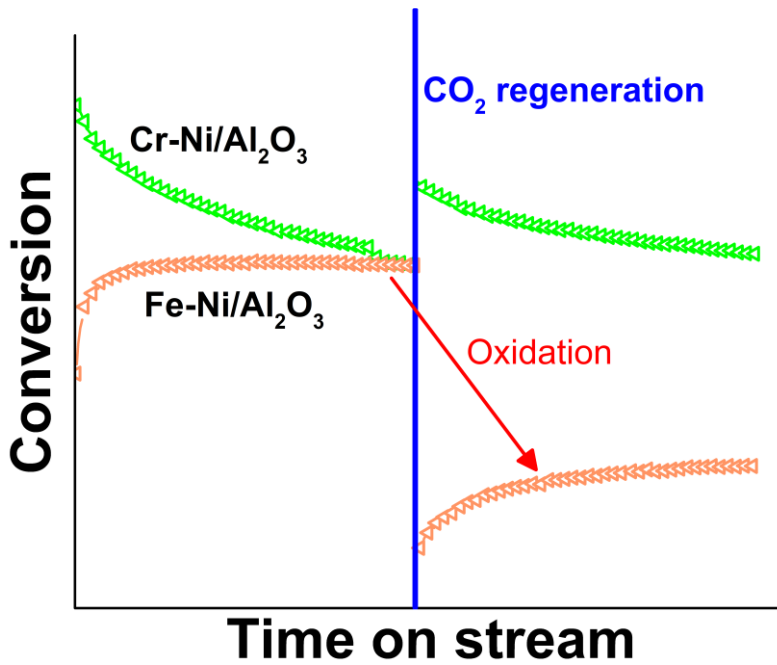


Fig. B7: CO₂ conversion for the catalysts without a passivation step between reduction and catalytic reaction

Chapter 4

Impact of promoter addition on the regeneration of Ni/Al₂O₃ dry reforming catalysts



Industrial-scale reforming of methane is typically carried out with an excess of oxidant to suppress coking of the catalyst. On the other hand, many academic studies on dry reforming employ a CO_2/CH_4 ratio of unity to quickly observe coking which can be reduced by adding a catalyst promoter. In this work Ni/ Al_2O_3 catalysts were tested for dry reforming of methane ($\text{CO}_2/\text{CH}_4 = 1$) with additional regeneration steps to test the resistance against an oxidation treatment. Thereby, we wanted to evaluate catalyst stability for industrial relevance. The effects of three promoters, Cr, Mn and Fe, that differ in their degree of CO_2 interaction, are compared. A higher iron loading on Ni/ Al_2O_3 leads to higher stability in dry reforming with lower coke formation. However, the higher the concentration of a promoter with high CO_2 affinity, the quicker the catalyst is oxidized during regeneration with CO_2 . Subsequent reduction of a catalyst oxidized with CO_2 leads to considerable sintering in all cases. This sintering induces formation of more coke during dry reforming. On such sintered samples only highly effective promoters in large concentrations still have a noticeable effect compared to unpromoted Ni/ Al_2O_3 .

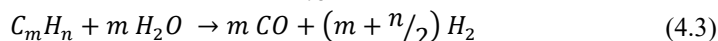
This chapter is based on the following publication:
R. Franz, D. Pinto, E. A. Uslamin, A. Urakawa and E. A. Pidko, *submitted*

4.1 Introduction

Dry reforming of methane is a reaction that has received a lot of attention in academic and industrial research in recent years. The growing issue of global warming requires society to find an effective approach to decrease the amount of CO₂ emissions into the atmosphere. One potential approach to achieve a reduction in emissions is to use CO₂ as a chemical resource. Good examples for this approach are reactions such as the hydrogenation of CO₂ to hydrocarbons^{1,2} and methanol³⁻⁵ or dry reforming of methane (DRM).⁶⁻⁸ The latter refers to the combined conversion of methane and CO₂ to synthesis gas or syngas:



This reaction has several important advantages. Firstly, not only CO₂ is used, but also methane, which is also a highly active greenhouse gas.⁹ Secondly, synthesis gas is an intermediate for many large-scale chemical reactions and widely synthesized via steam reforming of hydrocarbons:



DRM therefore represents a possible CO₂ utilization route that can draw on a vast amount of expertise and infrastructure already available within the chemical industry. In contrast to steam reforming of methane (SRM) the additional energy input for water evaporation is not necessary for DRM.⁸ Nevertheless, this reaction is only slowly being implemented in industry. The feed in DRM is more carbon rich than in SRM, leading to a higher propensity to coke formation and catalyst deactivation.^{8,10} The DRYREF process developed by BASF and Linde is less harsh than pure dry reforming since both steam and CO₂ are used as the oxidant. Even so, existing steam reforming catalysts were not sufficiently resistant to coke formation under these conditions, requiring an extensive period of catalyst optimization.¹¹

Commercial steam reforming catalysts are mostly Ni-based since it offers an acceptable compromise between activity, stability, cost and availability.^{8,12} To prevent excessive coke formation, different strategies have been reported in literature. The most common approach in catalyst design is to add another metal to the catalyst as a promoter. These metals can improve the performance in several different manners. It has been shown, that coke is mainly formed on larger Ni particles or on step-edge sites on the Ni surface.^{13,14} Promoters block such highly reactive sites and thus suppress coke formation. Most popular promoters of this type are alkali and earth alkali metals.¹⁵⁻¹⁸ A similar mode of action has also been reported for other common metal promoters such as Mn or Sn.¹⁹⁻²¹

Besides the site-blocking, promoters can introduce other beneficial effects. Alkali metals can enhance CO₂ adsorption via a carbonate cycle.^{16, 22} Mn, Sn and several noble metals stabilize small Ni particles.^{19, 23-26} Additionally, Mn has also been reported to increase the CO₂ affinity of the catalyst.²¹ A control over the particle size can also be achieved via the selection of catalyst support materials.^{27, 28} Lastly, promoters can bring about enhanced redox reactivity to help coke removal through a redox cycle of the promoter, i.e. via a Mars-van Krevelen mechanism. The prime example for such an effect is the addition of Fe to a Ni-based catalyst, which allows either for a chemical looping process or continuous operation with little coke deposition.²⁹⁻³²

Despite decades of research, catalyst deactivation due to coking is a persistent problem in DRM. This makes cyclic operation, in which the catalyst is periodically regenerated, an attractive strategy to manage carbon formation. Various procedures utilizing different regeneration gases and conditions are available.³³⁻³⁶ Coke can be removed from the catalyst surface either by oxidation with CO₂ or O₂ or by methanation with H₂. Oxidative regeneration is preferable in an industrial setting as it does not affect the overall yield of the target product H₂. A common drawback of this approach is the considerable sintering of the metal particles due to oxidation.^{33, 37} *Takenaka et al.* investigated the influence of the support on Ni stability in cycles of methane decomposition and coke gasification with CO₂.³⁶ Ni/SiO₂ was found to be the most prone to sintering. The increase of particle sizes due to the cyclic operation occurred to a lesser extent for Ni/TiO₂ and Ni/Al₂O₃. *Düdder et al.* demonstrated that CO₂ regeneration allows for the full recovery of the initial activity of a Ni/MgAlO_x catalyst.³⁴ However, no information on the effect of the regeneration on the Ni particles was presented.

In-situ XAS studies by *Steib et al.* demonstrated that a catalyst regeneration with CO₂ at 800 °C oxidizes the Ni phase on various supports.^{35, 38} Exposure of Ni/SiO₂ and Ni/ZrO₂ to the original reaction mixture of CH₄ and CO₂ is sufficient to reduce the Ni again. In contrast, more Ni is in the oxidized state in the second reaction cycle than in the first cycle for Ni/Al₂O₃.

This information on Ni oxidation during catalyst regeneration raises the question of what the impact of promoter addition is on catalyst stability during regeneration. The mechanisms, by which promoters increase catalyst stability, include differing degrees of interaction with CO₂. Therefore, in this work we compare the effect of promoters that vary in their degree of interaction with CO₂ on the stability of Ni/Al₂O₃ catalysts. Literature led us to Cr, Mn and Fe as representative promoters since they present a step-wise increase of the interaction with CO₂. Cr is not reported to noticeably increase the interaction of Ni-catalysts with CO₂, while Mn enhances the CO₂ adsorption on Ni/Al₂O₃ catalysts and Fe is redox active.^{20, 21, 31, 32} Our results show that the more the promoter interacts with CO₂ the more the catalyst is deactivated during a regeneration procedure consisting of a short exposure to a stream of diluted CO₂. We assume this deactivation to be due to catalyst oxidation. An additional reduction of a thus fully oxidized catalyst causes a significant increase in coke formation during dry reforming

compared to a fresh catalyst. Only high loadings of effective promoters limit this increase in coking after regeneration to a reasonable degree.

It must also be mentioned that commercial methane reforming is typically carried out with an excess of oxidant to suppress coke formation.⁷ The ensuing concentration gradient over the length of the catalyst bed results in an oxidizing atmosphere in the upper section of the catalyst bed where little methane conversion has taken place.³⁹ Thus, catalyst stability under oxidative environments is a relevant parameter in general. The research in this work can be seen as a set of model experiments investigating this stability making the conclusions relevant beyond the immediate application of catalyst regeneration.

4.2 Experimental

4.2.1 Chemicals

The following chemicals were used in this work: Ethylenediaminetetraacetic acid (EDTA, ThermoFisher 99%), NH₃ solution (VWR, 25 wt.%), γ -Al₂O₃ catalyst support (Alfa Aesar), Ni(NO₃)₂ · 6H₂O (Merck, analysis quality), Mn(NO₃)₂ · 4H₂O (Acros, analysis quality), Cr(NO₃)₃ · 9H₂O (Sigma Aldrich, 99%), Fe(NO₃)₃ · 9H₂O (Sigma Aldrich 98%).

All materials were used as received except for NH₃ (aq) and Al₂O₃. NH₃ (aq) was diluted with demineralized water to achieve concentrations of 12 wt.% and 5 wt.%. Al₂O₃ extrudates were ground to a particle size below 212 μ m and calcined at 800 °C for 4 h (10 °C min⁻¹ heating rate) before impregnation.

4.2.2 Catalyst synthesis

All samples were synthesized via sequential incipient wetness impregnation. In a typical synthesis EDTA and Ni(NO₃)₂ or the nitrate salt containing the promoter were dissolved in an aqueous ammonia solution and impregnated on the support. After each impregnation the sample was dried at 80 °C for 6 h and then calcined at 700 °C for 5 h (10 °C min⁻¹ heating rate). The solubility of the different nitrates and EDTA together in the aqueous ammonia solution varied. The amount of EDTA also had to be varied depending on the promoter to achieve reproducibility of the catalytic tests. For Ni, 12 wt.% NH₃ and a Ni/EDTA molar ratio of unity were used. The promoter was always impregnated before the nickel and in some cases over multiple impregnation steps. The catalysts with promoter are named according to the system y.yyX1Ni, in which y.yy is the molar ratio of the promoter X (Cr, Mn or Fe) to Ni. The final, optimized values are given in Table 4.1:

Table 4.1: Overview of the synthesis parameters

Sample name	Ni loading [g g _{support} ⁻¹]	$n(M^{n+})/n(Ni^{2+})$	$n(EDTA)/n(M^{n+})$	c(NH ₃) [wt.%]
REF	0.08	0	--	12%
1Mn1Ni	0.08	1	2	12%
0.5Mn1Ni	0.08	0.5	2	12%
0.25Mn1Ni	0.08	0.25	2	12%
1Cr1Ni	0.08	1	3	12%
0.5Cr1Ni	0.08	0.5	3	12%
0.25Cr1Ni	0.08	0.25	3	12%
1Fe1Ni	0.08	1	1	5%
0.5Fe1Ni	0.08	0.5	1	5%
0.25Fe1Ni	0.08	0.25	1	5%

4.2.3 Catalyst characterization

Temperature programmed reduction (TPR) was carried out in a home-built setup equipped with thermal conductivity detector (TCD) and mass spectrometer (MS). For TPR measurements, 100 mg of sample (particle size 212-355 μm) were filled into a quartz reactor (I.D. of 6 mm) and the reactor placed into the furnace. Afterwards, a flow of 30 mL min⁻¹ (10% H₂ in Ar) was started. The setup was heated to 950 °C with a ramp of 10 °C min⁻¹. H₂ consumption was monitored with the TCD downstream of the reactor.

CO₂ Temperature-programmed desorption (CO₂-TPD) was measured in the same setup as the TPR experiments. For each measurement 150 mg of sample (particle size 212-355 μm) were filled into a quartz reactor (I.D. of 6 mm) and the reactor placed into the furnace. In a first step, the sample was reduced using a flow of 30 mL min⁻¹ at 800 °C for 1 h (heating rate of 10 °C min⁻¹). Then the sample was cooled in 27 mL min⁻¹ of pure Ar to room temperature. After cooling, the sample was exposed to 25 mL min⁻¹ of CO₂ for 30 minutes. The flow was then switched again to 27 mL min⁻¹ of Ar and the system was purged until the CO₂ signal in a mass spectrometer downstream of the reactor was stable. Once the baseline was stable, the furnace temperature was increased to 800 °C with a rate of 10 °C min⁻¹.

NH₃-TPD was measured using a *Micromeritics Autochem II 2920* unit. For each measurement 200 mg of sample were loaded into the system and heated under H₂ flow to 800 °C (10 °C min⁻¹). After 1 h of reduction at this temperature the sample was cooled to a temperature of 200 °C under He flow. Once the sample was stabilized at this temperature the

flow was switched to 3% NH₃ in He and maintained for 1 h. Finally, after the exposure to NH₃, the flow was switched to He again and the sample was heated to 750 °C with a rate of 10 °C min⁻¹.

H₂-Chemisorption measurements were performed in a *Micromeritics ASAP 2020 C*. 400 mg of sample per measurement were loaded into the sample tube. The system was heated to 800 °C under H₂ flow (5 °C min⁻¹) and this temperature maintained for 1 h. The sample was then cooled to 35 °C and the H₂ uptake was measured. This was followed by two more measurement cycles for each sample. In the second cycle the samples were heated to 700 °C (5 °C min⁻¹) and exposed first to CO₂ for 30 min and then to H₂ for 30 minutes before cooling to measurement temperature. For the third cycle the original reduction procedure at 800 °C was used. To account for H₂ physisorption, all reported values are the difference in uptake between two consecutive H₂ chemisorption measurements with an evacuation step in between.

TEM images were obtained using a Jem JEOL 1400 transmission electron microscope. The equipment was operated at 120 kV using a single-tilt holder. Calcined catalysts were ground to a fine powder and dispersed in denatured ethanol. This dispersion was dropped onto Quantifoil R 1.2/1.3 holey carbon films supported on a Cu mesh.

4.2.4 Catalytic testing

The catalytic tests for dry reforming of methane were carried out in a single-reactor system. The reactor consists of a quartz tube (I.D. of 4 mm) in a furnace. Bronckhorst mass flow controllers upstream of the reactor control the flow of N₂, CH₄, CO₂ and H₂. Downstream of the reactor a compact GC equipped with a TCD was used for the online product analysis. Product separation was achieved using a micropacked column (ShinCarbon ST 80/100 2m, 0.53 mm I.D.). The conversion of methane and CO₂ was calculated using N₂ as the internal standard according to the following equation:

$$X_R = \frac{\left(\frac{A_R}{A_{N_2}}\right)_0 - \left(\frac{A_R}{A_{N_2}}\right)}{\left(\frac{A_R}{A_{N_2}}\right)_0} \quad (4.4)$$

where R is the reactant in question (either CH₄ or CO₂) and A is the peak area in the GC. In all experiments, 10 mg of sample (355-425 μm) were diluted in 140 mg of SiC (212-300 μm). This mixture was filled into the quartz reactor between two plugs of quartz wool and upstream of a 9 cm layer of SiC (212-425 μm). To pre-warm the feed a 7 cm bed of SiC (212-425 μm) was placed upstream of the catalytic bed. In all experiments the fresh

sample was heated in a stream of 10% H₂ in N₂ (50 mL min⁻¹) to 800 °C (10 °C min⁻¹) and reduced at this temperature for 1 h, before being cooled to 650 °C. Afterwards, the flow was switched to 100 mL min⁻¹ of 25% CH₄ and 25% CO₂ in N₂. Standard activity measurements consisted of 24 h of reaction. The sample was then either cooled down to room temperature or heated to 700 °C for a regeneration treatment. One treatment consisted of 30 min of CO₂ exposure (50 mL min⁻¹ of 40% CO₂ in N₂) followed by 30 min of reduction (50 mL min⁻¹ of 10% H₂ in N₂). The other regeneration protocol was an exposure to CO₂ of 4 min (50 mL min⁻¹ of 40% CO₂ in N₂). In all cases heating and cooling before and after the regeneration treatment were done under pure N₂ flow. A second reaction cycle of 24 h at 650 °C was added after the regeneration procedure if desired. Lastly, the entire system was cooled to room temperature under N₂ flow. After each catalytic experiment, the coke content of the sample was analyzed by TGA (Mettler-Toledo TGA/SDTA 851^e). For the activity measurements in standard dry reforming two different batches of catalyst were tested to determine the experimental error in both coke content and conversion.

The experiments to visually check for signs of catalyst oxidation under elevated CO₂ concentrations were carried out in two different setups. In one case 50 mg of undiluted catalyst (212–425 μm) were loaded into the setup described above and with the same amounts of SiC upstream and downstream of the catalyst bed. The catalyst was then reduced in 10% H₂ in N₂ (50 mL min⁻¹) at 800 °C for 1 h (10 °C min⁻¹). The reactor was afterwards cooled to 650 °C and the flow switched to 12.5% CH₄ and 25% CO₂ in N₂ (100 mL min⁻¹) and the reaction was carried out for 30 h.

Operando monitoring of the CO₂ regeneration was carried out in a different setup. It consists of a single quartz tube reactor (4 mm I.D.) in a furnace with Bronckhorst mass flow controllers upstream of the furnace. In this setup the quartz reactor is equipped with a steel jacket to ensure good heat transfer to the catalyst bed. This steel jacket contains an opening to allow for observation of the catalyst bed. Similarly, the wall of the furnace contains a hole above of which a digital microscope was positioned to take pictures of the catalyst bed during reaction. In total 50 mg of catalyst (212–425 μm) were placed in the reactor, heated to 800 °C in a flow of 50 mL min⁻¹ of H₂ (10 °C min⁻¹) and reduced at this temperature for 1 h. Afterwards the system was cooled to 650 °C and the sample exposed to 40 mL min⁻¹ of 10% CO₂ in He. During this time, the change in sample color was monitored with the digital microscope. Simultaneously, the outlet concentrations were measured with an ALPHA FTIR spectrometer (Bruker). For this the obtained data was Fourier-transformed and the absorbance peaks in the ranges of 2260–2280 cm⁻¹ and 2040–2060 cm⁻¹ used for CO₂ and CO quantification respectively. The degree of catalyst oxidation was calculated from the generated CO and the desired catalyst loading, using the following equation:

$$D_o(t) = \frac{n_{CO}(t)}{n_{Ni} + 1.5 * n_{Fe}} * 100 \quad (4.5)$$

in which $D_{O}(t)$ is the degree of oxidation at time t in %, $n_{CO}(t)$ the total molar amount of CO released until that time and n_{Ni} and n_{Fe} the molar amounts of Ni and Fe on the used sample. The factor of 1.5 stems from the assumption that Fe(0) is oxidized to Fe₂O₃. Ni(0) is assumed to be oxidized to NiO. The obtained pictures of the catalyst bed were processed with Adobe Photoshop 2018 (brightness and contrast) to highlight color changes in the catalyst bed.

4.3 Results and discussion

4.3.1 Catalyst characterization

Temperature-programmed reduction was carried out in a first step to obtain information on the reducibility of the promoted catalysts. The results in Figure 4.1 show that two peaks were detected for all samples containing the promoters Cr, Mn or Fe. The reduction at lower temperature takes place at 300-500 °C, depending on the sample, with a lower reduction temperature for the Cr-series. The second reduction occurs at 800-900 °C. For REF only a high-temperature reduction was detected and the intensity of the low-temperature peak increases with promoter loading. This clearly assigns the high-temperature reduction to Ni and the low-temperature reduction to the promoter. Especially for the Cr-containing samples the intensity of the promoter peak is more prominent in contrast to the other samples for which significantly less H₂ consumption could be measured.

Cr-Ni catalysts are known to form alloys upon reduction, making Cr(0) the probable final oxidation state.⁴⁰ At the same time, oxidized Cr can theoretically be present in different oxidation states up to Cr(VI). Considering the larger peak for Cr reduction compared to the other promoters, we assume that Cr is at least partially present in higher oxidation states than Cr(III). The changes in the Fe-series can at most be from Fe(III) to Fe(0) and these samples contain a significantly smaller promoter reduction peak.³² Reduction of supported Mn systems should lead to a maximum change in oxidation state from Mn(IV) to Mn(II).⁴¹

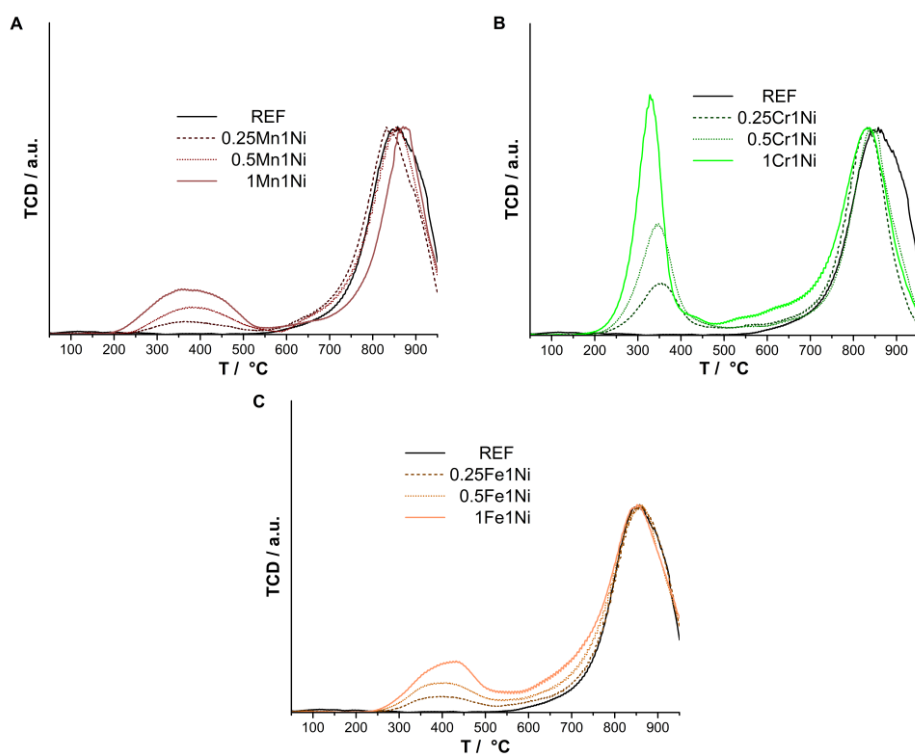


Figure 4.1: Temperature-programmed reduction of the as-prepared promoted Ni/Al₂O₃ samples: Mn-series (A), Cr-series (B) and Fe-series (C).

The promoters were added to the catalyst to increase the interaction of the catalyst with CO₂. To compare the influence of the different promoters on this parameter, temperature-programmed desorption of CO₂ (CO₂-TPD) was measured for the reference sample and all samples with a promoter/Ni ratio of unity. The resulting CO₂-signals shown in Figure 4.2 highlight that only the addition of manganese leads to a greater adsorption of CO₂ on the catalyst. Chromium and iron do not affect the CO₂ adsorption capacity to any significant degree. The total peak area is comparable for these two samples and the reference Ni/Al₂O₃. Therefore, when comparing the Cr-series and the Mn-series, an increase in CO₂ adsorption must be taken into account. For Fe-promoted Ni systems literature data show that at reaction conditions Fe increases the interaction via a redox cycle, which represents a noticeable increase of the interaction with CO₂.^{30, 32}

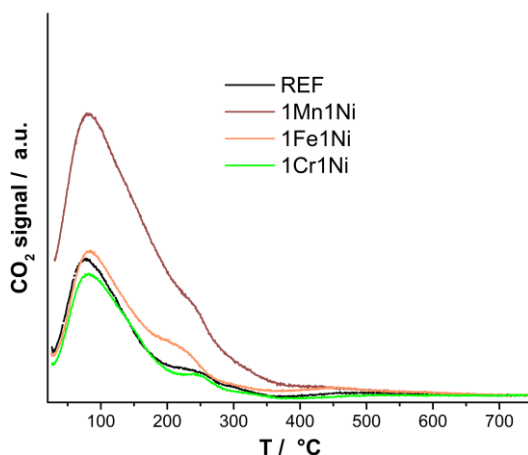


Figure 4.2: CO₂-TPD profiles for pure Ni/Al₂O₃ and all samples with a promoter/Ni ratio of unity

In addition, the catalysts were characterized with H₂ chemisorption. The promoter-Ni interactions can be evaluated by measuring the total metal surface area. Additionally, the regeneration procedures can be simulated in the setup and the impact on the metal surface area compared among the different promoters. The results are summarized in Figure 4.3. For each series of catalysts only the sample with the highest promoter loading was tested to determine trends. While the samples REF, 1Cr1Ni and 1Fe1Ni have a total metal surface area of approx. 2.5 m² g⁻¹ after the first reduction at 800 °C, only 1.5 m² g⁻¹ could be measured for 1Mn1Ni. It is important to note that H₂ chemisorption is not selective for specific metals. Consequently, the simultaneous uptake of H₂ on different metals must be taken into account. Mn is expected to remain in the oxidic state after reduction²⁰, while alloy formation has been reported for Cr-Ni and Fe-Ni systems.^{30, 32, 33, 40} Thus, Mn may block a significant portion of the Ni surface while for the other promoters the total metal surface area remains constant.

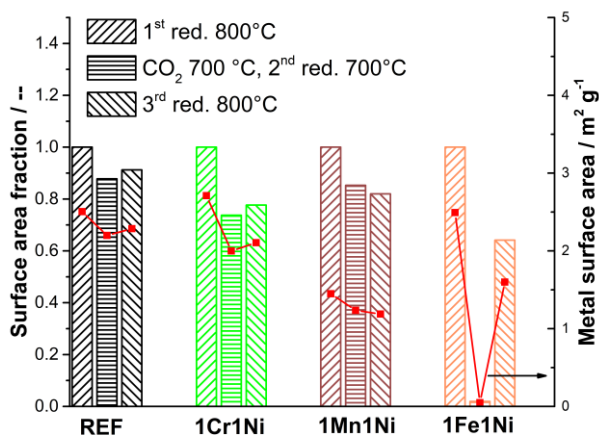


Figure 4.3: Fraction of metal surface area (columns), determined by H₂ chemisorption, available after CO₂ and/or reduction treatments relative to after the first reduction treatment. The absolute surface area values are shown with closed symbols.

Furthermore, the chemisorption setup was used to treat the samples consecutively with CO₂ and H₂ at 700 °C in a similar fashion to the redox regeneration procedure in catalytic testing. Figure 4.3 also demonstrates how the total metal surface area is affected by a simulated regeneration procedure. In all cases, exposing the catalyst to CO₂ flow and then H₂ flow for 30 min at 700 °C leads to a drop in total metal surface area. This drop is in the range of 10-20% of the original surface area for REF (2.5 to 2.2 m² g⁻¹) and 1Mn1Ni (1.5 to 1.3 m² g⁻¹). For 1Cr1Ni this decrease is almost 30% (2.7 to 2 m² g⁻¹) and for 1Fe1Ni almost no metal surface area could be measured after the redox treatment. A subsequent reduction in H₂ at 800 °C did not drastically change the surface area except for 1Fe1Ni. Approximately 60% of the original surface area was recovered for this sample (2.5 to 1.6 m² g⁻¹).

Previous studies have shown that exposing Ni catalysts to (diluted) CO₂ at elevated temperatures leads to NiO formation. Especially for Ni/Al₂O₃ the subsequent reduction can be unsuccessful at relatively low temperatures.^{35, 36, 38} For all tested samples except 1Fe1Ni the surface area increased only marginally after the additional reduction at 800 °C, which suggests that the observed surface area loss is not due to insufficient reduction. Sintering of the Al₂O₃-supported metal particles is the most credible explanation for the loss in surface area measured for REF, 1Mn1Ni and 1Cr1Ni. The reduction behavior of the Fe-Ni system is significantly more complex making it challenging to determine the degree of sintering. For further details we refer to Figure C1.

The catalyst support consists of γ -Al₂O₃ which, while providing a high surface area, contains a non-negligible amount of acid sites. NH₃-TPD was measured for the same samples that were characterized via H₂ chemisorption and CO₂-TPD to judge if the promoters influence the acidity (Figure C2). The addition of Mn appears to reduce the NH₃ uptake

slightly which may be related to the higher affinity of CO₂ for 1Mn1Ni. An improved CO₂ uptake has previously been linked to higher catalyst basicity.^{21, 42} For 1Fe1Ni NH₃ desorbs at slightly higher temperatures, indicating stronger acidity. Nevertheless, the NH₃ uptake appears to be in a similar order of magnitude for all catalysts.

4.3.2 Catalytic activity

The catalytic tests were carried out at 650 °C which represents a thermodynamic compromise between reforming and coking, allowing for a better insight into the effects of coke formation and the resulting catalyst deactivation.¹⁶ In a first step, the fresh catalysts were tested for dry reforming of methane without catalyst regeneration. In Figure 4.4 the methane conversion is plotted for the Mn-series and the Cr-series of catalysts. The coke contents determined after reaction are shown in Figure 4.5. The respective data for the Fe-series are summarized in Figure 4.6.

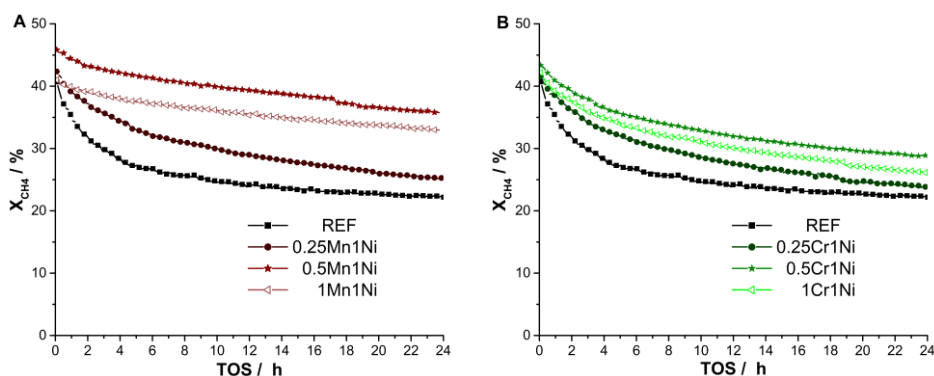


Figure 4.4: Methane conversion over TOS for Mn (A) and Cr-promoted (B) Ni/Al₂O₃ (10 mg sample, 650 °C, 100 mL min⁻¹ of 25% CH₄, 25% CO₂ in N₂).

Dry reforming of methane over fresh Ni/Al₂O₃ (REF) shows an initial methane conversion of approx. 40%. Within the first 6-8 h time on stream (TOS) a noticeable deactivation can be observed leading to a conversion of ca. 25%. In the next 16-18 h the deactivation slows down with a final conversion slightly higher than 20% after a total 24 h TOS. Compared to this, the addition of Mn or Cr has a qualitatively similar effect on the conversion. At higher loadings of the promoters the stability of the conversion is increased with a greater effect observed upon the addition of Mn. We attribute the more stable conversion observed for 1Mn1Ni and 0.5Mn1Ni to the higher CO₂ affinity of Mn-promoted catalysts. The experimental variation in conversion between different batches of the same catalyst appears to be greater for 1Mn1Ni and 0.5Mn1Ni than for the corresponding Cr-

promoted samples (Figures C3 and C4). Nevertheless, the higher activity for Mn-containing samples in Figure 4.4 appears to be a valid trend.

The comparison of the coke contents after reaction shown in Figure 4.5 reveals a similar trend for both Mn and Cr. The coke content is the lowest for the highest promoter loading and the samples 0.5X1Ni (X: Mn or Cr) contain the most coke in both series. The samples 0.25X1Ni only contain slightly less coke than the respective 0.5X1Ni. Interestingly, while for the Cr-series all promoted samples have a lower coke content than the reference sample, both 0.5Mn1Ni and 0.25Mn1Ni contain more coke than the reference Ni/Al₂O₃.

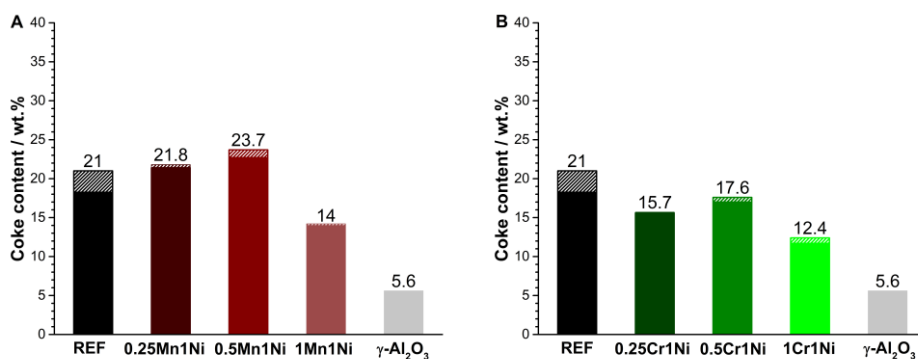


Figure 4.5: Coke contents as determined by TGA for the Mn-series (A) and Cr-series (B) after 24 h TOS; shaded areas show the observed variation between two measurements (10 mg sample, 650 °C, 100 mL min⁻¹ of 25% CH₄, 25% CO₂ in N₂).

In contrast, the addition of Fe to Ni/Al₂O₃ leads to quite different trends as shown in Figure 4.6. Especially 1Fe1Ni and 0.5Fe1Ni display an induction period and deactivate much less than the catalyst REF. 0.25Fe1Ni is mainly characterized by its slow but pronounced deactivation compared to the other Fe-containing samples. With increased Fe-loading, both the induction period and the stabilization of the conversion with TOS become more pronounced. In the case of 0.5Fe1Ni, the conversion first increases to ca. 42% in the first 60 min TOS, after which it decreases very slowly and reaches 40% after 24 h TOS. For the 1Fe1Ni catalyst the induction period is longer and it takes ca. 2 h TOS to reach a stable conversion of only 30% that remains unchanged during the subsequent 22 h. After the reaction 1Fe1Ni contains 2.4 wt.% coke, which is even less than half the amount formed over pure γ-Al₂O₃. Decreasing the Fe loading leads to increases in the coke content with 13.2 wt.% for 0.5Fe1Ni. To our surprise, a coke content of 33.2 wt.% was measured for 0.25Fe1Ni, which is more than 1.5 times the coke content of REF.

The low coke content for the catalysts with a high Fe-loading can be explained by the Mars-van Krevelen mechanism previously established for Fe-Ni samples, in which surface

Fe species actively oxidize coke by participating in a redox cycle.^{30, 32} This also explains the lower coke content for 1Fe1Ni compared to the pure support. The excessive amount of iron on the catalyst is in contact with carbon deposits forming on the support, oxidizing them as well. At the same time, an Fe-Ni alloy with a high Fe content is less active towards methane than pure Ni or an alloy with a low Fe content.^{43, 44} This explains the lower conversion values for 1Fe1Ni despite the improved stability. The negative effect of higher Fe contents in the alloy also partially explains the observed induction periods for 1Fe1Ni and 0.5Fe1Ni. In this context, it is important to mention that the Mars-van Krevelen mechanism leads to partial dealloying and the formation of FeO_x on the surface of the Ni-Fe particles.^{30, 32, 43} Thus, we speculate that in the initial phase of the reaction the reactive metal surface becomes more rich in Ni and more active towards methane with small clusters of Fe forming on top of the Fe-Ni particles.

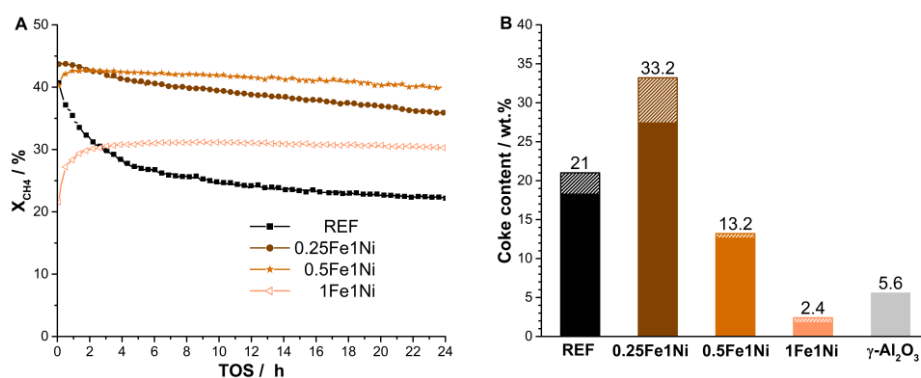


Figure 4.6: Conversion (A) and coke content after reaction (B) for the Fe-series of Ni/Al₂O₃ catalysts; shaded areas in coke content show the observed variation between different batches (10 mg sample, 650 °C, 100 mL min⁻¹ of 25% CH₄, 25% CO₂ in N₂).

The explanation for the higher coke contents for lower iron loadings is less straightforward. The experimental variation in coke content between different batches is larger for 0.25Fe1Ni than for the other samples. This suggests that the relative distribution of Fe and Ni and thus the degree of interaction between the two metals could at least be partially responsible. Previous studies showed that Ni-Fe systems with low Fe concentrations perform better when synthesized via hydrotalcite-like precursors³⁰ than through incipient-wetness impregnation.³² The synthesis route via such precursors improves the interaction between Ni and Fe, resulting in a higher catalyst stability.^{43, 45} It has been proposed that Fe can increase the lifetime of Ni catalysts for methane decomposition due to the faster diffusion of C through bulk Fe than through bulk Ni.⁴³ The presence of Fe in an Fe-Ni alloy thus promotes the diffusion of carbon away from the surface region where methane decomposition takes place,

preventing this active site to be blocked by carbon deposits. This implies that a small amount of Fe in the alloy prevents deactivation of the most coke-forming sites which increases the overall amount of coke formed during the reaction. Higher Fe loadings ensure a sufficient surface coverage with FeO_x to ensure a noticeable amount of coke removal via the Mars-van Krevelen mechanism.

Over 60 h TOS 1Fe1Ni also starts to show signs of deactivation but less so than REF, 1Mn1Ni and 1Cr1Ni (Figure C5). Only for 1Mn1Ni noticeable additional coke formation could be detected over the extended reaction period. Due to the small amounts of catalyst and the high dilution ratio, we were able to carry out these longer runs without any issues with reactor blocking observed by other researchers.^{20, 21} These results confirm that catalytic tests lasting 24 h are sufficient for the analysis of the effects of the regeneration procedures on the catalysts.

Previous studies reported the formation of NiO in supported Ni catalysts upon exposure to CO_2 at high temperatures.^{35, 38} To define the regeneration procedures, we investigated the effect of the duration of the CO_2 treatment at 700 °C on the reference catalyst after 24 h of reaction (Figure 4.7). Interestingly, successful regeneration can only be achieved with very short exposures to CO_2 . The obvious risk of Ni oxidation led to the investigation of the effects of catalyst oxidation with CO_2 , followed by reduction in H_2 . For this procedure a higher activity of the catalyst can be seen in the second reaction cycle. In literature this has been linked to the reduction of Ni in NiAl_2O_4 and similar species in successive redox cycles.^{46, 47}

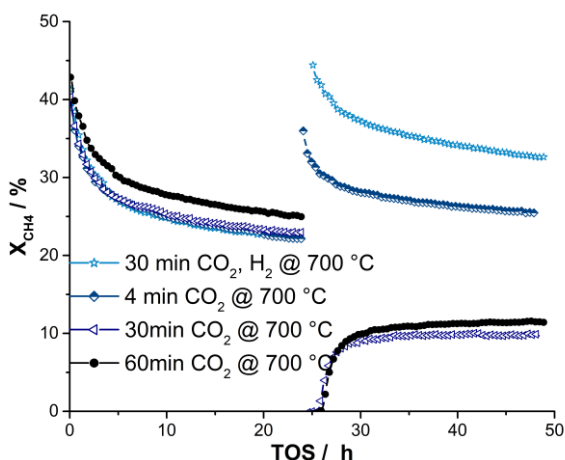


Figure 4.7: The effect of different regeneration protocols on pure Ni/ Al_2O_3 (10 mg sample, 650 °C, 100 mL min^{-1} of 25% CH_4 , 25% CO_2 in N_2).

Redox regeneration

In a first step the regeneration with a redox treatment, i.e. the sequential exposure to CO₂ and H₂, was investigated. In Figure 4.8 the methane conversion over TOS is shown for the Mn-series and Cr-series and the corresponding coke contents in Figure 4.9. The results in Figure 4.7 show that for REF such a redox procedure gives rise to a higher overall methane conversion in the second cycle of dry reforming. The initial methane conversion in both cycles is comparable but the regenerated sample deactivates less over TOS. The final conversion of approx. 22% after the first cycle increases to 31% after the second cycle. The effect of Mn and Cr on the conversion after regeneration is once again qualitatively comparable. The samples 1X1Ni and 0.5X1Ni (X: Mn or Cr) display a more stable conversion than REF. During the first reaction cycle 0.25Mn1Ni and 0.25Cr1Ni are still more active than REF. However, in the second cycle these two samples exhibit conversions that are already more comparable to that of pure Ni/Al₂O₃.

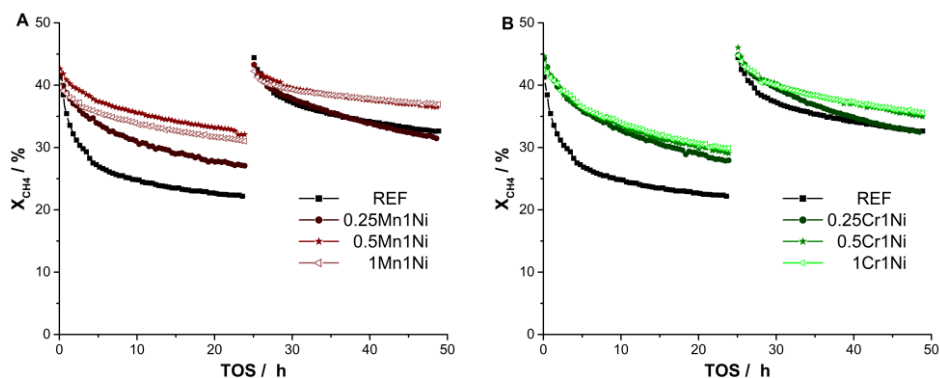


Figure 4.8: Methane conversion over TOS for the Mn-series (A) and the Cr-series (B) before and after regeneration with CO₂ and H₂ (10 mg sample, 650 °C, 100 mL min⁻¹ of 25% CH₄, 25% CO₂ in N₂).

The effect of redox regeneration on the coke content differs depending on the promoter and the loading as can be seen in Figure 4.9. The reference Ni/Al₂O₃ undergoes a relative increase in coke content by almost 70% after one redox regeneration cycle to almost 31 wt.%. For the samples 0.5X1Ni and 0.25X1Ni (X: Mn, Cr) the final coke content is in the range of 27-31 wt.%. The coke content after this extended testing procedure is only significantly lower than 30 wt.% for 1Mn1Ni and especially for 1Cr1Ni.

In our previous work we demonstrated that the catalyst must sinter to a significant degree for the conversion to be noticeably affected in dry reforming of methane. The coke content on the other hand already increases measurably if the catalyst only sinters slightly.⁴⁷ Thus, the general increase in coke content after regeneration is a strong indicator of sintering, in

accordance with the results of H₂ chemisorption. Additionally, we want to draw attention again to the fact that the observed conversion profiles of REF, 0.25Mn1Ni and 0.25Cr1Ni are significantly more comparable after redox regeneration than for the fresh samples. All these findings indicate that such redox cycles strongly diminish the effect of promoter addition to Ni/Al₂O₃ except for high promoter loadings and highly effective promoters (e.g. the high stability of 1Cr1Ni).

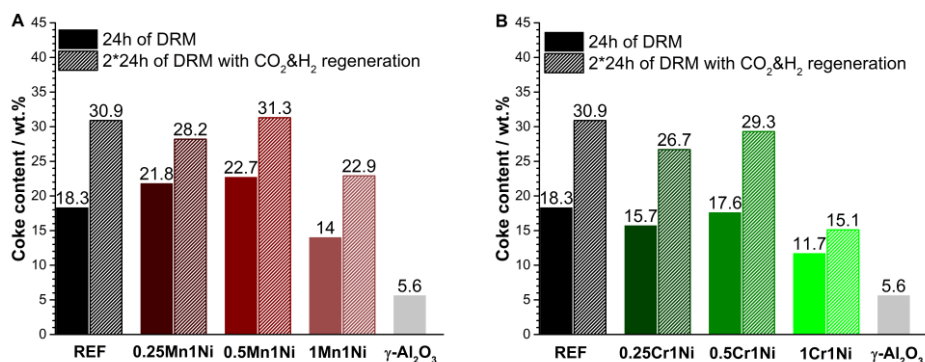


Figure 4.9: Coke contents as determined by TGA for the Mn-series (A) and Cr-series (B) after 24 h TOS (filled) or after 2 times 24 h TOS with a redox regeneration in between (shaded) (10 mg sample, 650 °C, 100 mL min⁻¹ of 25% CH₄, 25% CO₂ in N₂).

In contrast, the results in Figure 4.10 reveal little difference in the conversion between the two dry reforming cycles for the Fe-containing catalysts. Only 0.25Fe1Ni deactivates slightly less after a redox regeneration. At the beginning of both reaction cycles 1Fe1Ni undergoes an induction period starting from almost the same level of conversion. After regeneration and another 24 h of DRM, the coke content of 1Fe1Ni is the same as after 24 h of dry reforming. For the samples with less iron, an increase in the coke content can be observed. 0.5Fe1Ni contains a similar coke amount as REF after two reaction periods and redox regeneration (34.3 wt.% vs 30.9 wt.%). However, for 0.25Fe1Ni the coke content increases to almost 50 wt.%.

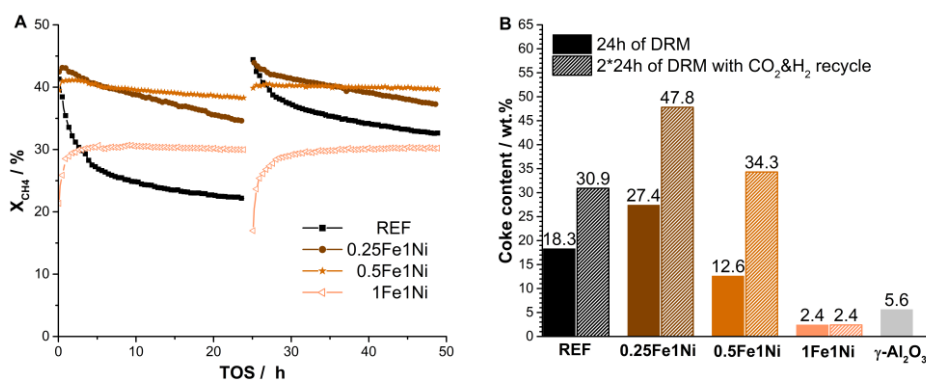


Figure 4.10: Conversion (A) and coke content (B – solid symbols 24 h of reaction, shaded symbols 2*24 h and regeneration) for two reaction periods and a redox regeneration procedure for the Fe-series of Ni/Al₂O₃ catalysts (10 mg sample, 650 °C, 100 mL min⁻¹ of 25% CH₄, 25% CO₂ in N₂).

The H₂ chemisorption study of 1Fe1Ni indicated that after a redox cycle at 700 °C the available metallic surface area is significantly lower than after a reduction at 800 °C (Figure 4.3). Even an additional reduction at 800 °C after a redox treatment can only recover ca. 60% of the original metal surface area. However, these observations are not reflected in the conversion profiles. The almost identical induction periods for 1Fe1Ni imply that also after reduction at 700 °C a high amount of Fe is incorporated into the Fe-Ni alloy. An analysis of the coke contents after reaction also does not support the theory of such strong sintering as indicated during the chemisorption experiments. For example, the final coke content after one and two cycles is identical for 1Fe1Ni. Such strong sintering should reduce the contact of Fe particles with coke formed over the γ-Al₂O₃ surface, increasing the measured coke levels. The chemisorption results for the Fe-Ni system should thus not be translated linearly into information on the degree of sintering. However, the combination of the chemisorption data and the increases in coke content after regeneration for 0.5Fe1Ni and 0.25Fe1Ni can be seen as an indication of the occurrence of sintering in general.

The specifics of Fe-Ni interaction make it difficult to judge from this data, if the degrees of sintering are comparable between REF and the Fe-containing samples. To recall, Fe(0) dissolved in the Ni particles aids carbon diffusion and thus coke formation. FeO_x on the surface aids carbon oxidation. For example, in the case of 0.5Fe1Ni the increase in coke content could be due to either larger Ni particles or less FeO_x clusters on the surface of these particles. The relative contributions of these two effects cannot be quantified from the available data.

To sum up, both the chemisorption and reactivity data are strong indicators of sintering being the result of a redox regeneration. The sintering is so pronounced that a positive impact

of the addition of Cr or Mn is mainly visible for high loadings. 1Mn1Ni still shows superior performance compared to REF but it is noticeably more affected than 1Cr1Ni. After redox regeneration it is also only for high Fe loadings that the coke content is still lower than for REF. For 0.5Fe1Ni and especially for 0.25Fe1Ni the coke content is higher than when using reference Ni/Al₂O₃.

Oxidative regeneration with CO₂

The results discussed in the previous section highlight the potential negative consequences of a redox regeneration. Furthermore, commercial applications of dry reforming are expected to involve ratios of CO₂/CH₄ larger than unity.⁴⁸ Especially in the upper section of a catalyst bed with little conversion the atmosphere can be oxidizing instead of reducing during methane reforming.³⁹ Therefore, it is of interest to determine how resistant a catalyst is to oxidation and what the effect of the promoter is on this. For this the regeneration procedure of 4 minutes of diluted CO₂ at 700 °C is a good benchmark.

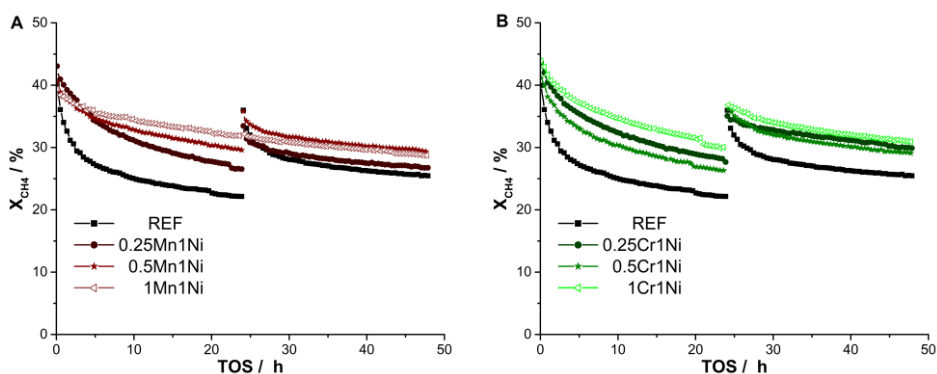


Figure 4.11: Methane conversion over TOS for the Mn-series (A) and the Cr-series (B) before and after regeneration with CO₂ (10 mg sample, 650 °C, 100 mL min⁻¹ of 25% CH₄, 25% CO₂ in N₂).

Figure 4.11 demonstrates the impact of such a regeneration procedure on the conversion for the Mn-series and Cr-series. The activity of reference Ni/Al₂O₃ after regeneration is slightly lower than for the first 24 h period. A similar effect was observed for all Cr-containing samples, 0.5Mn1Ni and 0.25Mn1Ni. For 1Mn1Ni with the highest Mn loading, the conversion remains unchanged after a short exposure to CO₂. The coke contents for REF and the Cr-series after dry reforming, oxidative regeneration and dry reforming are similar to the respective values after only 24 h of dry reforming. These four samples vary by approx. 2 wt.% carbon between the different experiments. The Mn-series on the other hand displays

a larger drop of the coke content for all samples. In particular the coke content of 1Mn1Ni drops by 50% (14 vs 7.8 wt.%) after the short CO₂ exposure.

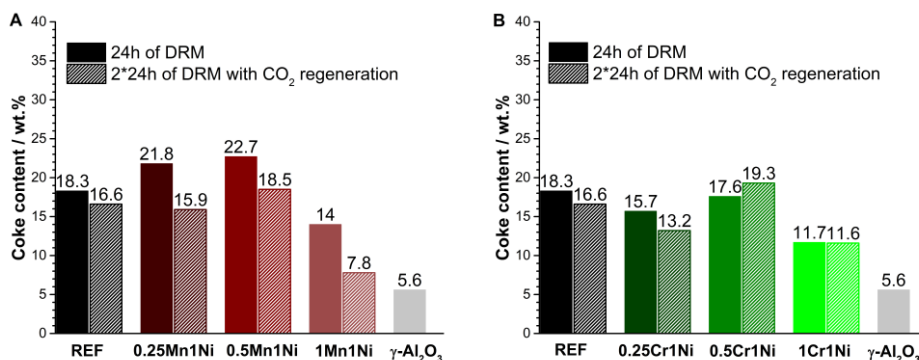


Figure 4.12: Coke contents as determined by TGA for the Mn-series (A) and Cr-series (B) after 24 h TOS (filled) or after 2 times 24 h TOS with a CO₂ regeneration in between (shaded) (10 mg sample, 650 °C, 100 mL min⁻¹ of 25% CH₄, 25% CO₂ in N₂).

The methane conversion and coke contents of the Fe-series for the oxidative regeneration experiments are shown in Figure 4.13. A short exposure clearly deactivates the samples with the adverse effect increasing with Fe loading. The sample 1Fe1Ni is almost completely inactive at the beginning of the second reaction cycle. The coke content also decreases for all samples except 1Fe1Ni after the CO₂ treatment. For the latter an increase from 2.4 wt.% to 3.8 wt.% was observed.

We propose that the short exposure to CO₂ removes most of the coke and oxidizes some Ni without affecting the stabilizing effect of Cr. The increased CO₂ affinity of Mn means that at a higher Mn-loading the oxidation of Ni is accelerated, reducing the activity. Fe has the strongest interaction with CO₂ and thus even more Ni is oxidized, possibly by reactive oxygen in the oxidized Fe. A higher percentage of NiO means that less coke can be formed. This is in line with the lower coke content after oxidative regeneration observed for 0.25Fe1Ni and 0.5Fe1Ni. The increase in coke content for 1Fe1Ni is most likely due to the extensive degree of catalyst deactivation during the regeneration. Exposing the thus deactivated catalyst to the reaction mixture would then lead to the formation of coke species not in contact with catalytically active metal particles on the catalyst surface. These deposits are then not oxidized by iron species during dry reforming.

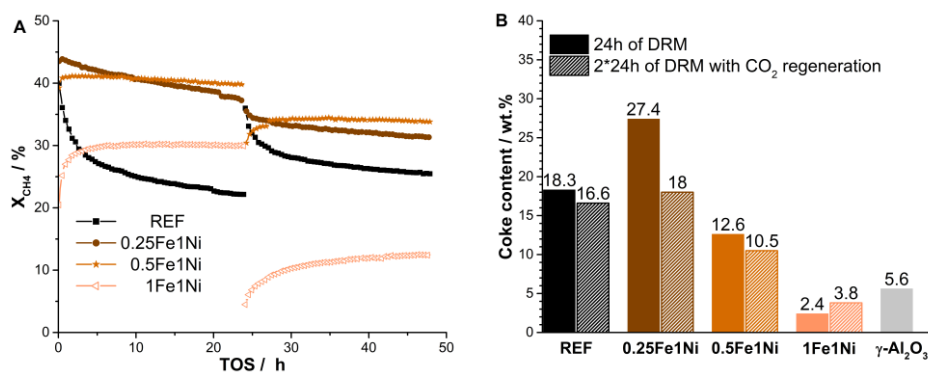


Figure 4.13: Conversion (A) and coke content (B – solid symbols 24 h of reaction, shaded symbols 2*24 h and regeneration) for two reaction periods and a CO₂ regeneration procedure for the Fe-series of Ni/Al₂O₃ catalysts (10 mg sample, 650 °C, 100 mL min⁻¹ of 25% CH₄, 25% CO₂ in N₂).

Furthermore, we analyzed the coke content after 4 minutes of exposure to CO₂ at 700 °C without any additional dry reforming afterwards (Figure C6). In most cases the remaining coke amount on the catalyst is comparable to the carbon deposited on pure γ -Al₂O₃. The only noteworthy exceptions are 0.25Fe1Ni and 0.5Mn1Ni with higher coke contents. TEM analysis clearly shows that most carbon is present as carbon fibers (Figure C7) but other carbon species may be formed as well. Carbon fibers are oxidized at 700 °C but species such as low-surface area graphite require higher oxidation temperatures.³⁴ This is a possible explanation but the impact of the promoters on the carbon structure is not within the scope of this work.

As discussed above, the choice of promoter has a strong impact on the rate of catalyst oxidation in the presence of CO₂. Therefore, we investigated the impact of an elevated CO₂ concentration on the catalyst stability. 50 mg of 1Fe1Ni were tested for 30 h in DRM with a CO₂/CH₄ ratio of 2. The elevated CO₂ concentration led to the detection of only 0.4 wt.% carbon after reaction. Figure 4.14 shows, that operation under such conditions leads to a distinct color change in the upper section of the catalyst bed. The reduced Ni catalysts studied in this work are always black, whereas the upper section of the catalyst bed is brown, i.e. the color of the freshly calcined sample. This is a clear sign of oxidation.

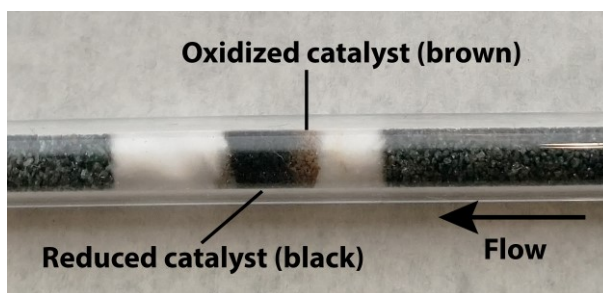


Figure 4.14: 1Fe1Ni after 30 h of reaction (50 mg sample, 650 °C, 100 mL min⁻¹ of 12.5% CH₄, 25% CO₂ in N₂).

To further investigate the impact of CO₂ on this catalyst, freshly reduced 1Fe1Ni was treated with diluted (10% in He) CO₂ at 650 °C in another setup allowing for simultaneous operando monitoring of the catalyst bed and of the outlet gas composition with an IR detector. As shown in Figure 4.15, a color change over the catalyst bed could be observed over the course of the CO₂ treatment. Monitoring the outlet gas composition via FTIR led to the detection of a CO signal over the entire experimental runtime of 50 minutes. At the very beginning of the measurement a peak in the CO signal of around 2 vol% was detected with a subsequent continuous drop of the measured concentration. After around 10 minutes TOS the CO concentration was in the range of 0.1 vol% and stayed in this order of magnitude. The combination of color change and CO detection in the outlet stream strongly supports the previous assumption of catalyst oxidation for the experiment with CO₂/CH₄=2.

The calculated degree of oxidation is also shown in Figure 4.15. The CO production peak in the first 10 minutes TOS corresponds to an oxidation of 50% of the metal deposited on the catalyst surface. After 10 min TOS, the degree of oxidation increased at a lower and almost constant speed to approx. 86% at the end of the experiment. We attribute these two phases of oxidation to a fast oxidation of iron and a slow oxidation of Ni. Consequently, the CO peak represents a full oxidation of the Fe species of the catalyst in the initial phase of the CO₂ treatment.

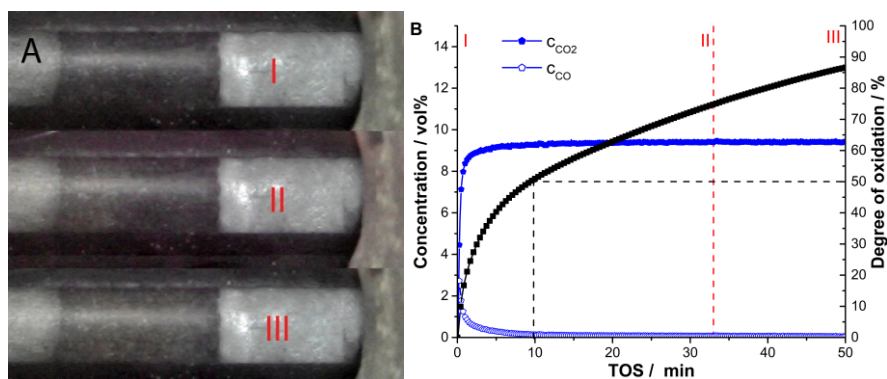


Figure 4.15: 1Fe1Ni during exposure to CO₂ at 650 °C (A – operando images, B – CO and CO₂ outlet concentrations and total degree of catalyst oxidation; 50 mg, 40 mL min⁻¹ of 10% CO₂ in He).

The low CO concentration after 10 minutes TOS means that the calculated degree of Ni oxidation may not be an exact value. A small difference between the calculated and the actual CO concentration over 40 minutes could result in a non-negligible offset in the degree of oxidation as well. However, the data allow for two statements. The oxidation of Ni appears to be the decisive parameter for a color change of the catalyst. Additionally, a full oxidation of all Ni is not necessary for a color change. After 50 minutes the rate of CO generation is still constant despite the color change being complete (Figures C11 and C12). These considerations also explain why after 33 min TOS (point II) only 30-40% of the catalyst had changed color when the CO quantification indicates a total degree of oxidation of 70-80%, i.e. 40-60% of Ni oxidation.

4.4 Conclusion

The impact of the CO₂ affinity of different promoters was tested on the stability of Ni/Al₂O₃ catalysts for dry reforming of methane. The main focus of this comparison was to subject the catalysts to different regeneration procedures with CO₂ and H₂. Many academic studies use a CO₂/CH₄ ratio of unity. Under industrial conditions the feed will contain significantly greater oxidant (CO₂ or H₂O) concentrations. The differing regeneration procedures were implemented to simulate the impact of higher oxidant concentrations on a timescale sufficiently short for academic research. To back up the conclusions drawn from the activity tests the samples were also characterized with methods such as H₂ chemisorption, TPR and

TEM. The promoters in question (Cr, Mn and Fe) were chosen to increase the CO₂ affinity step by step while keeping the promoter characteristics as similar as possible.

The combination of activity measurements and characterization clearly showed that regeneration of the catalysts via redox cycles leads to considerable sintering and thus an increase in coke formation. The sintering during regeneration also causes positive effects of promoter addition to disappear quickly unless a considerable amount of promoter is present on the samples. Additionally, the higher the CO₂ affinity of the promoter in question, the more quickly the respective catalysts appear to be oxidized by a treatment with CO₂. This research clearly emphasizes downsides of promoters such as Fe, that reduces the coke content via a Mars-van Krevelen mechanism. Consequently, if such promoters are desired in an industrial catalyst, the sintering resistance of the catalyst must be increased by other means, e.g. an improved support or improved synthesis methods such as via hydrotalcite-like precursors.⁴⁵

4.5 References

1. A. Ramirez, A. Dutta Chowdhury, A. Dokania, P. Cnudde, M. Caglayan, I. Yarulina, E. Abou-Hamad, L. Gevers, S. Ould-Chikh, K. De Wispelaere, V. van Speybroeck and J. Gascon, *ACS Catal.*, 2019, **9**, 6320-6334.
2. J. Wei, Q. Ge, R. Yao, Z. Wen, C. Fang, L. Guo, H. Xu and J. Sun, *Nat. Comm.*, 2017, **8**, 15174.
3. A. Bansode and A. Urakawa, *J. Catal.*, 2014, **309**, 66-70.
4. E. Lam, K. Larmier, P. Wolf, S. Tada, O. V. Safonova and C. Copéret, *J. Am. Chem. Soc.*, 2018, **140**, 10530-10535.
5. J. Zhong, X. Yang, Z. Wu, B. Liang, Y. Huang and T. Zhang, *Chem. Soc. Rev.*, 2020, **49**, 1385-1413.
6. S. Arora and R. Prasad, *RCS Adv.*, 2016, **6**, 108668-108688.
7. J. R. Rostrup-Nielsen, J. Sehested and J. K. Nørskov, in *Adv. Catal.*, Academic Press, 2002, vol. 47, pp. 65-139.
8. K. Wittich, M. Krämer, N. Bottke and S. A. Schunk, *ChemCatChem*, 2020, **12**, 2130-2147.
9. IPCC, *Climate Change 2007: Synthesis Report. Contribution of Working Groups I, II and III to the Fourth Assessment Report of the Intergovernmental Panel on Climate Change*, Geneva, Switzerland, 2007.
10. T. Roussière, PhD thesis, Karlsruhe Institute of Technology, 2013.

11. Technologies that do more with less, <https://www.linde-engineering.com/en/about-linde-engineering/success-stories/technologies-more-with-less.html>, (accessed Nov. 19, 2019).
12. Y. T. Shah and T. H. Gardner, *Catal Rev*, 2014, **56**, 476-536.
13. H. S. Bengaard, J. K. Nørskov, J. Sehested, B. S. Clausen, L. P. Nielsen, A. M. Molenbroek and J. R. Rostrup-Nielsen, *J. Catal.*, 2002, **209**, 365-384.
14. J. R. Rostrup-Nielsen, *J. Catal.*, 1984, **85**, 31-43.
15. H. S. Bengaard, I. Alstrup, I. Chorkendorff, S. Ullmann, J. R. Rostrup-Nielsen and J. K. Nørskov, *J. Catal.*, 1999, **187**, 238-244.
16. R. Franz, T. Kuhlewind, G. Shterk, E. Abou-Hamad, A. Parastaev, E. Uslamin, E. J. M. Hensen, F. Kapteijn, J. Gascon and E. A. Pidko, *Catal. Sci. Tech.*, 2020, **10**, 3965-3974.
17. J. Juan-Juan, M. C. Román-Martínez and M. J. Illán-Gómez, *Appl. Catal., A*, 2006, **301**, 9-15.
18. T. Osaki and T. Mori, *J. Catal.*, 2001, **204**, 89-97.
19. Z. Hou, O. Yokota, T. Tanaka and T. Yashima, *Appl. Surf. Sci.*, 2004, **233**, 58-68.
20. S.-H. Seok, S. H. Choi, E. D. Park, S. H. Han and J. S. Lee, *J. Catal.*, 2002, **209**, 6-15.
21. S.-H. Seok, S. H. Han and J. S. Lee, *Appl. Catal., A*, 2001, **215**, 31-38.
22. M. Németh, D. Srankó, J. Károlyi, F. Somodi, Z. Schay, G. Sáfrán, I. Sajó and A. Horváth, *Catal. Sci. Tech.*, 2017, **7**, 5386-5401.
23. Z. Hou and T. Yashima, *Catal. Lett.*, 2003, **89**, 193-197.
24. D. Pakhare and J. Spivey, *Chem. Soc. Rev.*, 2014, **43**, 7813-7837.
25. B. Pawelec, S. Damyanova, K. Arishtirova, J. L. G. Fierro and L. Petrov, *Appl. Catal., A*, 2007, **323**, 188-201.
26. W. L. Vrijburg, G. Garbarino, W. Chen, A. Parastaev, A. Longo, E. A. Pidko and E. J. M. Hensen, *J. Catal.*, 2020, **382**, 358-371.
27. M. Akri, S. Zhao, X. Li, K. Zang, A. F. Lee, M. A. Isaacs, W. Xi, Y. Gangarajula, J. Luo, Y. Ren, Y.-T. Cui, L. Li, Y. Su, X. Pan, W. Wen, Y. Pan, K. Wilson, L. Li, B. Qiao, H. Ishii, Y.-F. Liao, A. Wang, X. Wang and T. Zhang, *Nat. Comm.*, 2019, **10**, 5181.
28. T. Roussière, K. M. Schelkle, S. Titlbach, G. Wasserschaff, A. Milanov, G. Cox, E. Schwab, O. Deutschmann, L. Schulz, A. Jentys, J. Lercher and S. A. Schunk, *ChemCatChem*, 2014, **6**, 1438-1446.
29. M. Amey, B. Saurabh and V. Götz, *Energy Technol-Ger*, 2016, **4**, 1147-1157.
30. S. M. Kim, P. M. Abdala, T. Margossian, D. Hosseini, L. Foppa, A. Armutlulu, W. van Beek, A. Comas-Vives, C. Copéret and C. Müller, *J. Am. Chem. Soc.*, 2017, **139**, 1937-1949.

31. S. A. Theofanidis, R. Batchu, V. V. Galvita, H. Poelman and G. B. Marin, *Appl. Catal. B*, 2016, **185**, 42-55.
32. S. A. Theofanidis, V. V. Galvita, H. Poelman and G. B. Marin, *ACS Catal.*, 2015, **5**, 3028-3039.
33. N. N. Nichio, C. E. Quincoces, M. G. González and P. Moral, in *Stud. Surf. Sci. Catal.*, eds. J. J. Spivey, G. W. Roberts and B. H. Davis, Elsevier, 2001, vol. 139, pp. 263-269.
34. H. Düdder, K. Kähler, B. Krause, K. Mette, S. Kühn, M. Behrens, V. Scherer and M. Muhler, *Catal. Sci. Tech.*, 2014, **4**, 3317-3328.
35. M. Steib, Y. Lou, A. Jentys and J. A. Lercher, *ChemCatChem*, 2017, **9**, 3809-3813.
36. S. Takenaka, E. Kato, Y. Tomikubo and K. Otsuka, *J. Catal.*, 2003, **219**, 176-185.
37. A. Gil, A. Diaz and M. Montes, *J. Chem. Soc., Faraday Trans.*, 1991, **87**, 791-795.
38. M. Steib, A. Jentys and J. A. Lercher, *Journal of Physics: Conference Series*, 2016, **712**, 012049.
39. A. Giehr, L. Maier, S. A. Schunk and O. Deutschmann, *ChemCatChem*, 2018, **10**, 751-757.
40. M. G. González, N. N. Nichio, B. Moraweck and G. Martin, *Mater. Lett.*, 2000, **45**, 15-18.
41. F. Kapteijn, A. D. Vanlangeveld, J. A. Moulijn, A. Andreini, M. A. Vuurman, A. M. Turek, J. M. Jehng and I. E. Wachs, *J. Catal.*, 1994, **150**, 94-104.
42. W. L. Vrijburg, E. Moiola, W. Chen, M. Zhang, B. J. P. Terlingen, B. Zijlstra, I. A. W. Filot, A. Züttel, E. A. Pidko and E. J. M. Hensen, *ACS Catal.*, 2019, **9**, 7823-7839.
43. K. Tomishige, D. Li, M. Tamura and Y. Nakagawa, *Catal. Sci. Tech.*, 2017, **7**, 3952-3979.
44. G. Wang, Y. Jin, G. Liu and Y. Li, *Energy Fuels*, 2013, **27**, 4448-4456.
45. D. Li, M. Koike, L. Wang, Y. Nakagawa, Y. Xu and K. Tomishige, *ChemSusChem*, 2014, **7**, 510-522.
46. L. Silvester, D. Ipsakis, A. Antzara, E. Heracleous, A. A. Lemonidou and D. B. Bukur, *Energy Fuels*, 2016, **30**, 8597-8612.
47. R. Franz, F. D. Tichelaar, E. A. Uslamin and E. A. Pidko, *Appl. Catal., A*, 2021, **612**, 117987.
48. A. Ramirez, K. Lee, A. Harale, L. Gevers, S. Telalovic, B. Al Solami and J. Gascon, *ChemCatChem*, 2020, **12**, 5919-5925.

Appendix C

C1 Catalyst characterization

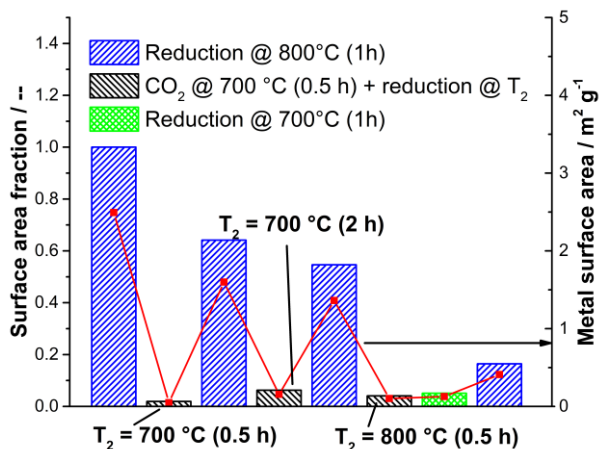


Figure C1: Surface area of 1Fe1Ni after varying oxidation and reduction protocols with T_2 representing the varying reduction conditions in the redox treatment.

The total metal surface area of 1Fe1Ni after different treatment steps is shown in Figure C1. In a first step, the reduction in H_2 at 700 °C immediately after CO_2 exposure was extended to two hours. This did not have a significant effect. Heating to 800 °C in vacuum afterwards to reduce at higher temperatures caused an irreversible loss of metallic surface area. Afterwards even a standard reduction procedure of heating to 800 °C in H_2 flow could not recover a similar surface area as before. This observation is independent of the number of previous redox cycles the sample has been exposed to. Even a fresh sample undergoes this considerable loss of surface area if oxidized at 700 °C, heated in vacuum to 800 °C and then reduced. It is unclear what exactly causes this loss of surface area after heating a CO_2 -treated sample in vacuum. This is not the relevant aspect, however. The quite pronounced effects of reduction conditions on 1Fe1Ni make it difficult to judge the degree of sintering during a redox treatment for this sample using H_2 chemisorption. For all other samples clear signs of sintering could be observed during regeneration procedures with H_2 chemisorption measurements.

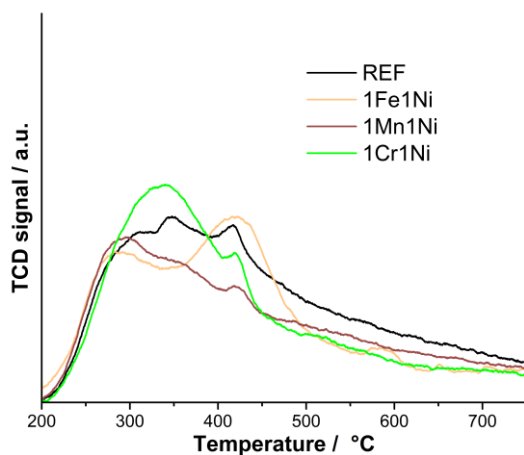


Figure C2: NH₃-TPD results for catalysts reduced at 800 °C under H₂ flow.

C2 Catalytic activity

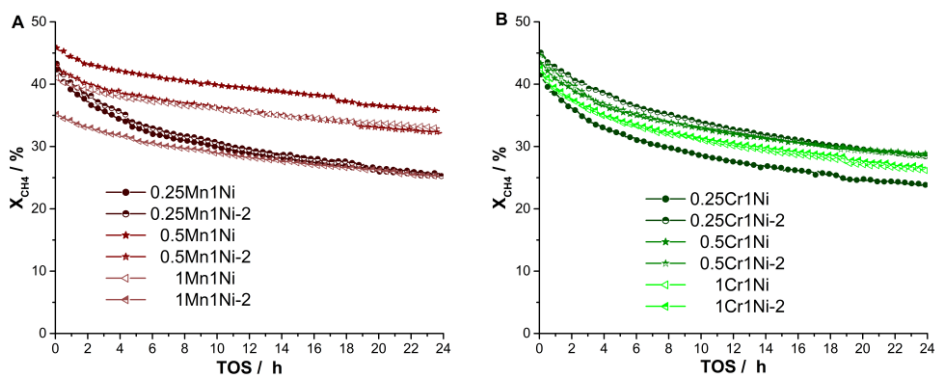


Figure C3: Experimental variation observed between two batches of the same catalyst for the Mn-series (A) and Cr-series (B) (10 mg sample, 650 °C, 100 mL min⁻¹ of 25% CH₄, 25% CO₂ in N₂).

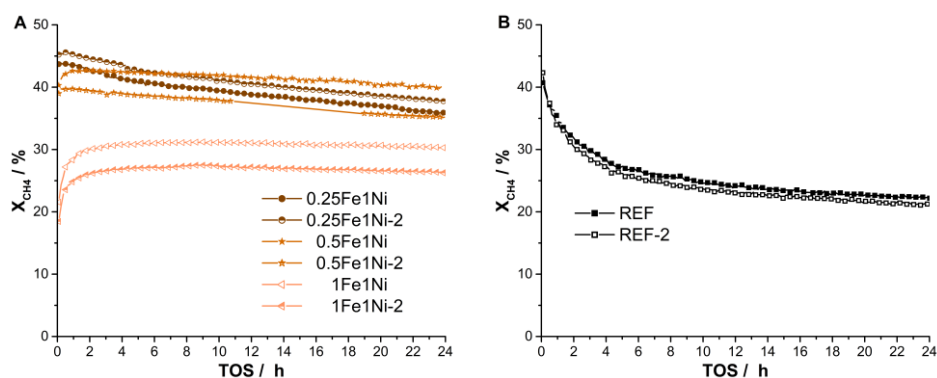


Figure C4: Experimental variation observed between two batches of the same catalyst for the Fe-series (A) and Ni/Al₂O₃ (B) (10 mg sample, 650 °C, 100 mL min⁻¹ of 25% CH₄, 25% CO₂ in N₂).

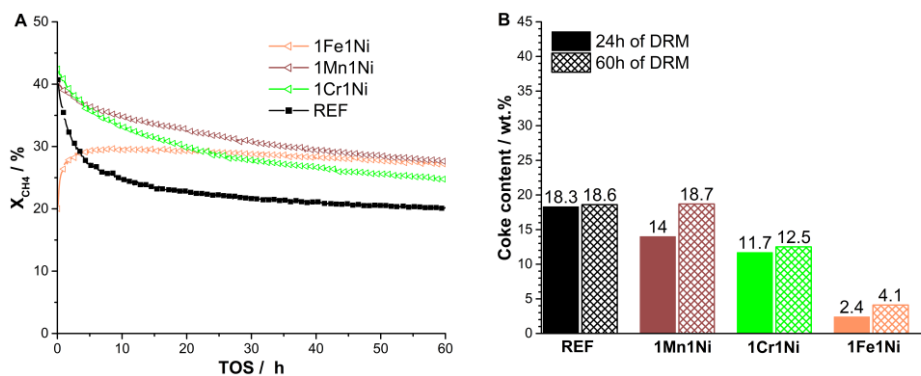


Figure C5: Conversion (A) and coke content after reaction (B) over 50 h TOS for pure Ni/Al₂O₃ and all samples with a 1:1 ratio of promoter to Ni (10 mg sample, 650 °C, 100 mL min⁻¹ of 25% CH₄, 25% CO₂ in N₂).

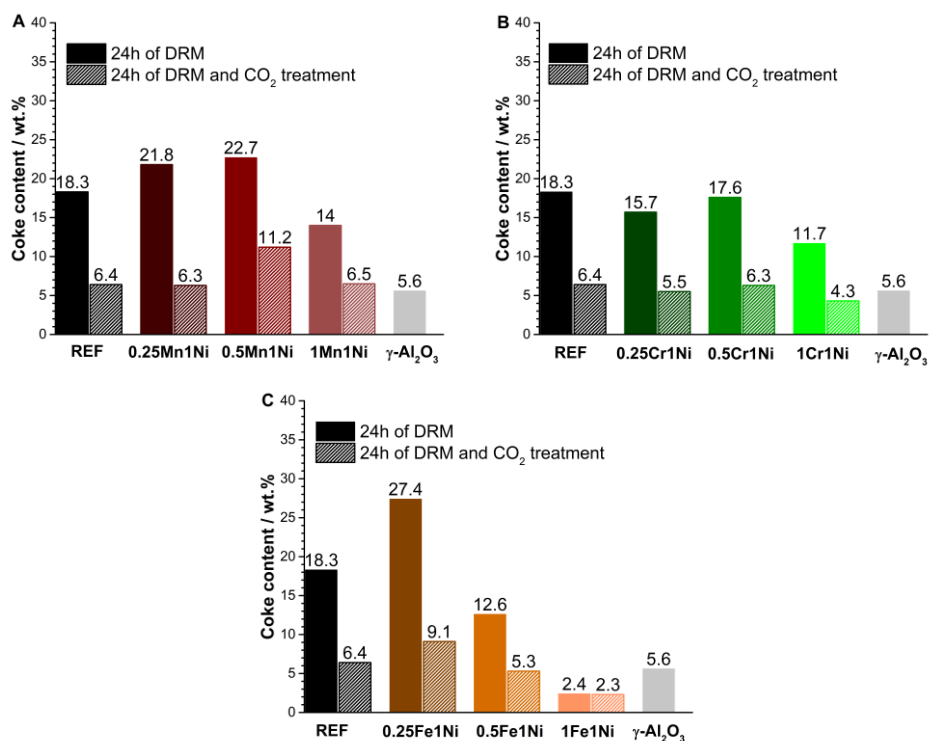


Figure C6: Coke contents as determined by TGA for the Mn-series (A), Cr-series (B) and the Fe-series (C) after 24 h TOS with (shaded) and without (filled) a 4 min CO₂ treatment at 700 °C between (10 mg sample, 650 °C, 100 mL min⁻¹ of 25% CH₄, 25% CO₂ in N₂).

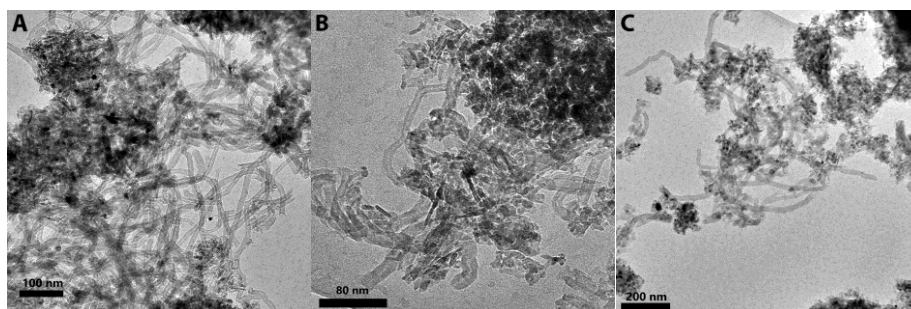


Figure C7: Coke structures on 1Mn1Ni (A, B) and 1Fe1Ni (C) after 24 h of reaction.

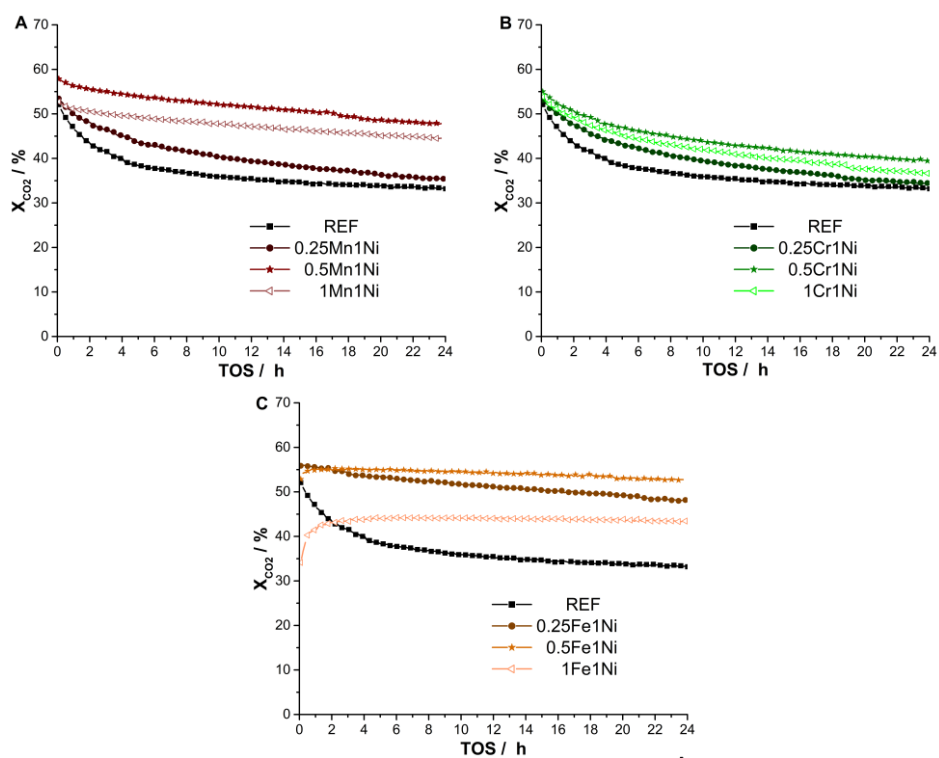


Figure C8: CO₂ conversion over TOS for the Mn-series (A), Cr-series (B) and Fe-series (C) (10 mg sample, 650 °C, 100 mL min⁻¹ of 25% CH₄, 25% CO₂ in N₂).

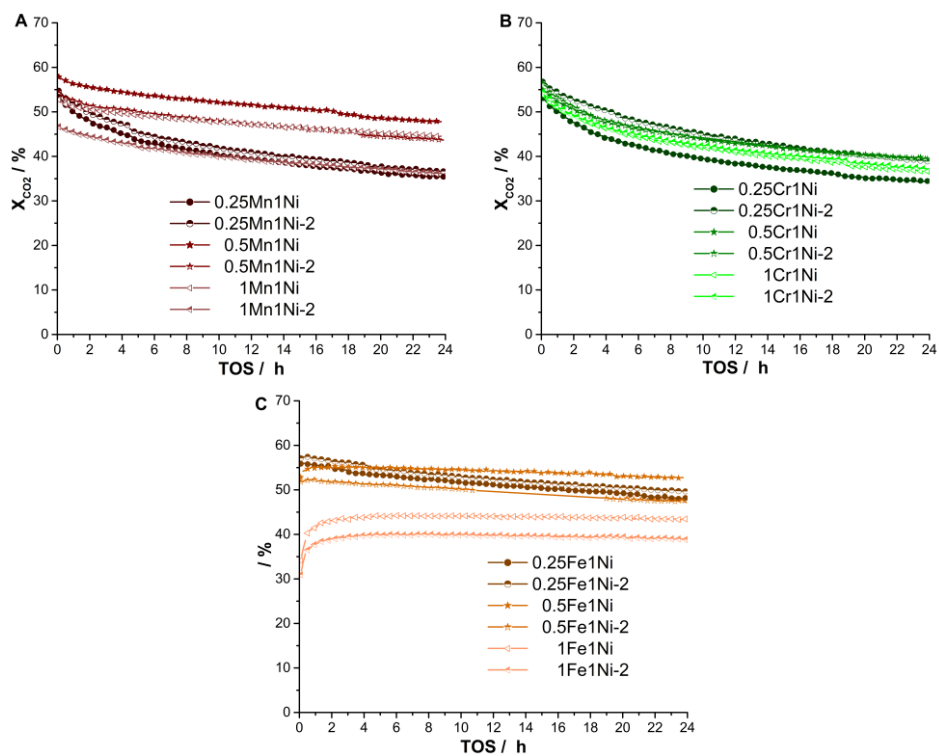


Figure C9: Experimental variation observed in the CO₂ conversion between two batches of the same catalyst for the Mn-series (A), Cr-series (B) and Fe-series (C) (10 mg sample, 650 °C, 100 mL min⁻¹ of 25% CH₄, 25% CO₂ in N₂).

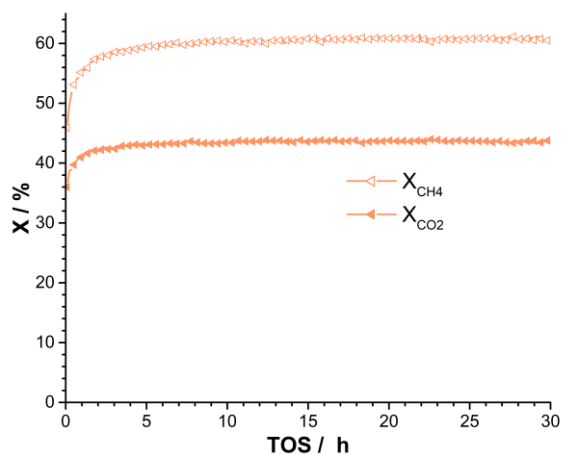


Figure C10: Conversion over TOS for 1Fe1Ni (50 mg sample, 650 °C, 100 mL min⁻¹ of 12.5% CH₄, 25% CO₂ in N₂).



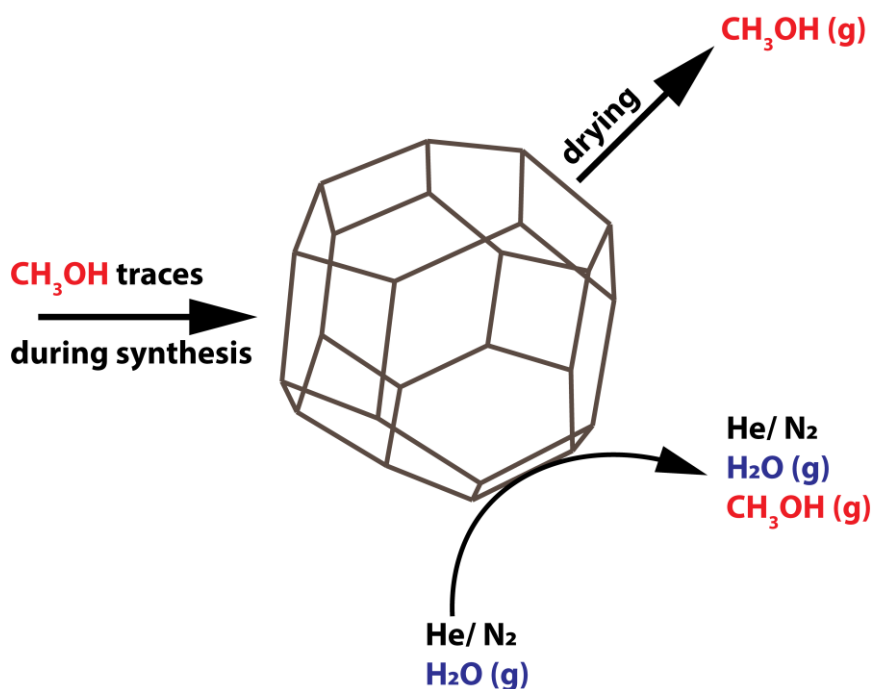
Figure C11: A picture of the 1Fe1Ni catalyst bed oxidized after CO₂ treatment (50 mg sample, 650 °C, 40 mL min⁻¹ of 10% CO₂ in He).



Figure C12: Unprocessed operando images of the 1Fe1Ni catalyst bed at the three different points in time (50 mg sample, 650 °C, 40 mL min⁻¹ of 10% CO₂ in He).

Chapter 5

Potential for false positive in methane to methanol conversion experiments due to MOF contamination and the impact on apparent productivity



Metal-Organic Frameworks (MOFs) are an attractive material group to serve as a basis for the development of next-generation heterogeneous catalysts for the direct oxidative conversion of methane to methanol. While the wide range of design options of MOFs allows for great flexibility in design of the active site and their environments, the well-known stability issue is of major importance for this type of catalysis. Additionally, MOFs cannot be calcined like zeolites to remove impurities. Thus, MOF degradation under reaction conditions is one challenge but impurities remaining after synthesis may also obscure the observed methanol signal. Indeed, during experiments on the continuous oxidation of methane to methanol we found that the combination of water-containing feeds and contaminations present in the MOFs can lead to false positive measurement of catalytic activity. We propose that especially for catalytically less active MOFs, this can lead to a significant relative error of measured productivity. Such effects must be taken into account when designing experiments for the conversion of methane to methanol over MOF-based catalysts.

5.1 Introduction

Directly converting methane to methanol is in theory the most attractive route for methane valorization. It would allow for a single-step, low temperature and exothermic conversion of methane into an energy-rich liquid.^{1, 2} Current industrial methane conversion is based on first generating synthesis gas from methane as an intermediate which is a highly energy-intensive process.³ The direct conversion of methane to methanol is not only a single-step synthesis of a desirable end product. With the current knowledge on methanol to hydrocarbons (MTH), methanol could also serve as an attractive platform chemical.^{4, 5}

Among different process options and catalytic materials considered for the direct conversion of methane^{6, 7}, particular attention has been devoted to the development of the low temperature oxidation of methane to methanol by zeolite-based heterogeneous catalysts modified by Fe^{8, 9} or Cu^{10, 11} species that are stabilized by the framework. The exact nature of these intrazeolitic active sites and their roles in both the selective conversion of methane and the different side-reactions are still under discussion.¹² However, concepts like a high structural homogeneity¹³ and a better control over the confinement environment^{14, 15} are seen by many researchers as key to improve the selectivity and activity during catalytic conversion of methane. Such an improved control over the speciation of the reactive centers can be achieved with catalysts based on Metal-Organic Frameworks.^{16, 17} Metal-Organic Frameworks (MOFs) are coordination polymers consisting of metal ion nodes connected by organic linker molecules. Besides the possibility to construct the reactive centers with atomic precision, this material class offers more options than zeolites to fine-tune hydrophobicity and microscopic transport parameters to facilitate product removal from the reactive porous space and thus enhance the overall selectivity. However, the nature of MOFs poses its own problems. Successful use of MOFs as catalysts has been reported previously (see e.g. refs. 18, 19) but the considerable pore space can also lead to problems such as pore blockage.²⁰ Pristine MOFs can already exhibit issues with pore accessibility.²¹ Degradation of the framework (e.g. due to air or vapor exposure) may easily lead to diffusional barriers within the framework.²² This is especially important for a catalytic usage as catalyst degradation is typically encountered in both industrial and academic environments. Furthermore, unlike the pure inorganic materials such as oxides and zeolites, the robust and reliable calcination procedure cannot be applied to most of the MOF-catalysts leaving therefore behind a substantial uncertainty about the level of contamination of the porous space and its impact on the observed chemical and catalytic properties.

In the context of methane oxidation, MOF-based catalytic systems have received considerable attention in the last years. So far, three different systems have been reported in literature. *Ikuno et al.* and *Zheng et al.* used Zr-based NU-1000 that was functionalized with Cu species via atomic layer deposition (ALD) or via ion exchange, respectively.^{23, 24} Similarly *Baek et al.* also grafted Cu-species on a Zr-based MOF, choosing MOF 808.²⁵ The

exception is the MIL-53 (Al) reported by *Osadchii et al.* Here, Fe was incorporated into the framework structure during the electrochemical synthesis of the framework itself.²⁶ Table 5.1 summarizes the key characteristics of the reported MOF-catalyzed methane oxidation systems reported so far.

Table 5.1: Summary of published literature on MOFs as catalysts for methane to methanol conversion.

MOF	T_R [°C]	Active metal	Oxidant	MeOH yield [$\mu\text{mol/g}$]	Ref.
NU-1000	150 – 200 °C	Cu	O ₂	18	23
NU-1000	150 – 200 °C	Cu	O ₂	0.5 - 18	24
MOF-808	150 °C	Cu	O ₂	30 – 70	25
MIL-53	60 °C	Fe	H ₂ O ₂	14	26

In all four instances, a non-continuous approach was chosen for these experiments. *Osadchii et al.* carried out their experiments in a batch reactor using an aqueous solution of H₂O₂ as the oxidant.²⁶ *Ikuno et al.*, *Zhang et al.* and *Baek et al.* on the other hand, performed methane oxidation with molecular O₂ or N₂O in a gas-phase cyclic operation, previously established for zeolite-based catalysts (see e.g. ref. 11).²³⁻²⁵ In this approach, as shown in Figure 5.1, the fixed bed of catalyst is first oxidized in a flow of a (diluted) oxidant such as O₂ or N₂O. The system is then purged and methane is flown through the bed. In the last step, the catalyst bed is exposed to a mixture of steam and inert to extract the generated methanol. This last step stems from previous work on zeolites in which formed methoxy species only desorb from the active sites in the presence of water.⁸

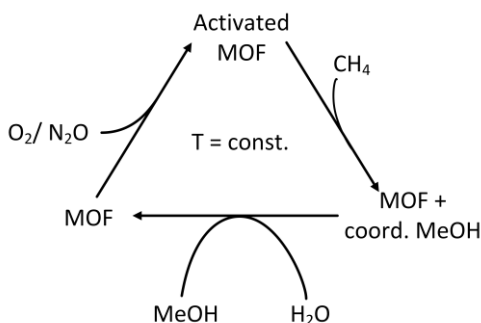


Figure 5.1: Schematic of the cyclic approach to methane oxidation with MOFs

The difference in testing parameters cannot explain the observed variation in catalytic activity of the different frameworks. The yield over NU-1000 depends on the Cu loading and the synthesis approach and is in the range of 0.5-18 $\mu\text{mol g}_{\text{cat}}^{-1}$.^{23, 24} MIL-53 yields 15 $\mu\text{mol g}_{\text{cat}}^{-1}$, despite completely different experimental conditions.²⁶ Three different variations of MOF-808 were reported by *Baek et al.*, which vary in productivity by over 100% between the samples (30 – 70 $\mu\text{mol g}_{\text{cat}}^{-1}$).²⁵ Careful and deliberate optimization of the framework design should therefore be able to provide considerable insight into the function of the active site.

Interestingly, the highest methanol yield obtained with MOF-808 is already comparable with the results for Cu-exchanged zeolites. Yields of slightly below 100 $\mu\text{mol g}_{\text{cat}}^{-1}$ or 100-200 $\mu\text{mol g}_{\text{cat}}^{-1}$ have been mentioned for Cu-exchanged ZSM-5 and MOR respectively.^{11, 27} For these zeolites a high-temperature activation step with O₂ (450 °C or higher) is necessary to achieve these yields. Isothermal operation generates a different, less active species.²⁸ For an isothermal cyclical treatment of Cu-MOR a productivity of 5 $\mu\text{mol g}_{\text{cat}}^{-1}$ has been reported in literature, which is substantially lower than the productivity of the MOF catalysts.²⁹ Under isothermal conditions, continuous gas-phase oxidation can also be carried out, using either O₂ or N₂O as an oxidant and feeding this together with H₂O and CH₄.^{28, 30-32} Results have so far only been published for zeolites. The productivity here is strongly affected by the choice of the oxidant and reaction conditions. For Cu-exchanged zeolites and O₂ at 200 °C, a productivity of up to 6 $\mu\text{mol h}^{-1} \text{g}_{\text{cat}}^{-1}$ has been reported.³⁰

The definition of a suitable testing protocol is especially important when using MOF catalysts for oxidative conversion of methane. Regardless of continuous or cyclical testing the catalyst will be exposed to considerable amounts of water vapor and oxygen at elevated temperature. This raises concerns regarding the structural integrity and the long-term stability of the hybrid organic-inorganic MOF frameworks. Indeed, the instability of many MOF structures towards hydrolysis is a well-known phenomenon.³³⁻³⁵ The stability of various MOF materials under humid conditions has been reviewed by *Burtch et al.* They reported only few MOF structures with sufficient structural stability to liquid water.³⁵ Stability against higher concentrations of water vapor is easier to achieve since this hydrolysis in the gas phase is a question of kinetic instead of thermodynamic stability. This means, that due to a hydrophobic environment or steric obstacles, the water vapor cannot hydrolyze the metal-ligand bonds in the framework despite hydrolysis being thermodynamically feasible. However, a nominal resistance to water vapor may not be seen as a final evaluation. For example, NU-1000 was listed as a MOF with high kinetic stability to water vapor by *Burtch et al.* Nevertheless, *Ikuno et al.* reported a decrease in the methanol productivity upon the recycling of Cu/NU-1000 catalyst, which has been attributed to the decarboxylation of the organic linkers.²³

With the methanol outlet concentration on the ppm-scale, a decarboxylation of the framework can quickly obscure the true catalyst activity and selectivity. It must be clearly established for these tests, if and how MOF instability issues affect the catalyst behavior. For such questions, continuous oxidative methane conversion is desirable. It provides a higher

density of data points, making it easier to establish trends and correlations. Therefore, in this work the focus was on continuous methane oxidation experiments in which all reactants are co-fed. Despite an expected lower conversion we believe this method is more suitable to answer the above-mentioned question about framework stability and durability. Our research focused on two different types of framework: MIL-53 and MIL-100. For both frameworks the focus was on mixed-metal MOFs. This was based on previous reports, where the insertion of small amounts of iron in MIL-53 (Al) provided a stable methane oxidation catalyst.²⁶ The framework syntheses and initial characterization are described first, followed by testing results and characterization of the frameworks post reaction.

5.2 Experimental

5.2.1 Chemicals

Chemicals: 2-Aminoterephthalic acid (99%, Aldrich), terephthalic acid (98%, Aldrich), aluminum nitrate nonahydrate (98% Aldrich), 1,3,5-benzenetricarboxylic acid (95%) (trimesic acid, Aldrich), sodium chloride (99%, Acros), iron(III) chloride hexahydrate (FeCl_3) (98%, Aldrich), N,N-dimethylformamide (DMF) (Aldrich, 99.8%), methanol (technical, VWR), ethanol (96%, FMVG L&M), absolute ethanol (Merck), iron powder (Aldrich). All chemicals were used as delivered by the supplier without any further purification.

5.2.2 Syntheses of MIL-53

Both NH_2 -MIL-53 (Al, Fe) and MIL-53 (Al, Fe) were synthesized using the modified electrochemical procedure previously described by *Osadchii et al.*²⁶ In a batch reactor, two aluminum plates in PTFE holders were used as the electrodes. Except for a hole of 25 mm diameter, the PTFE holders completely encased the electrodes. These were placed in a solution of 0.73 g NaCl and either 0.6 g terephthalic acid or 0.65 g aminoterephthalic acid in a mixture of 90 mL H_2O and 10 mL DMF. A syringe containing 0.191 g FeCl_3 in 1 mL DMF and 9 mL H_2O was so connected that the needle tip was situated between the two uncovered parts of the Al plates. The system was then heated up to 80 °C under constant stirring. Once at temperature, 20 mA of potential were applied for 4 h (with an AUTOLAB PGSTAT128N in galvanic mode), while the solution was injected with a rate of 0.6 mL h^{-1} . Post synthesis the samples were washed in a Teflon-lined autoclave in DMF at 130 °C overnight followed by denatured ethanol at 70 °C for 4.5 h.

Similarly, a sample of MIL-53 (Al) was synthesized hydrothermally and Fe coordinated to it as described previously.²⁶ 2 g of terephthalic acid and 8 g of $\text{Al}(\text{NO}_3)_3 \cdot 9 \text{H}_2\text{O}$ were dispersed in 30 mL of demin. water and kept in a Teflon-lined autoclave for 72 h at 220 °C.

Afterwards, the solid was filtered and washed in DMF at 130 °C (overnight) and methanol at 70 °C (5 h), again in a Teflon-lined autoclave, followed by drying in air at 100 °C.

For the coordination of iron, 2.1 g of $\text{Fe}(\text{NO}_3)_3 \cdot 9\text{H}_2\text{O}$ was dissolved in 20 mL of demin. water (instead of DMF as before²⁶). This solution was filled in a Teflon-lined autoclave together with 1.1 g of MIL-53 (Al). After 12 h at 80 °C, the solid was filtered off and washed with water on the filter. Afterwards, the solid was filtered off and dried at 100 °C in air overnight. This sample shall be referred to as MIL-53 (HS).

5.2.3 Syntheses of MIL-100

MIL-100 (Fe) was synthesized according to the procedure reported by *Yoon et al.*³⁶ In short 336 mg of Fe(0), 842 mg of trimesic acid and 252 mg were dispersed in 30 mL of demin. H₂O in a Teflon-lined autoclave. Afterwards, 200 μL of HF was added, the autoclave was sealed and hydrothermal synthesis was carried out at 150 °C for 12 h. The solid was then filtered off and washed in water at 80 °C for 5 h and denatured ethanol for 3 h. In a last step, the solid was dried in vacuum at 80 °C overnight.

The synthesis of MIL-100 (Fe, Ni) was also based on a previously reported procedure.³⁷ Trimesic acid (1.68 g – 8 mmol), a total of 12 mmol Fe(0) and Ni acetate (molar ratios of Ni/Fe = 0.01 and 0.111 for Ni contents of 2% and 7%), 90 mL of dist. H₂O and 5 mmol of HNO₃ were mixed in a Teflon-lined autoclave. This autoclave was closed and heated to 85 °C for 24 h. Afterwards, the solid was filtered off, washed with water and then washed in 30 mL of absolute ethanol for 12 h at 60 °C. In a last step, this solid was then again filtered and washed with water before drying at 80 °C in air.

5.2.4 Catalyst testing

Catalytic experiments were carried out in a fixed-bed tubular reactor with an outer diameter of 6.35 mm (0.25 “) and an inner diameter of 3.81 mm (0.15 “). A quartz plug was used to support the catalyst bed with a thermocouple positioned just downstream of the quartz plug. Per experiment 250 mg of pelletized sample were used. CH₄, He and 1% O₂ in He were connected to the setup via Bronkhorst mass flow controllers (MFCs). The general gas stream could be fed either through a saturator filled with demineralized H₂O at room temperature or directly to the reactor, to test dry feeds. Downstream of the reactor, an additional MFC was connected to feed 1% n-butane in He as an internal standard for analysis. All gases were supplied as 5.0 quality by Airgas. The product stream was analyzed with an Agilent online GC employing an FID and a TCD and a HP-PLOT Q PT column (length: 30 m, I.D.: 0.53 mm, film thickness: 40 μm).

The catalytic testing was carried out under different conditions. In a typical experiment the sample was heated to 200 °C in a flow of 20 mL min⁻¹ of inert, before switching to a mixture of reactant gases. While varying the inlet gas composition, the dry gas flowrate was

kept constant at 24.25 mL min⁻¹ with an O₂ level of 600 ppm. The CH₄ content was either 94% or 0% with He as the balance. Lastly, both wet and dry feeds were tested to gauge the impact of water. All tests were carried out in a continuous operation.

5.2.5 Catalyst characterization

X-ray diffraction (XRD) measurements were carried out in a Bruker D8 Advance Diffractometer with monochromatic Co *K* α radiation ($\lambda = 0.179026$ nm) at room temperature. The scan speed was set at 0.2 s deg⁻¹.

Physisorption measurements were carried out both with N₂ and CO₂ as probe molecules. In both cases the samples were first dried in sample tubes at 150 °C under N₂ flow overnight. Afterwards the dried samples were loaded into a micromeritics TriStar II. The analysis temperature depended on the gas used for porosity analysis: 273 K for CO₂ physisorption and 77 K in case of N₂.

5.3 Results and discussion

5.3.1 Characterization

All samples described in this work (MIL-53 (Al, Fe), NH₂-MIL-53 (Al, Fe), MIL-100 (Fe, Ni), MIL-53 (HS)) were characterized by XRD and N₂ physisorption before testing. For the MIL-53 samples CO₂ physisorption was carried out as well. The focus of this work was on mixed-metal MOFs, partially involving multi-step syntheses to include different metals. Therefore, these samples have to be characterized over different steps. XRD and N₂ physisorption show the successful synthesis of the desired MOF structures in the first step. In Figure 5.2, the XRD patterns and N₂ isotherms of MIL-100 species are shown with good agreement in the XRD for the different loadings of Ni. Minor shifts in the XRD patterns can be attributed to small differences in sample height within the diffractometer. N₂ physisorption provided a total gas uptake in the desired range. The uptake of the classically synthesized MIL-100 (Fe) is lower than previously reported.³⁶ Therefore, there seems to be a variation within the synthesis itself. Nevertheless, it appears as though an increase in Ni content leads to a decrease in N₂ uptake. This is in agreement with literature, where it was proposed that for higher Ni contents, the percentage of Ni outside the framework forming NiO clusters increases.³⁷

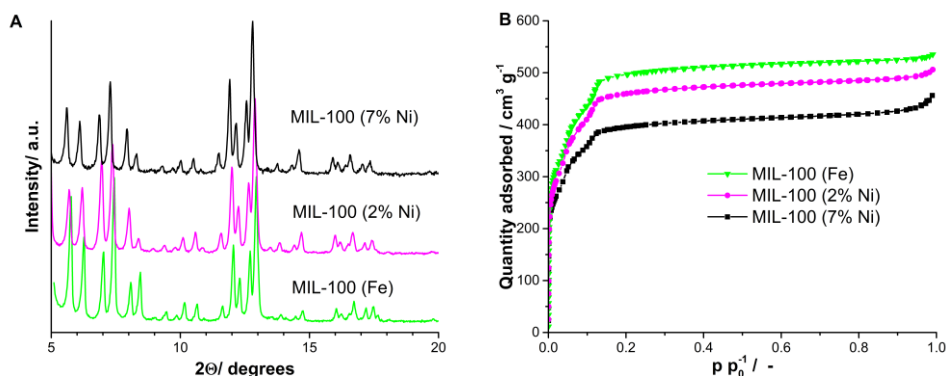


Figure 5.2: XRD (A) and N₂ physisorption (B) results for MIL-100 with 0%, 2% and 7% Ni.

As reported in literature for the electrochemical synthesis of MIL-53, the XRD patterns of MIL-53 (Al, Fe) and NH₂-MIL-53 are rather broad compared to hydrothermal synthesis.^{26, 38} This has previously been correlated to the smaller crystal particles that result from this synthesis method.^{26, 38} Figure 5.3 shows the XRD patterns of the three different MOFs after synthesis. It can be seen that the hydrothermal synthesis yields a framework almost exclusively in the narrow pore configuration (distinctive peaks around e.g. $2\Theta = 15^\circ$, 21° , 29°). The electrochemically synthesized frameworks on the other hand have a large pore configuration (distinctive peaks at $2\Theta = 18^\circ$, 21°). The preference for large pore configuration in electrochemical synthesis has been reported before, if DMF is used as a solvent.³⁸ However, for the hydrothermally synthesized MIL-53, this is not the final synthesis step. After coordination of iron as described in the experimental section, the XRD pattern changes considerably. Part of the change in the XRD pattern could be explained by a switch from narrow pore the large pore configuration (a peak at $2\Theta = 18^\circ$ instead of $2\Theta = 15^\circ$). This does not explain the appearance of the many additional peaks however.

Osadchii et al. carried out a similar synthesis for MIL-53 (Al) with externally coordinated iron.²⁶ In their case, DMF was the solvent instead of H₂O. Despite the detection of larger clusters of iron in HAADF-STEM and Raman, they did not observe a change of the XRD pattern. It stands to reason, that the post-synthesis treatment of MIL-53 (Al) with an aqueous iron solution degrades the framework. Analysis of the physisorption data leads to the same conclusion. The N₂ uptake of the final stage of MIL-53 (HS) is significantly reduced compared to the pristine MIL-53 (Al) (see Figure 5.4) and no CO₂ uptake could be measured for MIL-53 (HS). This is despite the final XRD pattern of MIL-53 (HS) being more in keeping with large pore than narrow pore configuration. Thus, the additional peaks seen in Figure 5.3 for MIL-53 (HS) can be attributed to structural changes in or degradation of MIL-53 (Al).

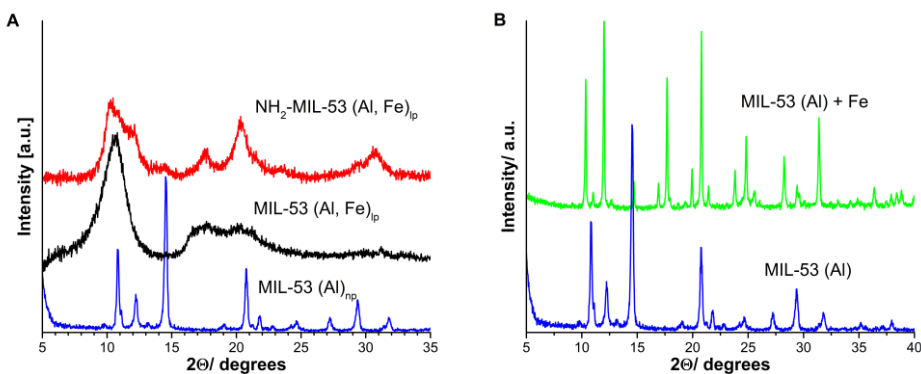


Figure 5.3: Comparison of the different MIL-53 species after framework synthesis in large pore (lp) and narrow pore (np) configuration (A) and MIL-53 (HS) before and after iron was coordinated to the pure MIL-53 (Al) (B).

Similarly to the final MIL-53 (HS), $\text{NH}_2\text{-MIL-53 (Al, Fe)}$ shows significantly lower N_2 uptake than reported for MIL-53. The electrochemically synthesized MIL-53 (Al, Fe) does show a level of uptake in accordance with literature but the uptake was too slow to be able to measure even a full adsorption branch (see Figure 5.4). Incomplete N_2 adsorption isotherms for individual batches of MIL-53 (Al, Fe) have been observed in our group before. Slow gas uptake during physisorption is typically seen as an indicator of diffusion limitation.³⁹ CO_2 physisorption at 273 K allows for much faster diffusion due to the increased temperature and the higher overall pressure used during measurement. However, for Metal-Organic Frameworks the uptake can be affected by the interaction between CO_2 and the polar sites within the framework, necessitating extra care during data analysis.⁴⁰ No CO_2 uptake could be measured for MIL-53 (HS) which underlines the degradation of the framework due to the iron coordination. This result was obtained despite residual porosity remaining in the framework. If CO_2 uptake on MIL-53 (Al, Fe) and $\text{NH}_2\text{-MIL-53 (Al, Fe)}$ were exclusively due to CO_2 coordination to polar groups, CO_2 uptake should also be observable for MIL-53 (HS).

Both MIL-53 (Al, Fe) and $\text{NH}_2\text{-MIL-53 (Al, Fe)}$ show CO_2 -uptakes in a similar range when measured at 273 K. The uptake is also in accordance with previously published data for batches of MIL-53 (Al, Fe), where full N_2 physisorption could be measured.²⁶ Literature does not indicate strong chemical interactions between CO_2 and the NH_2 -groups of $\text{NH}_2\text{-MIL-53}$.⁴¹ While we cannot rule out CO_2 coordination to polar groups within the frameworks, these results indicate pore accessibility issues within $\text{NH}_2\text{-MIL-53 (Al, Fe)}$, compared to MIL-53 (Al, Fe).

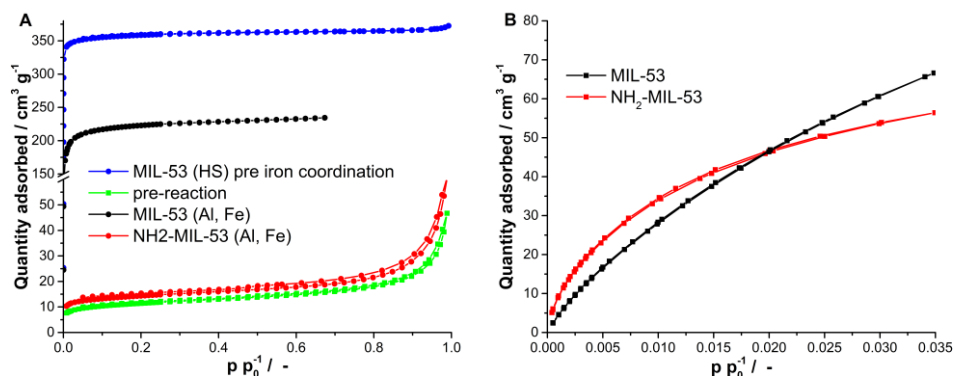


Figure 5.4: N₂ isotherms for MIL-53 (HS) before and after iron coordination (A) and CO₂ isotherms for the electrochemically synthesized samples (B).

To sum up, for three out of four samples, the desired structure was obtained: MIL-100 (Fe, 7%Ni), MIL-53 (Al, Fe) and NH₂-MIL-53 (Al, Fe). MIL-100 is both highly porous and there is little indication of pore accessibility issues. In contrast for MIL-53 (Al, Fe) and NH₂-MIL-53 (Al, Fe) physisorption strongly indicates issues with pore accessibility. MIL-53 (HS) cannot be described as a MIL-53 structure anymore. Instead, the iron coordination has strongly degraded the framework, leading to a severe drop in pore volume.

5.3.2 Catalytic testing results

To test the catalytic properties of the four different frameworks for direct synthesis of methanol from methane, catalytic experiments were carried out at elevated temperature. MIL-53 (Al, Fe), MIL-100 (Fe, 7% Ni), NH₂-MIL-53 (Al, Fe) and MIL-53 (HS) were heated to 200 °C and exposed to flows of He, CH₄, O₂ and H₂O (either all gases or only a selection of these). Feeding all of these gases with a Weight hourly space velocity (WHSV) of 6000 mL g⁻¹ h⁻¹ led to a detection of methanol at a concentration of around 1 ppm and lower. When the sample loading was decreased at a constant flow to achieve a WHSV of 10000 mL h⁻¹ g⁻¹ however, no methanol could be detected anymore by GC analysis. To determine the origin of the methanol signal, more work was carried out at a WHSV of 6000 mL g⁻¹ h⁻¹.

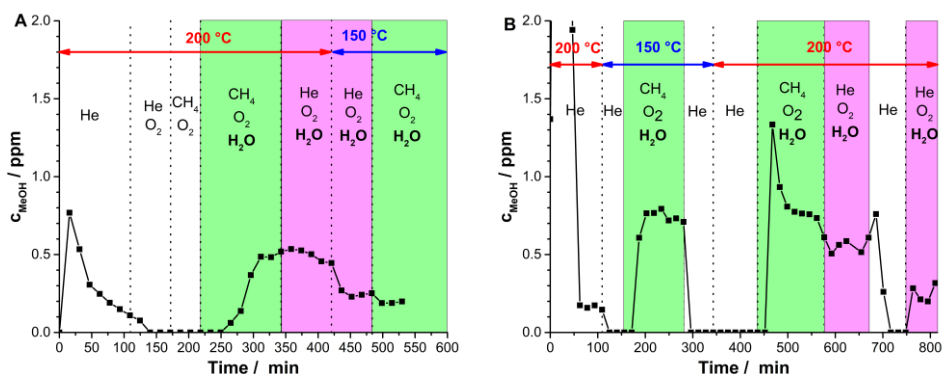


Figure 5.5: Methanol concentration for MIL-100 (Fe, 7% Ni) – A and NH₂-MIL-53 (Al, Fe) – B as a function of TOS and inlet gas composition.

After the presence of methanol was established, the gas composition was varied. Figure 5.5 summarizes the results of methane activation tests over MIL-100 (Fe, 7% Ni) and NH₂-MIL-53 (Al, Fe) under different conditions. The aim was to clearly identify the role of the different gases (CH₄, O₂ and H₂O) in the generation of the methanol signal. Therefore, the samples were first exposed to pure He to remove methanol residues. Afterwards, the gas composition was varied to see which gases are indeed necessary to detect methanol in the outlet stream. This was done at temperatures of both 200 °C and 150 °C. As can be seen in Figure 5.5, the essential parameter is the presence of water in the feed gas.

Traces of methanol can be observed, when first heating the framework in a flow of helium. Additionally, the presence of water also causes a methanol signal to appear in the GC. This led us to question what happens, if a MOF is exposed to a combination of helium and water at 200 °C, without first being exposed to methane and/ or oxygen. Consequently, MIL-53 (Al, Fe) was treated in a stream of 15 mL (He and 3% H₂O) at 200 °C for a period of 9 h before varying the inlet concentration. Figure 5.6 shows the outlet concentration of methanol both during pretreatment and the main experiment. In this context it must be mentioned, that at 200 °C, CO₂ could be observed in the GC for all samples. Since a reliable quantification could not be established, the data is not shown in this work.

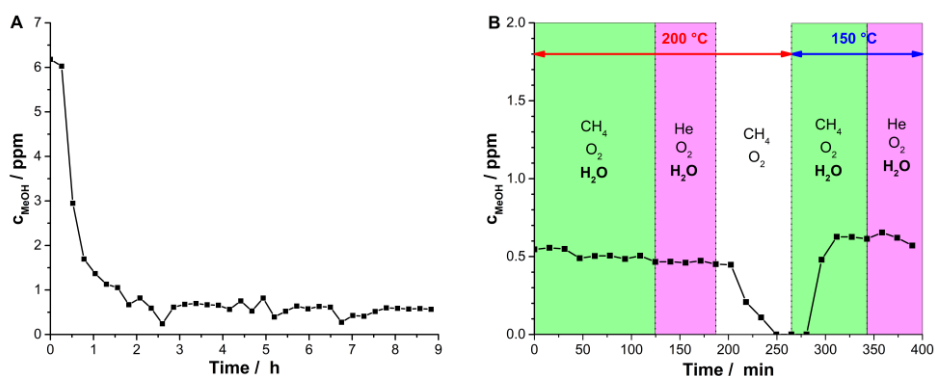


Figure 5.6: Methanol concentration for MIL-53 (Al, Fe) measured during treatment with He and H₂O (A) and different gas mixtures (B).

The left graph of Figure 5.6 shows that in the presence of steam, the initial methanol signal that was also observed for MIL-100 (Fe, 7% Ni) and NH₂-MIL-53 (Al, Fe) does not disappear. This is in contrast to the experiments shown in Figure 5.5, where the original methanol signal disappears after approx. 2 h in a dry feed. After the initial drop in methanol concentration, the signal stays in the same order of magnitude (slightly below 1 ppm) as observed for MIL-100 (Fe, 7% Ni) and NH₂-MIL-53 (Al, Fe). After the switch from He and H₂O to mixtures containing CH₄ and O₂, methanol can be observed in the same order of magnitude (Figure 5.6, right). Once again, the detection of methanol is dependent on the presence of steam in the inlet stream.

The catalytic testing of MIL-53 (HS) leads to similar observations. For this sample, almost no methanol could be detected, when heating in a helium stream. As soon as the inlet stream contains water, the methanol signal increases noticeably. Adding methane and oxygen to the feed stream does not increase the methanol signal. This observation is valid both at 200 °C and at 150 °C (see Figure 5.7). In summary, for all four samples tested, methanol could be observed in the outlet stream, if water was present in the inlet. However, the presence of methane and oxygen had no impact on the methanol signal. Even if the sample was only heated in helium and water added to the feed at elevated temperatures, a stable presence of methanol in the outlet stream could be established.

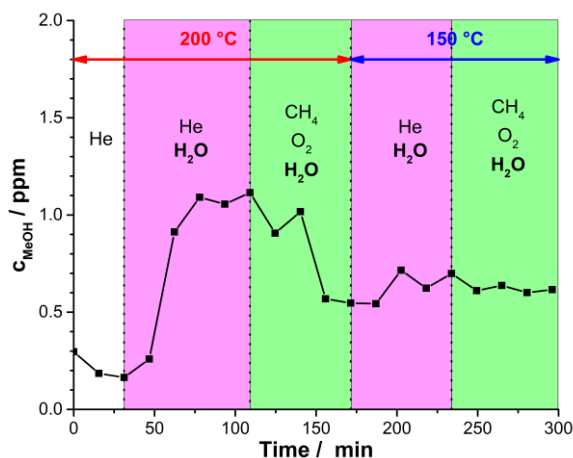


Figure 5.7: Methanol concentration for different feed compositions when testing MIL-53 (HS).

5.3.3 Post-reaction characterization

The MIL-100 (Fe, 7% Ni) used for catalytic experiments shows no signs of having been affected by the catalytic testing. No relevant difference can be detected between the different N₂ isotherms and XRD patterns shown in Figure 5.8. Consequently, for the timescales investigated in this work, the MOF can be considered stable.

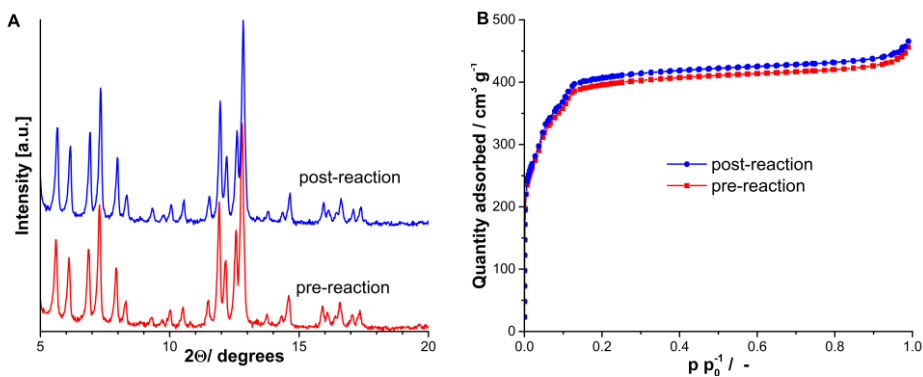


Figure 5.8: Characterization of MIL-100 (Fe, 7% Ni) with XRD (A) and N₂ physisorption (B).

For MIL-53 (HS) both XRD and N₂ adsorption together show a further degradation of the sample due to the catalytic testing. Additional peaks appear in the XRD pattern (e.g. $2\theta = 13^\circ$) after the catalytic test. Furthermore, N₂ uptake is reduced after catalytic testing. While the shape of the isotherm is not affected noticeably, the uptake is in general reduced by approx. $5 \text{ cm}^3 \text{ g}^{-1}$. For a significant section of the isotherm, this represents a drop by 50%.

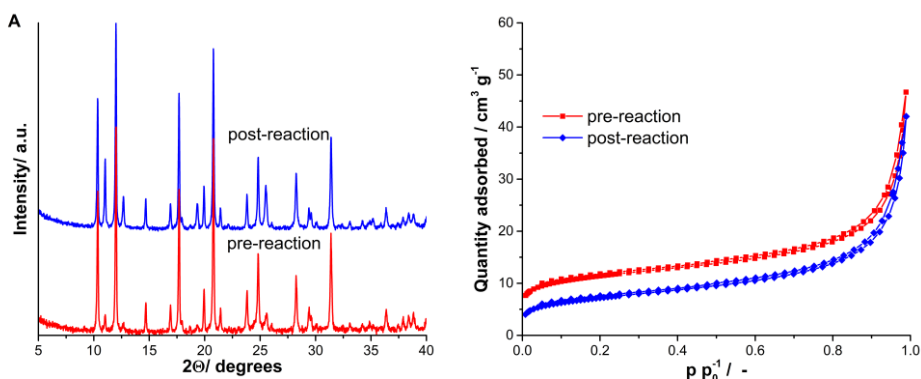


Figure 5.9: XRD patterns (A) and N₂ isotherms (B) of MIL-53 (HS) with coordinated Fe before and after catalytic testing.

In case of the electrochemically synthesized MIL-53 samples (MIL-53 (Al, Fe) and NH₂-MIL-53 (Al, Fe)), there is little information available to indicate framework degradation. As can be seen in Figure 5.10, the XRD patterns of both MIL-53 (Al, Fe) and NH₂-MIL-53 (Al, Fe) are practically identical before and after catalytic testing.

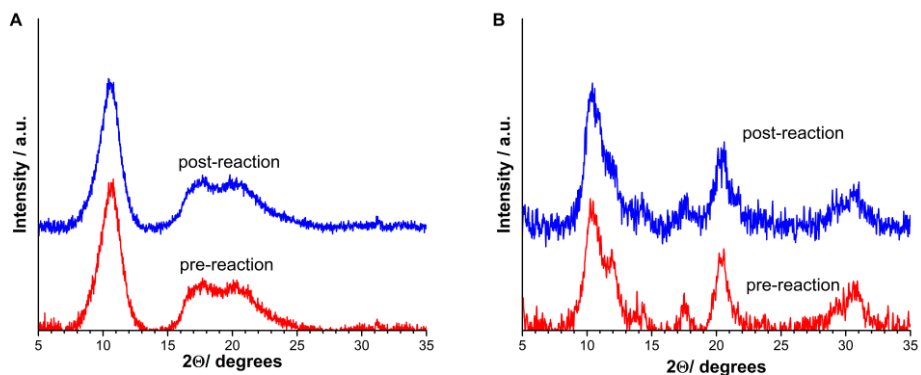


Figure 5.10: XRD patterns of MIL-53 (A) and NH₂-MIL-53 (B) before and after catalytic testing.

Gas adsorption shows small differences in the case of MIL-53 (Al, Fe). With N_2 as a probe molecule, the gas uptake for MIL-53 (Al, Fe) was too slow to measure a complete branch of the isotherm. After reaction however, the uptake is slightly accelerated, allowing for measurement of additional points on the isotherm. For NH_2 -MIL-53 (Al, Fe) on the other hand, no differences could be detected either with CO_2 or N_2 as a probe molecule (see Figure 5.12).

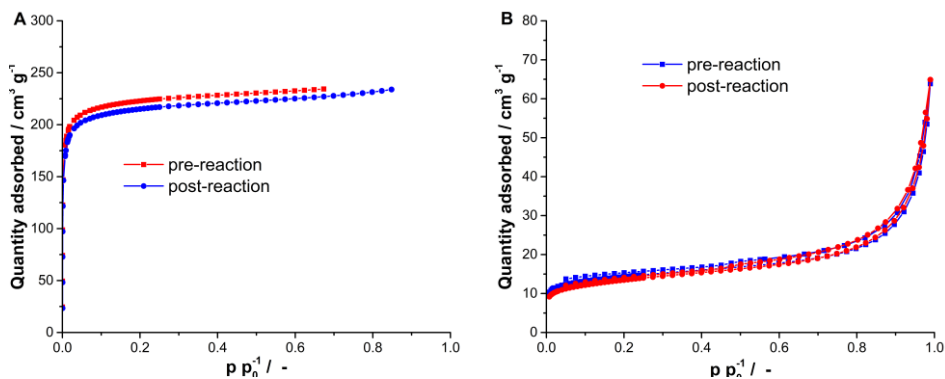


Figure 5.11: N_2 isotherms of MIL-53 (left) and NH_2 -MIL-53 (right) before and after catalytic testing.

In conclusion, NH_2 -MIL-53 (Al, Fe) does not appear to have been affected by the catalytic tests, just like MIL-100 (Fe, 7% Ni). For MIL-53 (Al, Fe) there is no indication of noticeable framework degradation. The improved N_2 uptake at 77 K could be seen as a slight improvement in pore accessibility. In contrast to this, MIL-53 (HS) clearly shows signs of degradation as a result of the catalytic testing.

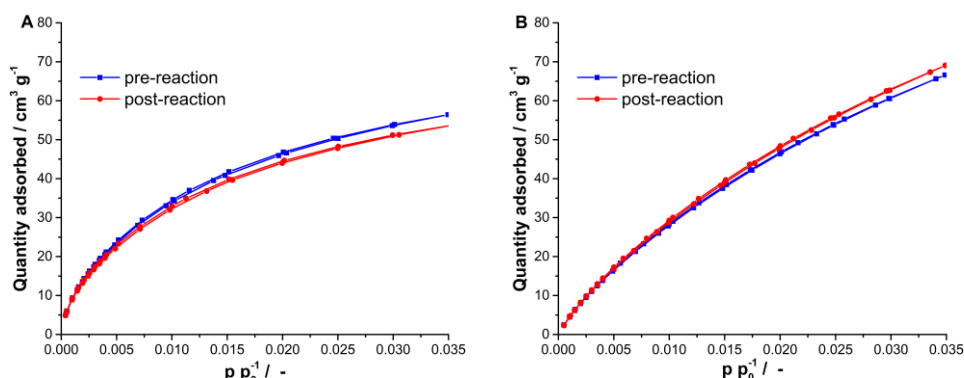


Figure 5.12: CO₂ isotherms of MIL-53 (A) and NH₂-MIL-53 (B) before and after catalytic testing.

5.3.3 Discussion

The results of the catalytic testing clearly show that the methanol signal is not the product of methane conversion. The next step is to define, how important such low signals of methanol could be, when a catalytically active MOF is tested. The overall amount of methanol extracted during the 6 hours of varying feed composition for MIL-53 (Al, Fe) (Figure 5.6, right graph) is less than 1 $\mu\text{mol g}^{-1}$. As mentioned before, in step-wise catalytic operation productivities of 0.5-80 $\mu\text{mol g}_{\text{cat}}^{-1}$ have been reported.^{24, 25} At the same time, such operation limits the exposure of the catalyst to steam to periods of 3 h or less.^{23, 24} In periods of 2-3 h, catalysts such as MIL-100 (Fe, 7%Ni) or NH₂-MIL-53 gave false positive methanol yields of 0.3-0.4 $\mu\text{mol g}_{\text{cat}}^{-1}$. Thus, especially for catalysts with a low concentration of active sites, this contamination signal is quite relevant and in the same order of magnitude as the signal.

As mentioned in the introduction, no published literature to date has shown the productivity of MOF-based catalysts in continuous isothermal oxidation of methane. A first estimate of contamination errors can be given based on the data available for zeolitic systems. The influence of a high temperature treatment step on zeolite activity means however, that many reported values cannot be used for this extrapolation.²⁸ Tomkins *et al.* did show the productivity of Cu-MOR for an isothermal cyclical treatment.²⁹ Starting from the Na-form of MOR (Si/Al = 6.5) they achieved a productivity of approx. 5 $\mu\text{mol g}_{\text{cat}}^{-1}$ per cycle. An H-MOR (Si/Al = 11.5) sample was one of zeolites tested by Narsimhan *et al.* in continuous operation.²⁸ For a WHSV of 2400 mL g⁻¹ h⁻¹, they report a productivity of approx. 0.8 $\mu\text{mol g}^{-1}$ h⁻¹. With our experimental parameters, an outlet concentration of 0.5 ppm corresponds to a methanol rate of 0.15 $\mu\text{mol g}^{-1}$ h⁻¹. This would be a relative error of around 20%.

The two MOR samples differed noticeably in their specifications, so the productivity of $5 \mu\text{mol g}_{\text{cat}}^{-1}$ cannot be seen as the critical limit. The zeolite tested by *Tomkins et al.* had a higher Cu loading but also contained significant amounts of CuO clusters and other Cu species.²⁹ Additionally, the productivity of a Cu-exchanged H-MOR (Si/Al = 10.5) is 5-6 times as high as a Cu-exchanged Na-MOR (Si/Al = 6.5).⁴²

Given this uncertainty, a minimum productivity level, beyond which MOF contamination will clearly not play a role anymore, cannot be defined. Additionally, two studies report a significant decrease in catalytic activity of the MOFs, when repeating the oxidation cycle.^{23, 25} We observed false positive methanol signals that were visible for up to 13 h of continuous operation. Thus, the continuous testing of a moderately active MOF (e.g. comparable to Cu-exchanged NU-1000) with limited stability over TOS may be affected by such phenomena to an unacceptable degree.

It is preferable, if such samples can still be analyzed in a continuous approach. To do this, the source of the methanol signal needs to be identified and the issue resolved. Analysis of the previously described experimental results clearly shows that the MOFs themselves are the source of the methanol signal. The only correlation between the methanol signal and a feed component is with water. However, a decrease of MOF loading from 0.25 g to 0.15 g at constant gas flow rate (i.e. an increase in the WHSV) causes the disappearance of the methanol signal. A contamination of the water source can therefore be ruled out.

Limited MOF decomposition might take place in a humid atmosphere at elevated temperatures. However, a fragmentation of linker molecules beyond decarboxylation reactions under such conditions has not been reported and is not expected. The more likely explanation is the coordination of methanol molecules to the metal centers of the MOF samples. Solvent coordination and solvent molecule exchange in MOFs has been frequently studied in literature.^{43, 44} The most important detail from these studies are the rather elaborate methods necessary to remove all possible solvent molecules from the samples.

Consequently, methanol coordination to the framework appears to be the most credible theory on the origin of the methanol signal. The next step is to determine, if methanol coordination to the framework can be prevented. The MOFs can be classified according to solvent usage and porosity.

- Solvent usage: The MIL-53 samples (electrochemical synthesis) were synthesized using denatured ethanol as a solvent. In contrast only ultra-high purity ethanol and water were used during the syntheses of the MIL-100 samples. However, ultra-high purity ethanol also contains trace amounts of methanol (typically less than 0.1 vol%). For MIL-53 (HS) methanol itself was used as a solvent in the washing procedure.
- Porosity and pore accessibility: The MIL-100 has high porosity and pore accessibility. For MIL-53 and NH₂-MIL-53 the (accessible) pore volume is

significantly reduced. In the case of MIL-53 (HS) the overall pore volume is minimal and the framework shows signs of degradation when being exposed to steam at 200 °C.

The methanol signal measured by GC does not appear to be much affected by either of these categorizations. Especially the question of methanol impurities in the solvents is significant here. The guaranteed maximum concentration of methanol was 0.1 vol% in absolute ethanol. If these concentrations are sufficient to cause such experimental issues, MOF syntheses for this kind of chemistry need to be adapted to avoid solvents typically containing traces of methanol.

At the same time, the exact experimental conditions of the testing protocol are also extremely important. The electrochemically synthesized MIL-53 (Al, Fe) was synthesized in exactly the same manner as that used for liquid-phase methane oxidation experiments previously published.²⁶ In blank runs of the liquid-phase experiments, no methanol could be detected via NMR.

5.4 Conclusions

Bimetallic MOFs belonging to the subgroups MIL-53 and MIL-100 were tested in the continuous gas-phase oxidation of methane. Methanol signals observed during the measurements turned out to be false positives. Feed streams containing water led to the detection of methanol traces in an online GC. Further analysis of the synthesis procedures and the reactivity tests indicate that the MOFs were all contaminated with methanol after synthesis. Traces of methanol in used solvents seem to be sufficient to have methanol coordinated to the frameworks after drying. Steaming the MOFs at elevated temperatures then leads to an exchange of the coordinated molecules and the detection of methanol. For samples with low catalytic activity this could cause significant experimental errors. Thus, any syntheses of MOFs for such work must be carried out with great care and all solvents analyzed for possible methanol contamination before usage. Preferably, syntheses should be adapted to avoid critical solvents (such as other short-chain alcohols), that are easily contaminated with methanol.

5.5 References

1. A. I. Olivos-Suarez, Á. Szécsényi, E. J. M. Hensen, J. Ruiz-Martinez, E. A. Pidko and J. Gascon, *ACS Catal.*, 2016, **6**, 2965-2981.
2. M. Ravi, M. Ranocchiari and J. A. van Bokhoven, *Angew. Chem. Int. Ed.*, 2017, **56**, 16464-16483.
3. A. Holmen, *Catal. Today*, 2009, **142**, 2-8.
4. U. Olsbye, S. Svelle, M. Bjørgen, P. Beato, T. V. W. Janssens, F. Joensen, S. Bordiga and K. P. Lillerud, *Angew. Chem. Int. Ed.*, 2012, **51**, 5810-5831.
5. I. Yarulina, A. D. Chowdhury, F. Meirer, B. M. Weckhuysen and J. Gascon, *Nat. Catal.*, 2018, **1**, 398-411.
6. P. Schwach, X. Pan and X. Bao, *Chem. Rev.*, 2017, **117**, 8497-8520.
7. C. Karakaya and R. J. Kee, *Progr. Energy Combust. Sci.*, 2016, **55**, 60-97.
8. V. I. Sobolev, K. A. Dubkov, O. V. Panna and G. I. Panov, *Catal. Today*, 1995, **24**, 251-252.
9. N. S. Ovanesyan, K. A. Dubkov, A. A. Pyalling and A. A. Shteinman, *J. Radioanal. Nucl. Chem.*, 2000, **246**, 149-152.
10. M. H. Groothaert, P. J. Smeets, B. F. Sels, P. A. Jacobs and R. A. Schoonheydt, *J. Am. Chem. Soc.*, 2005, **127**, 1394-1395.
11. S. Grundner, M. A. C. Markovits, G. Li, M. Tromp, E. A. Pidko, E. J. M. Hensen, A. Jentys, M. Sanchez-Sanchez and J. A. Lercher, 2015, **6**, 7546.
12. P. Tomkins, M. Ranocchiari and J. A. van Bokhoven, *Acc. Chem. Res.*, 2017, **50**, 418-425.
13. D. K. Pappas, A. Martini, M. Dyballa, K. Kvande, S. Teketel, K. A. Lomachenko, R. Baran, P. Glatzel, B. Arstad, G. Berlier, C. Lamberti, S. Bordiga, U. Olsbye, S. Svelle, P. Beato and E. Borfecchia, *J. Am. Chem. Soc.*, 2018, **140**, 15270-15278.
14. F. Göttl, C. Michel, P. C. Andrikopoulos, A. M. Love, J. Hafner, I. Hermans and P. Sautet, *ACS Catal.*, 2016, **6**, 8404-8409.
15. Á. Szécsényi, E. Khramenkova, I. Y. Chernyshov, G. Li, J. Gascon and E. A. Pidko, *ACS Catal.*, 2019, DOI: 10.1021/acscatal.9b01914.
16. P. Valvekens, F. Vermoortele and D. De Vos, *Catal. Sci. Tech.*, 2013, **3**, 1435-1445.
17. J. Gascon, A. Corma, F. Kapteijn and F. X. Llabrés i Xamena, *ACS Catal.*, 2014, **4**, 361-378.
18. A. Dhakshinamoorthy, A. M. Asiri, J. R. Herance and H. Garcia, *Catal. Today*, 2018, **306**, 2-8.

19. H. G. T. Nguyen, N. M. Schweitzer, C.-Y. Chang, T. L. Drake, M. C. So, P. C. Stair, O. K. Farha, J. T. Hupp and S. T. Nguyen, *ACS Catal.*, 2014, **4**, 2496-2500.
20. A. Dhakshinamoorthy, M. Alvaro and H. Garcia, *ACS Catal.*, 2011, **1**, 48-53.
21. F. Hibbe, C. Chmelik, L. Heinke, S. Pramanik, J. Li, D. M. Ruthven, D. Tzoulaki and J. Kärger, *J. Am. Chem. Soc.*, 2011, **133**, 2804-2807.
22. L. Heinke, Z. Gu and C. Wöll, *Nat. Comm.*, 2014, **5**, 4562.
23. T. Ikuno, J. Zheng, A. Vjunov, M. Sanchez-Sanchez, M. A. Ortuño, D. R. Pahls, J. L. Fulton, D. M. Camaioni, Z. Li, D. Ray, B. L. Mehdi, N. D. Browning, O. K. Farha, J. T. Hupp, C. J. Cramer, L. Gagliardi and J. A. Lercher, *J. Am. Chem. Soc.*, 2017, **139**, 10294-10301.
24. J. Zheng, J. Ye, M. A. Ortuño, J. L. Fulton, O. Y. Gutiérrez, D. M. Camaioni, R. K. Motkuri, Z. Li, T. E. Webber, B. L. Mehdi, N. D. Browning, R. L. Penn, O. K. Farha, J. T. Hupp, D. G. Truhlar, C. J. Cramer and J. A. Lercher, *J. Am. Chem. Soc.*, 2019, **141**, 9292-9304.
25. J. Baek, B. Rungtaweevoranit, X. Pei, M. Park, S. C. Fakra, Y.-S. Liu, R. Matheu, S. A. Alshimiri, S. Alshehri, C. A. Trickett, G. A. Somorjai and O. M. Yaghi, *J. Am. Chem. Soc.*, 2018, **140**, 18208-18216.
26. D. Y. Osadchii, A. I. Olivos-Suarez, Á. Szécsényi, G. Li, M. A. Nasalevich, I. A. Dugulan, P. S. Crespo, E. J. M. Hensen, S. L. Veber, M. V. Fedin, G. Sankar, E. A. Pidko and J. Gascon, *ACS Catal.*, 2018, **8**, 5542-5548.
27. M. A. C. Markovits, A. Jentys, M. Tromp, M. Sanchez-Sanchez and J. A. Lercher, *Top. Catal.*, 2016, **59**, 1554-1563.
28. K. Narsimhan, K. Iyoki, K. Dinh and Y. Román-Leshkov, *ACS Cent. Sci.*, 2016, **2**, 424-429.
29. P. Tomkins, A. Mansouri, S. E. Bozbag, F. Krumeich, M. B. Park, E. M. C. Alayon, M. Ranocchiaro and J. A. van Bokhoven, *Angew. Chem. Int. Ed.*, 2016, **55**, 5467-5471.
30. K. T. Dinh, M. M. Sullivan, K. Narsimhan, P. Serna, R. J. Meyer, M. Dincă and Y. Román-Leshkov, *J. Am. Chem. Soc.*, 2019, **141**, 11641-11650.
31. B. Ipek and R. F. Lobo, *Chem. Commun.*, 2016, **52**, 13401-13404.
32. M. V. Parfenov, E. V. Starokon, L. V. Pirutko and G. I. Panov, *J. Catal.*, 2014, **318**, 14-21.
33. D.-D. Zu, L. Lu, X.-Q. Liu, D.-Y. Zhang and L.-B. Sun, *J. Phys. Chem. C*, 2014, **118**, 19910-19917.
34. E. V. Khramenkova, M. V. Polynski, A. V. Vinogradov and E. A. Pidko, *Phys. Chem. Chem. Phys.*, 2018, **20**, 20785-20795.
35. N. C. Burtch, H. Jasuja and K. S. Walton, *Chem. Rev.*, 2014, **114**, 10575-10612.
36. J. W. Yoon, Y.-K. Seo, Y. K. Hwang, J.-S. Chang, H. Leclerc, S. Wuttke, P. Bazin, A. Vimont, M. Daturi, E. Bloch, P. L. Llewellyn, C. Serre, P. Horcajada,

- J.-M. Grenèche, A. E. Rodrigues and G. Férey, *Angew. Chem. Int. Ed.*, 2010, **49**, 5949-5952.
37. M. Giménez-Marqués, A. Santiago-Portillo, S. Navalón, M. Álvaro, V. Briois, F. Nouar, H. Garcia and C. Serre, *J. Mater. Chem. A*, 2019, **7**, 20285-20292.
38. A. Martinez Joaristi, J. Juan-Alcañiz, P. Serra-Crespo, F. Kapteijn and J. Gascon, *Cryst. Growth Des.*, 2012, **12**, 3489-3498.
39. C. Erkey, in *Supercritical Fluid Science and Technology*, ed. C. Erkey, Elsevier, 2011, vol. 1, pp. 41-77.
40. M. Thommes, *Chem. Ing. Tech.*, 2010, **82**, 1059-1073.
41. E. Stavitski, E. A. Pidko, S. Couck, T. Remy, E. J. M. Hensen, B. M. Weckhuysen, J. Denayer, J. Gascon and F. Kapteijn, *Langmuir*, 2011, **27**, 3970-3976.
42. M. Dyballa, D. K. Pappas, K. Kvande, E. Borfecchia, B. Arstad, P. Beato, U. Olsbye and S. Svelle, *ACS Catal.*, 2019, **9**, 365-375.
43. C. K. Brozek, V. K. Michaelis, T.-C. Ong, L. Bellarosa, N. López, R. G. Griffin and M. Dincă, *ACS Cent. Sci.*, 2015, **1**, 252-260.
44. J. Bae, J. S. Choi, S. Hwang, W. S. Yun, D. Song, J. Lee and N. C. Jeong, *ACS Appl. Mater. Interfaces*, 2017, **9**, 24743-24752.

Summary and outlook

Summary

Methane is one of the most abundant hydrocarbons available to society. At the same time the industrially available routes to use methane as a chemical feedstock are limited. Until now, the high temperature conversion of methane to synthesis gas is an essential first step on the path of chemical upgrading. This first step is typically carried out by steam reforming or autothermal reforming of methane. This situation must be improved for several reasons.

The high temperatures necessary for the generation of synthesis gas only make this process commercially viable at very large scales. Smaller amounts of methane for example as a by-product of oil extraction cannot yet be profitably converted to useable chemicals. Instead, the so-called associated petroleum gas is flared to prevent the emission of methane into the earth's atmosphere. This is the lesser of two evils but also not ideal considering the global issue of growing CO₂ emissions. The goal is therefore, to develop a process that can utilize these smaller methane reservoirs on a commercial basis. In lieu of that an optimization of existing methane conversion pathways in combination with CO₂ utilization would already represent progress.

Consequently, this thesis deals with two different reactions. Chapters 2-4 focuses on dry reforming of methane. This reaction is closely related to steam reforming of methane but utilizes CO₂ instead of steam to oxidize methane. Chapter 5 on the other hand deals with the direct partial oxidation of methane to methanol.

The high degree of similarity between commercially applied steam reforming and dry reforming of methane result in a high degree of understanding of catalyst design. Cost considerations have led to Ni being the active metal of choice in most commercial steam reforming catalysts. The disadvantage of Ni over more expensive noble metals is the higher propensity to sinter during reaction. At the same time, coking is a major issue and requires a minimum Ni particle size. Strategies to manage coke formation in steam reforming have already been developed. The higher carbon levels in the reactor during dry reforming and the fact that CO₂ is a softer oxidant than H₂O make coke formation a major stumbling block in the commercialization of dry reforming. Consequently, chapters 2-4 of this thesis focus on providing a deeper insight into both the coking and sintering mechanisms of Ni-based dry reforming catalysts.

A simple model system is used to study coke formation in **Chapter 2**. Ni/ZrO₂ catalysts are promoted with several different metals at low loadings: Na, K, Cs and Mn. It has been reported in literature, that addition of small amounts of additional elements such as Au, K or S can deactivate the most active coke forming sites of Ni-based methane reforming catalysts. The aim of this chapter is to determine, if there are quantitative differences in the influence of different promoters. There does not appear to be any effect on methane or CO₂ conversion activity. However, all promoters suppress coke formation but to differing degrees. TGA

shows, that Na and Cs-promoted Ni/ ZrO₂ contain the smallest amounts of coke. Addition of K and Mn is less effective at reducing the overall coke content. The latter two promoters result in similar coke amounts but TEM and ¹³C-NMR show that K-addition leads to less carbon fibers than Mn-addition. Furthermore, NMR indicates the existence of carbonates in the presence of Na or Cs. We assume this to be due to increased coke gasification activity in these cases, which would explain the lower carbon content. Literature also implies that the surprisingly high effectivity of Na is due to Na-ZrO₂ interactions, which aid in the gasification of coke.

Thus, even for a relatively inert support such as ZrO₂ metal-support interactions cannot be ignored. Therefore, Al₂O₃-supported catalysts are the focus of the next two chapters. Such systems are well-known for potential metal-support interactions. Using Al₂O₃ as a support allows us to take such important effects into account while at the same time providing us with a considerable amount of literature reports, detailing for example the formation of mixed NiO-Al₂O₃ phases. To further understand such effects in combination with Ni sintering, **Chapter 3** focuses on the study of passivation and reactivation of Ni/Al₂O₃ catalysts with dry reforming as a probe reaction. Passivation refers to the controlled formation of oxide layers on reduced catalysts, to protect the metal core from uncontrolled oxidation on contact with air. Ni/Al₂O₃ has frequently been reported to undergo a loss of Ni surface during passivation. We use the fact, that large Ni facets form more coke than several smaller Ni surfaces in dry reforming to track sintering, even when working only with several mg of sample. STEM-EDX measurements confirm our results. In the end, we are able to show that sintering of Ni due to local overheating is an issue except when working with very low loadings of Ni or extremely low O₂ concentrations. Furthermore, we highlight the excellent suitability of dry reforming as a probe reaction for such questions.

In **Chapter 4** we combine the knowledge gained on catalyst sintering and coke formation in the previous two chapters. Ni/Al₂O₃ is promoted with Cr, Mn and Fe and the effect of the promoters on catalyst regeneration compared. All three promoters are, in theory, capable of forming mixed oxide phases with the support but differ in their degree of interaction with CO₂. Regeneration consists of either short oxidation periods with CO₂ or longer oxidation periods with CO₂ followed by reduction with H₂. Literature details the difficulty of reducing Ni²⁺ with methane on an Al₂O₃ support. Our experiments show that a promoter with higher CO₂ affinity leads to quicker Ni oxidation in the absence of H₂. This especially problematic as regeneration by consecutive exposure to CO₂ and H₂ increases Ni sintering and thus the amount of formed coke.

The focus of **Chapter 5** is the development of Metal-Organic Framework (MOF) based catalysts for the direct conversion of methane to methanol. In recent years many publications on this topic focused on zeolite-based catalysts operating at temperatures of 200 °C or lower. The aim of such an approach is to obtain well-defined active sites within the zeolite or MOF lattice. In theory MOFs offer more control over the achievable active site which is why we focus on this topic. Based on previous results obtained at TU Delft, several mixed-metal

MOFs of the structure MIL-53 (Al, Fe), NH₂-MIL-53 (Al, Fe), MIL-100 (Fe, Ni) and MIL-53 (Al) with externally coordinated iron are synthesized and investigated. The attempt to oxidize methane with O₂ at 200 °C in a fixed-bed reactor does indeed lead to the detection of methanol in the range of 1-2 ppm. However, it becomes apparent, that this methanol signal is independent of the presence of both CH₄ and O₂ in the feed. Detailed analysis and sample characterization lead to the conclusion that water in the feed streams removes impurities still coordinated to the frameworks after synthesis and purification. Traces of methanol in used solvents are already sufficient to cause such signal. The methanol signal obtained is in the same order of magnitude as the methanol signal that can be expected from a catalytically active MOF. Thus, the applicability of MOFs for this kind of research appears limited at best.

Outlook

Methane valorization remains an important industrial and societal challenge and thus merits extensive further research. Methane to methanol remains a highly attractive option on paper and thus merits further research but the focus should be on yield optimization. Less challenging reactions involving partial oxidations of hydrocarbons are already limited by unsatisfactory yields of the target products. Therefore, some more out of the box thinking appears essential for methane to methanol to become a viable process.

Too much work remains focused on avenues that, while known to produce traces of methanol, are highly unlikely to ever yield relevant levels of conversion. A prime example are Cu and Fe-exchanged zeolites. Instead, concepts such as protective groups or scavenger molecules that allow for more than traces of methanol must find more implementation. Without such steps forward, the direct synthesis of methanol will remain a “dream reaction”.

Dry reforming on the other hand is already a lot closer to industrial implementation. The major roadblocks towards industrially viable catalysts are well-known in academia: coke formation and catalyst sintering. Undoubtedly, many studies are being carried out to provide more insight into deactivation mechanisms and catalyst design parameters. Some industrially relevant aspects could be put into more focus. In this context, we refer to **Chapter 4**, where the impact of higher CO₂ levels is studied and the fact that industrial steam reforming typically operates with excess amount of steam.

Samenvatting en vooruitblik

Samenvatting

Methaan is een van de meest beschikbare koolwaterstoffen. Tegelijkertijd is het moeilijk om methaan als grondstof in de chemische industrie te kunnen gebruiken. Tot nu is de conversie van methaan naar synthesesgas bij hoge temperaturen een essentiële eerste stap. De opties hiervoor zijn vooral steam reforming en autothermal reforming. Er zijn meerdere redenen waarom deze processen verbeterd moeten worden.

Door de hoge temperaturen tijdens de productie van synthesesgas is een dergelijk proces alleen op grote schaal rendabel. Kleinere hoeveelheden methaan, bijv. het bijproduct van oliewinning, kunnen tot nu nog niet naar bruikbare chemicaliën omgezet worden. In plaats daarvan wordt het tijdens de oliewinning geproduceerde gas afgefakkeld, om de uitstoot van methaan te voorkomen. De te hoge CO₂ emissies zijn een mondiaal probleem. Het affakkelen van methaan is dus ook niet een ideale oplossing. Het doel is om een proces te ontwikkelen dat op kleinere schaal methaan om kan zetten. Als dat niet lukt, dan zou de optimalisatie van bestaande processen een grote stap voorwaarts zijn.

Daarom worden in deze proefschrift twee verschillen reacties onderzocht. Hoofdstukken 2-4 behandelen dry reforming van methaan. Deze reactie is vergelijkbaar met steam reforming van methaan, maar in plaats van stoom wordt CO₂ als oxidatiemiddel gebruikt. In hoofdstuk 5 wordt de directe conversie van methaan naar methanol onderzocht.

Dry reforming van methaan lijkt sterk op de al industrieel gebruikte stoomreforming, waardoor er al veel kennis over katalysatorontwerp bestaat. In de meeste gevallen wordt nikkel vanwege de kosten als katalytisch actief metaal gebruikt. Het nadeel van nikkel tegenover duurder edelmetalen is de neiging om te sinteren. Tegelijkertijd is cokesvorming een belangrijk probleem maar er is een bepaalde minimale diameter van nikkelpartikels nodig voor het ontstaan van cokes. Voor stoomreforming bestaan al manieren om de cokesvorming te kunnen controleren en onderdrukken. De hogere concentraties van koolstof in de reactor tijdens droogreforming en het feit dat CO₂ een zwakker oxidatiemiddel is dan stoom maken cokesvorming een groot hindernis in de commercialisering van droogreforming.

In **hoofdstuk 2** wordt een eenvoudig modelstelsel gekozen, om de cokesvorming te onderzoeken. Ni/ZrO₂ katalysatoren worden met lage concentraties verschillen metalen als promotoren voorzien: Na, K, Cs en Mn. In de literatuur is al beschreven dat kleine hoeveelheden van elementen zoals Au, K of S de meest actieve cokesvormende centra in Ni-gebaseerde reformingkatalysatoren deactiveren. De bedoeling van dit project is het om te onderzoeken of er kwantitatieve verschillen in de invloed van verschillen promotors zijn. Er kan geen verschil in de conversie van methaan en CO₂ worden gedetecteerd. Alle promotors verminderen de cokesvorming, maar verschillen qua effectiviteit. Via TGA is duidelijk te zien, dat Ni/ZrO₂ met Na of Cs het minst cokes bevat. De aanwezigheid van K of Mn reduceert de hoeveelheid cokes iets minder. De toevoeging van deze twee promotors leidt tot vergelijkbare cokeslevels, maar in TEM en ¹³C-NMR is te zien dat er bij toevoer van K minder

vezelcokes is. Bovendien geeft ^{13}C -NMR het bestaan van carbonaten bij aanwezigheid van Na of Cs aan. Dit is een indicatie dat deze twee promotors ook cokesvergassing katalyseren en zo lagere cokeslevel veroorzaken. De onverwacht hoge effectiviteit van Na is volgens de literatuur waarschijnlijk afkomstig in Na-ZrO₂ interacties, die bij de cokesgasificatie helpen.

De interacties tussen nikkel en drager zijn dus ook voor relatief inerte dragers belangrijk. Op basis van deze besef wordt de focus op Al₂O₃ als drager gericht. Ni-Al₂O₃ katalysatoren zijn welbekend voor de mogelijke interacties tussen Ni/ NiO en Al₂O₃. Dit is dus een systeem dat met zulke belangrijke effecten beter rekening houdt. Tegelijkertijd levert literatuur gedetailleerde informatie zoals details over de formatie van gemengde NiO-Al₂O₃ fases. Om deze effecten in combinatie met sinteren beter te verstaan wordt in **hoofdstuk 3** passivering en reactivering middels dry reforming als testreactie onderzocht. Passivering betekent de gecontroleerde oxidatie van de nikkeloppervlakte, om de metalen kern van de nikkeldeeltjes voor contact met zuurstof in de lucht te beschermen. Het is al vaker gerapporteerd, dat Ni/Al₂O₃ tijdens de passivering nikkeloppervlakte verliest. Dankzij het feit dat een groot nikkeldeeltje meer cokes vormt dan meerdere kleine nikkeldeeltjes kan met dry reforming sinteren nagegaan worden. Voor deze experimenten zijn alleen enkele milligrammen monster nodig. De resultaten worden ook met STEM-DEX metingen gesteund. Uiteindelijk is te zien dat sinteren van nikkel door lokale oververhitting snel een probleem is, behalve men werkt met lage concentraties van Ni of O₂. Bovendien kan men in dit hoofdstuk de geschiktheid van dry reforming als testreactie voor dit soort onderzoek duidelijk herkennen.

In **hoofdstuk 4** worden de nieuwe inzichten in sinteren en cokesformatie uit **hoofdstukken 2 & 3** gecombineerd. Ni/Al₂O₃ monsters worden voorzien met Cr, Mn of Fe en de effect van deze promotors op katalysatorregeneratie vergeleken. Alle drie promotors kunnen in theorie gemengde oxidefases met de drager vormen maar verschillen in de sterkte van hun interactie met CO₂. Regeneratie bestaat of uit een korte oxidatieperiode met CO₂ of een langer oxidatieperiode met CO₂ gevolgd van een reductie met H₂. In de literatuur is namelijk beschreven, dat de reductie van Ni/Al₂O₃ met CH₄ moeilijk is. De experimenten tonen dat een promotor met een sterkere interactie met CO₂ de nikkeloxidatie in de afwezigheid van H₂ versnelt. Dit is vooral problematisch omdat regeneratie bestaand uit redoxcycli met CO₂ en H₂ het sinteren van Ni en dus de cokesvorming versterkt.

Hoofdstuk 5 focust op de ontwikkeling van op Metal-Organic Frameworks (MOFs) gebaseerde katalysatoren voor de directe conversie van methaan naar methanol. In de afgelopen jaren werd veel gepubliceerd over zeoliet-gebaseerde katalysatoren, die bij temperaturen van 200 °C en lager actief zijn. Het doel van dit soort onderzoek is de synthese van een goed-gedefinieerd katalytisch actief centrum. De focus ligt op MOFs, omdat ze in theorie meer controle over de actieve centra bieden. Uitgaand van eerdere resultaten vanuit TU Delft worden MOFs met meerdere metalen en de volgende structuren gesynthetiseerd en onderzocht: MIL-53 (Al, Fe), NH₂-MIL-53 (Al, Fe), MIL-100 (Fe, Ni) en MIL-53 (Al) met extern gecoördineerd ijzer. Tijdens de pogingen om methaan bij 200 °C met zuurstof te oxideren wordt er inderdaad een methanol signaal van 1-2 ppm gedetecteerd. Evenwel is het

signaal noch van de aanwezigheid van methaan noch van de aanwezigheid van zuurstof in de toevoer afhankelijk. Nauwkeurige analyse en monsterkarakterisering leiden tot de conclusie, dat stoom in de toevoer onzuiverheden verwijderd, die na synthese en opzuivering nog aan de MOFs gecoördineerd zijn. Sporen van methanol in de gebruikte oplosmiddelen zijn voldoende om dergelijke onzuiverheden te veroorzaken. Het methanolsignaal is in dezelfde orde van grootte, als tijdens een katalytische reactie te verwachten is. MOFs zijn dus blijkbaar niet geschikt als katalysatoren voor dit soort onderzoek.

Vooruitblik

De valorisatie van methaan is een belangrijke industriële en maatschappelijke uitdaging en verdient dus uitgebreid verder onderzoek. De directe conversie van methaan naar methanol blijft op papier een zeer aantrekkelijke optie. Verder onderzoek is aan te bevelen maar met een duidelijke focus op een optimalisatie van de methanolopbrengst. Bij minder uitdagende reacties die partiele oxidatie van koolwaterstoffen inhouden is de opbrengst vaak al onbevredigend laag. Daarom lijkt out of the box denken essentieel te zijn om uit methaan naar methanol een rendabel proces te maken.

Te veel aandacht blijft op systemen gevestigd die sporen van methanol produceren, maar waarschijnlijk nooit belangrijke conversielevels kunnen bereiken. Een goed voorbeeld zijn met Cu of Fe voorziene zeolieten. In plaats daarvan zijn oplossingen met potentieel hogere opbrengsten zoals beschermende groepen of “scavenger” moleculen duidelijk meer aandacht waard. Zonder zulke stappen zal de directe synthese van methanol alleen een “droomreactie” blijven.

Anderzijds is dry reforming al duidelijk dichterbij een industriële toepassing. De grootste problemen voor industrieel toepasbare katalysatoren zijn in de academische wereld welbekend: cokesvorming en katalysatorsinteren. Er zijn zeker vele onderzoeksprojecten, die al uitgevoerd worden en meer inzicht in deactivering en ontwerpparameters zullen leveren. Sommige industrieel belangrijke punten zouden hierbij meer onderzocht kunnen worden. Een voorbeeld is dat voor steam reforming normaal gesproken hoge stoomconcentraties worden gebruikt. In **hoofdstuk 4** is te zien, dat hogere CO₂-concentraties een negatief invloed op bepaalde katalysatoren hebben.





Acknowledgements

After a bit more than four years of doing research, it is now my time to write the acknowledgements to this thesis. There were a few changes in topics, setups, buildings and supervisors and I want to thank the people who helped me during these ups and downs. I apologize already for switching languages in between. This was one of the really nice perks of such an international environment and I enjoyed it too much to waste this opportunity. I realized that on the following pages I mention discussions, chats, etc. frequently. It is not the result of laziness or lack of vocabulary but genuinely what I greatly enjoyed during my time in Delft.

Evgeny, I want to start by thanking you for being my supervisor over the last couple of years. We started working together when I came back from MIT and was a bit frustrated by how my first project had completely disintegrated. You then insisted that I must find my own project. I'm very grateful that you gave me this amount of scientific freedom. Also in terms of data presentation and building a coherent storyline for the right audience I learned quite a lot from you.

Jorge and Freek, it's a pity that our cooperation was cut short but nevertheless I want to thank you for all the feedback you provided and for the opportunity to do a PhD in Delft. Jorge, I also want to thank you for arranging the research stays at MIT and KAUST. Also a big thank you Atsushi, for agreeing to be my co-promotor. It's nice to see how research on heterogeneous catalysis is growing again at TU Delft.

I would also like to thank all members of my defense committee for taking the time to be part of my defense. A big thanks goes to the members of the CatC1Chem consortium for the feedback during the update meetings and showing that methane chemistry is always tricky. Michiel, dankjewel voor al jouw kritische vragen over mijn onderzoek. Jouw feedback was misschien niet altijd een leuke ervaring maar zeker nuttig!

Within TU Delft, there are some people, whose contribution is often under the radar, but in no way less important because of it. Els en Karin, bedankt voor jullie hulp met al de administratieve taken. Bart, het lukt je toch iedere keer om de opstellingen te repareren als weer iemand een "betere" manier heeft gevonden om onderzoek te doen. Dankjewel voor jouw feedback over waar mogelijke foutbronnen in mijn experimenten kunnen zitten. Harrie, dankjewel voor jouw hulp in het oude gebouw, tijdens de verhuizing en in het hogedruklab. Willy, met al die verschillende onderzoeksprojecten tijdens mijn PhD kwamen er ook vele manieren om monsters te karakteriseren. Dankjewel voor al jouw hulp en advies! Liliana, thanks a lot for the help with GCs in the lab and all the nice chats outside the lab.

During my PhD I had the chance to be in two different research groups: Catalysis Engineering and Inorganic Systems Engineering. Alma, I'd like to start by thanking you for the essential support when I started my PhD. Our discussions really pushed me to change my project as quickly as possible. I don't know how much time I would've lost otherwise.

Similarly, I also want to thank Agi for all the support on the topic of methane activation and the fun period as office mates. When I started my PhD, I struggled quite a bit due to the differences to what I expected from Germany. Ina, vielen Dank für deine Hilfe beim Verarbeiten dieses Kulturunterschieds! Jara, me impresiona la habilidad que tienes de saber pedir ayuda en el momento y a la gente adecuada. Muchas gracias por tus consejos y, por supuesto, el libro. Edu, no importaba que pasara durante tu tesis, siempre mantuviste tu buen humor. No podía seguir tu ejemplo, pero gracias por mostrar que eso es posible. I am also very happy that outside of work all of us had the opportunity to spend so much time together, be it drinks, restaurants or vacations together. In this context, also a big thanks to Ivo, Mate, Lennart and Elmar. These shared activities outside of the office helped a lot to maintain my sanity during the PhD.

Dima, the two of us were some of the last people to leave the old building and we managed to not go completely crazy. All the nice chats probably helped - Thanks! Donato, how many times have you tried to explain the difference between empanadas and panzerotti? Thanks a lot for all the fun times, and for keeping up the social vibe in the group. Davide, somehow I never managed to convince you to stop working on MOFs. Thanks for all the fun random conversations! Thanks also to Adrian, Alla, Anahid, Atul, Han, Irina, Meixia, Nastya, Nat Oleksii, Riming, Rob, Sorin, Srinidhi, Stefano, Thomas, Tim, Yixiao and all the other people that were part of CE.

Of course I wasn't planning on forgetting the ISE group. Robbert, thank you for translating/ interpreting Evgeny's comments on my drafts, the general advice on how to sell my science and of course the sometimes serious and sometimes random but always fun discussions. Annika vielen Dank für all die netten Gespräche über die letzten Jahre und die Unterstützung beim Coverdesign! Evgeny Jr./ Shenya thanks a lot for all the discussions about science and the black humor that you brought to the office. I really appreciate you teaching me highly applicable Russian. Chuncheng, thanks for supporting the heterogeneous catalysis section of ISE! It was great having you as a sparring partner for science talks. Lena, I'm terribly sorry that I shocked you so much with my cooking. Good luck with your work on methane activation! Dankjewel Christophe dat ik me ook een keer klein kon voelen! Ali, thanks a lot for the awesome introduction to Persian food and good luck with the science! Georgy, thanks a lot for all the chats at random in the corridors. Guanna, Dapeng, Wenjun and everyone else who at some point was in the group – thanks a lot for the nice atmosphere.

I also want to use this opportunity to thank the students I supervised over the years for their input and the opportunity to improve my teaching skills: Yeabsira, Elias and Tobias. Dominik, Shaurya, Aswin, Zaid, Isabel and Alberto it's been a pleasure having you guys as office neighbors. In PPE gallows humor is luckily not only appreciated but you showed me how much I can still learn.

A big thank you to the many people that helped me a lot during my research stays at MIT and KAUST. Thanks to Yuriy and Jorge for hosting me. Yuriy, it was a pleasure to experience this very infectious enthusiasm that you have for science. Kim, you helped me a lot with the

practicalities of methane oxidation and really helped me to finish this project. Thanks a lot for all the discussions we could have. Philipp and Yidi, die Gespräche über Wissenschaft und Gott und die Welt mit euch haben echt Spaß gemacht. From the Román group I also want to acknowledge Karthik. We only met shortly but it was a relief to hear that methane oxidation didn't only affect my mood. Nastya, my stay in Saudi would probably have been a lot less productive without your help in organizing everything. Abhay, Abhishek and Javier, thanks a lot for all the nice talks we could have over that time.

Life during PhD shouldn't only be limited to university, however. I want to start with the people from Rotaract Scheveningen. In the early phase of my PhD this was such a pleasant escape from the frustrations of academia. Catie, Cyriel and Yildiz our time together in Rotaract may now be over but I'm happy that we still manage to meet up for drinks or dinner and catch up.

One of the important ways for me to maintain some balance during PhD was the Latin dance scene here. Gracias a Constantino, Víctor y Leon. No hubiera descubierto tantas fiestas sin vosotros. Masha danki Chris for getting me hooked on bachata. Your advice to head to Bachata Passion was definitely worth it. Also thanks to all the people at BP for the fun times, especially the online classes and socials during COVID! Ik kan hier helaas niet iedereen noemen, dus: Geno en Steffie dank jullie wel voor de uitstekende lessen en de leuke sfeer! Anne thank you for all the dances, cooking sessions and the many chats and discussions in between! Xavier, thanks a lot for the dinners and nights out during which we both did our best to combat PhD fatigue.

Last but not least I want to mention my family. Liebe Ulrike, vielen lieben Dank für all deine Unterstützung, die unzähligen Gespräche, Notfallpakete und das Wissen, dass ich mich bei Bedarf immer melden kann. In diesem Zusammenhang natürlich auch vielen Dank an Sebastian und inzwischen an Julius! Lieber Papa, dir möchte ich natürlich zu guter Letzt auch danken. Egal was sich in den letzten Jahren ergeben hatte, konnte ich mir immer deiner Unterstützung sicher sein. Allein schon bei der Dissertation gab es doch einige Baustellen. Da war es unheimlich hilfreich zu wissen, dass ich mich immer bei dir melden konnte, wenn es etwas zu besprechen gab. Jetzt sind wir ja nicht mehr durch eine Grenze und Quarantänepflicht getrennt. Ich bin aber unheimlich dankbar, dass ich von euch allen genauso viel Unterstützung erfahren habe, als das noch der Fall war. Vielen lieben Dank!



List of publications and presentations

Publications within the scope of this thesis:

R. Franz, E.A. Pidko, Challenges for the usage of methane as a chemical feedstock, *in preparation*

R. Franz, D. Pinto, E.A. Uslamin, A. Urakawa, E.A. Pidko, Impact of promoter addition on the regeneration of Ni/Al₂O₃ dry reforming catalysts. *submitted*

R. Franz, F.D. Tichelaar, E.A. Uslamin, E.A. Pidko, Dry reforming of methane to test passivation stability of Ni/Al₂O₃ catalysts. *Appl. Catal., A*, **2021**, *612*, 117987

R. Franz, T. Kühlewind, G. Shterk, E. Abou-Hamad, A. Parastaev, E. Uslamin, E. J. M. Hensen, F. Kapteijn, J. Gascon, E. A. Pidko, Impact of small promoter amounts on coke structure in dry reforming of methane over Ni/ZrO₂. *Catal. Sci. Tech.*, **2020**, *10*, 3965-3974.

Publications outside the scope of this thesis:

A. V. Bavykina, A. I. Olivos-Suarez, D. Osadchii, R. Valecha, R. Franz, M. Makkee, F. Kapteijn and J. Gascon, Facile Method for the Preparation of Covalent Triazine Framework coated Monoliths as Catalyst Support: Applications in C1 Catalysis. *ACS Appl. Mater. Interfaces*, **2017**, *9*, 26060-26065.

J. Rischard, R. Franz, C. Antinori, O. Deutschmann, Oxidative dehydrogenation of butenes over Bi-Mo and Mo-V based catalysts in a two-zone fluidized bed reactor. *AIChE J.*, **2017**, *63*, 43-50.

Presentations:

Dry reforming of methane to test passivation stability of Ni/Al₂O₃ catalysts. *NCCC 2020 (The Netherlands' Catalysis and Chemistry Conference)*, **March 2020** Noordwijkerhout, The Netherlands, **oral**

Impact of small amounts of promoters for Ni-based dry reforming catalysts. *NCCC 2019 (The Netherlands' Catalysis and Chemistry Conference)*, **March 2019** Noordwijkerhout, The Netherlands, **poster**

On the applicability of MOFs as catalysts for low temperature methane to methanol conversion. *NCCC 2018 (The Netherlands' Catalysis and Chemistry Conference)*, **March 2018** Noordwijkerhout, The Netherlands, **poster**





Curriculum Vitae

Robert Franz was born on the 22nd of June, 1992 in Ludwigshafen am Rhein, Germany. In March 2010, he received his Abitur (high school diploma), then went on to start his military service in April and, to round off the year, he enrolled in the B.Sc. program of Chemical and Process Engineering in October 2010 at the Karlsruhe Institute of Technology (KIT) in Karlsruhe, Germany. During his studies, which were supported by a scholarship from the Konrad Adenauer Foundation, Robert was active both in the students' parliament of KIT and the Model United Nations Karlsruhe. In 2013 he completed his B.Sc. degree with a thesis in the group of Prof. Dr.-Ing. T. Wetzel entitled "Surface and Microstructure Analysis of Separators for Li-Ion Cells". Afterwards, he moved to the Basel area in Switzerland to complete an internship with Syngenta AG in the process development department.



Robert returned to Karlsruhe in April 2014 to start his M.Sc. degree in Chemical and Process Engineering. During this program, Robert was given the opportunity to carry out another internship, with BASF (China) Co. Ltd., in Shanghai. In April 2016, he finished his M.Sc. degree with a thesis in the group of Prof. Dr. O. Deutschmann, entitled "Oxidative Dehydrogenation of n-Butane and Butenes over Mo-Based Catalysts in a Two-Zone Fluidized Bed Reactor".

The exposure to catalysis research convinced Robert to start a PhD in this field. Therefore, in September 2016 he started his PhD on methane catalysis at TU Delft, first under prof. dr. F. Kapteijn and prof. dr. J. Gascon, then under prof. dr. E. Pidko. During this time, Robert had the opportunity to carry out research stays at MIT and KAUST. The results of this work are described in this thesis. Since February 2021, Robert is working as a process development engineer in the petrochemicals division of BASF SE on reducing the CO₂ emissions during chemical production processes.

